Computational Analysis of Woven Fabric Composites: Single- and Multi-Objective Optimizations and Sensitivity Analysis in Meso-scale Structures

DISSERTATION

Zur Erlangung des akademischen Grades eines
Doktor-Ingenieur (Dr.-Ing.)
an der Fakultät Bauingenieurwesen
der Bauhaus Universität Weimar

vorgelegt von

Ilyani Akmar ABU BAKAR
(externe Doktorandin)

aus

Kuala Lumpur, Malaysia

Mentor (Betreuer): Prof. Dr.-Ing. Timon Rabczuk

Weimar, Februar 2020

To my beloved family ...

Acknowledgements

Completing the journey of PhD is totally the most challenging thing that I went through in my life. The up-and-down moments of my doctoral journey have been shared with many individuals and I am deeply thankful to them. Without their support, this study could not be completed. It has been a great privilege to spend several years in Institute of Structural Mechanics, Faculty of Civil Engineering at Bauhaus Universität Weimar and the members are always be precious to me.

First and foremost, an endless gratitude to my academic supervisor, Professor Dr.-Ing. Timon Rabczuk who also the Chair of Computational Mechanics, Institute of Structural Mechanics, at Bauhaus Universität Weimar. He patiently provides the vision, encouragement and advises for me to proceed through the doctoral programme and completes my study. He has been a supportive person and has given me the freedom to pursue various projects without objection. He has also provided insightful discussions about the research and exposed me to the world of publication. Special thanks to my committee, Professor Dr. rer. nat. Tom Lahmer and Professor Dr. Oliver Kramer for their support, guidance and helpful suggestions. Their guidance has served me well and I owe them my heartfelt appreciation. I also would like to thank Professor Dr. Stephane Bordas and Dr. Lars A. A. Beex from University of Luxembourg for their collaborations and getting me started in the right direction for all the projects involvement.

A special thanks to Universiti Teknologi MARA (UiTM) and the Ministry of Education Malaysia (MoE) for their financial support during my stay in Weimar. I would like to express my sincere appreciation to my Vice-Chancellor, Prof. Emeritus Dato' Dr. Hassan Said, my former Vice-Chancellor, Tan Sri Dato' Sri Prof. Ir. Dr. Sahol Hamid Abu Bakar, the dean of Faculty of Civil Engineering, Prof. Dr. Zakiah Ahmad, the former dean of Faculty of Civil Engineering, Prof. Dr. Azmi Ibrahim, the officers and staff members of Consulate General of Malaysia, MoE and UiTM's Registar office (Sponsorship Department); Khairul Nizam Jamalus, Mohd Zamani Harun, Mohd Ajmi Osman, Sham Azura Ahmad, Nurul Haninah Salleh, Rohanah A. Kadir, Noriah Mohamed Ali, Murni Mohamed Yahya and Subihidin Ghaif.

Members of Institute of Structural Mechanics also deserve my sincerest thanks, their friendship and assistance have meant more to me than I could express. They have kept me entertained during my time in Weimar and without the invaluable kindness, I certainly could not complete my work. Special thanks to Dr.-Ing. Sofyan Ahmad, Dr.-Ing. Nhon Nguyen-Thanh, Dr. Yancheng Zhang,

Dr.-Ing. Zarina Itam, Nadia Sapee, Dr.-Ing. Mohammed Altay', Juan Michael Sargado, Dr.-Ing. Vu Bac Nam and countless others. Thanks are due to Heiko Beinersdorf, Michael Schwedler and Daniel Arnold for their technical support in familiarizing with the Institute facilities.

Not to forget my friends in Malaysia who create a wonderful joy, laughter and support. Special thanks go to Dr. Jurina Jaafar, Dr. Suzana Ramli, Dr. Amnorzahira Amir, Dr. Syahriza Ismail, Suzaini Samsudin, Noririnah Omar, Dr. Norbaya Sidek, Azianabiha A. Halip, Faizah Kamarudin, Nadiah Saari, Fauzilah Ismail and Dr. Aminuddin Baki. I am very happy that in many cases, our friendships have extended well beyond our shared time in Malaysia.

I am most grateful to my mother, Kamariah Ramli and my siblings for their belief in me and their constant prayers. Their endless love inspired me to strive till the end and made me stronger day by day. I owe them everything and I wish I could show them how much I love and appreciate them. I would like to acknowledge my beloved husband, Nor Al Azrin Al Junid for his incredible patience and precious support. Without his continuous support, understanding and encouragement, all my achievements would not be possible. To my little caliphs, Ghazi Al Firas, Ghazi Al Harith and Ghazi Al Aisy, I beg an apology for the limited time that I spent with three of you. Believe me, I love you more than I have. I also would like to thank my in-laws for their unconditional support. Last but not least this dissertation is dedicated to my late father, Abu Bakar Mohd Mokhter who has been my constant source of inspiration. Dad, this is for you.

Weimar, Februar 2020

ILYANI AKMAR ABU BAKAR

Abstract

This study permits a reliability analysis to solve the mechanical behaviour issues existing in the current structural design of fabric structures. Purely predictive material models are highly desirable to facilitate an optimized design scheme and to significantly reduce time and cost at the design stage, such as experimental characterization.

The present study examined the role of three major tasks; a) single-objective optimization, b) sensitivity analyses and c) multi-objective optimization on proposed weave structures for woven fabric composites. For single-objective optimization task, the first goal is to optimize the elastic properties of proposed complex weave structure under unit cells basis based on periodic boundary conditions. We predict the geometric characteristics towards skewness of woven fabric composites via Evolutionary Algorithm (EA) and a parametric study. We also demonstrate the effect of complex weave structures on the fray tendency in woven fabric composites via tightness evaluation. We utilize a procedure which does not require a numerical averaging process for evaluating the elastic properties of woven fabric composites. The fray tendency and skewness of woven fabrics depends upon the behaviour of the floats which is related to the factor of weave. Results of this study may suggest a broader view for further research into the effects of complex weave structures or may provide an alternative to the fray and skewness problems of current weave structure in woven fabric composites.

A comprehensive study is developed on the complex weave structure model which adopts the dry woven fabric of the most potential pattern in single-objective optimization incorporating the uncertainties parameters of woven fabric composites. The comprehensive study covers the regression-based and variance-based sensitivity analyses. The second task goal is to introduce the fabric uncertainties parameters and elaborate how they can be incorporated into finite element models on macroscopic material parameters such as elastic modulus and shear modulus of dry woven fabric subjected to uni-axial and biaxial deformations. Significant correlations in the study, would indicate the need for a thorough investigation of woven fabric composites under uncertainties parameters. The study describes here could serve as an alternative to identify effective material properties without prolonged time consumption and expensive experimental tests.

The last part focuses on a hierarchical stochastic multi-scale optimization approach (fine-scale and coarse-scale optimizations) under geometrical uncertainties parameters for hybrid composites considering complex weave structure. The fine-scale optimization is to determine the best lamina pattern that maximizes its macroscopic elastic properties, conducted by EA under the following

uncertain mesoscopic parameters: yarn spacing, yarn height, yarn width and misalignment of yarn angle. The coarse-scale optimization has been carried out to optimize the stacking sequences of symmetric hybrid laminated composite plate with uncertain mesoscopic parameters by employing the Ant Colony Algorithm (ACO). The objective functions of the coarse-scale optimization are to minimize the cost (C) and weight (W) of the hybrid laminated composite plate considering the fundamental frequency and the buckling load factor as the design constraints.

Based on the uncertainty criteria of the design parameters, the appropriate variation required for the structural design standards can be evaluated using the reliability tool, and then an optimized design decision in consideration of cost can be subsequently determined.

Contents

List of Figures

List of Tables

Nomenclature

Latin Symbols

$\bar{Q}_{ij}^{(k)}$ Plane stress reduced stiffness component of the k^{th} ply

c_{AlO} Unit cost of Alumina Oxide-Aluminum ply

c_{SiC} Unit cost of Silicon Carbide-Aluminum ply

E Strain energy of the unit cell

e° Misalignment in yarn angle

E_l Longitudinal stiffness

E_t Transverse stiffness

E_x/E_{xx}, E_{yy}/E_y, E_z/E_{zz} Modulus of elasticity

F Pareto-optimal solutions minimization

f Fundamental frequency

F_x, F_y, F_z, F_{xy}, F_{xz}, F_{yz} Concentrated forces of the unit cell

G_{lt} Longitudinal shear stiffness

G_{tt} Transverse shear stiffness

G_{xy}, G_{xz}, G_{yz} Modulus of rigidity

m, n Vibration mode shape

M_x, M_y Bending moments in the x and y directions

N_{AlO} Number of Alumina Oxide-Aluminum ply

N_{SiC} Number of Silicon Carbide-Aluminum ply

N_x, N_y, N_{xy} Axial load in x-, y-directions

q_0 Constant parameter of state transition rule

Q_{ij} Stiffness of composite along principal axes

r Ply angle array

R^2 Coefficient of determination (C.O.D.)

R^2_{adj}	Adjusted coefficient of determination
r_i	Radius value
s_y	Yarn spacing
t_y	Yarn height
u, v, w	Displacements in unit cell
W	Work done by the force of the unit cell
w	Deflection in the z-direction
w_y	Yarn width
x, y, z	Coordinates in unit cell
x_i	One independent variable
$\mathcal{P}'$	new population
$\mathcal{P}$	initial population

Greek Symbols

α	Multiplier values
α_i	Inner angle of warp/weft direction
$\bar{x}$, $\bar{y}$	Mean value of the x_i and y_i values
$\bar{Y}$	Mean value of Y_i
β; $\hat{\beta}$	Regression coefficient vector / Regression coefficient / Standardized regression coefficient
β_i	Yarn packing factor
ϵ^0_x, ϵ^0_y, ϵ^0_z, γ^0_{yz}, γ^0_{xz}, γ^0_{xy}	Macroscopic strains
ϵ_i	Error term
$\hat{a}$, $\hat{b}$	Uncertainty parameters
λ	Random number
λ_b	Buckling load factor
λ_b^{min}	Minimum buckling load factor
λ_{cb}	Critical buckling load
μ	Friction coefficient

ν	Poisson's ratio
ν_{lt}	Longitudinal Poisson's ratio
ν_{tt}	Transverse Poisson's ratio
ω_{mn}	Natural frequency of the vibration mode (m, n)
$\rho^{(k)}$	Mass density of the material in the k^{th} ply
ρ_{AlO}	Density of Alumina Oxide-Aluminum
ρ_i	Volumetric density of yarn
ρ_{SiC}	Density of Silicon Carbide-Aluminum
σ_x^0, σ_y^0, σ_z^0, τ_{yz}^0, τ_{xz}^0, τ_{xy}^0	Macroscopic stress
τ_0	Initial amount of the pheromone
θ	Ply angle in degree
θ_{wc}	Crimp angle for warp yarn in general configuration
θ_{wt}	Crimp angle for warp yarn in tight configuration
$\Phi(x_i)$	Fitness function for a weave pattern simulation run per individual

Abbreviations

A, **B**	Data matrices
a	Length of hybrid laminated composite plate
A_i	Cross-sectional area
AR_f	Weft yarn cross-sectional shape factor
AR_i	Cross-sectional shape factor
AR_y	Yarn cross-sectional aspect ratio
b	Width of hybrid laminated composite plate
b_i	Yarn width
C	Cost
c	Cost factor
d_f	Weft yarn thickness
D_{ij}	Bending stiffness
d_i	Yarn thickness

d_w	Warp yarn thickness
f_{Wa}	Warp float
f_{We}	Weft float
GA	Genetic algorithm
h	Total laminate thickness
H_u	Thickness of unit cell
k	Input uncertainty variables
L_i	Yarn length
L_{wgt}	Gap length of tight configuration
L_{wg}	Gap length of general configuration
L_{ws}	Length of straight part of warp yarn in general configuration
L_{wt}	Yarn-to-yarn distance of tight configuration
L_w	Yarn-to-yarn distance of general configuration
L_x	Length of unit cell in x-direction
L_y	Length of unit cell in y-direction
LHS	Latin Hypercube Sampling
MCS	Monte Carlo Sampling
N	Sample size / number of samples / number of plies
n	Data inputs
N_i	Inner ply
N_o	Outer ply
$N_{liaison}$	Number of transitions of warp/weft yarns from one side of the fabric to another
N_{Wa}	Number of warp yarn
N_{We}	Number of weft yarn
$NSGA-II$	Non-dominated sorting genetic algorithm
PSO	Particle swarm optimization
Q'	Image of Point Q
s	Step or move

NOMENCLATURE

S_i, $\hat{S}_i$	First-order sensitivity index / Main effect index
S_{Ti}, $\hat{S}_{Ti}$	Total-order sensitivity index / Total effect index
SA	Simulated annealing
SS	Scatter search
SS_E	Sum squared errors
SS_T	Total sum squared
t	Layer thickness / Ply thickness
T_i	Yarn linear density
V	Total volume of fibre in the unit cell
V_f	Total fibre volume fraction
v_f	Yarn fibre volume fraction
V_i	Volume of each yarn
V_u	Volume of unit cell
W	Weight
$z^{(k)}$	Distance from the middle plane of the laminate to the top of the k^{th} ply
5HS	Harness-Satin 5
8HS	Harness-Satin 8
ACO	Ant Colony Optimization
DOF	Degree(s) of freedom
EA	Evolutionary Algorithm
EP	Ellipse shape
FE	Finite Element
KES	Kawabata Evaluation System
LCR	Lenticular shape
PE	Power ellipse shape
PTFE	Polytetrafluoroethylene
PVC	Polyvinyl chloride
RVC	Representative volume cell
RVE	Representative Volume Element

Chapter 1

Introduction

In recent years, considerable attention has been devoted to woven fabric composite materials and realistic fabric geometric description is essential for modelling of the mechanical and physical properties of textiles and textile composites which in similar to the work discovered by Lin *et al.* (LZS$^+$12, LBL11). In addition, a reasonable cost of manufacturing, an easy handling in dry or preforms, and a good drapability factor also play a major role to its selection. This chapter highlights the state-of-art of textile composites, research overview of a single objective optimization precisely on Evolutionary Algorithm (EA), sensitivity analysis and a hierarchical stochastic multi-scale optimization using Ant Colony Optimization (ACO) in order to obtain a broad view of the fields and identify the gaps in the literature of this study.

1.1 Textile composites: State-of-art

A composite material is defined as an engineering material made from two or more constituent materials that remain separate and distinct on a microscopic level while forming a single component. There are two categories that comprise constituent materials: the matrix and the reinforcement. The matrix material encompasses and upholds the reinforcement materials by sustaining their relative positions. Reinforcements impart their special mechanical and physical properties to enhance the matrix properties. A synergy generates the robust material properties that are unavailable from the individual constituent materials.

Textile composites are a subclass of composites where the reinforcement is a textile material comprised of a network of natural or artificial fibres, typically arranged as tows or yarns. Textile composites encompass a wide variety of textile structures, which include braids, weaves, knitting and non-crimp fabrics. The difference between these types of woven fabrics arises from the way that yarns are placed and bonded together (KM10). Woven fabric is the most common type used in the industry which is made through the yarn interlacement. Braided fabric is manufactured by interweaving three or more strands of yarn whilst knitted fabric is produced by inter-looping yarn in a horizontal or vertical direction. The stitched fabric also known as non-crimp fabric, the yarns are stitched to each other. According to Ansar *et al.* (AXC11), textile composite structures can be categorized as: (i) laminated composites which are composed by stacking a number of unidirectional lamina, (ii) 2D fabric composites and (iii) structural composites for example 3D fabric composites in which the fibrous reinforcements are interlaced in multi-directions. A 3D fabric is defined as a single-fabric system, the constituent yarns of which are supposedly disposed in

a three mutually perpendicular plane relationship (Una12). The thickness or Z-direction dimension is considerable relative to X and Y dimensions in 3D-fabric structures. Fibres or yarns are intertwined, interlaced or intermeshed in the X (longitudinal), Y (cross), and Z (vertical) directions (Una12). In contrast, the 2D-woven fabric is defined as interlacement of two orthogonal sets of yarns in warp and weft directions. Fundamentally, the textile composites are fabricated of two-dimensional or three dimensional repetitions of a weave structure known as representative unit cell (RUC) or unit cell.

Textile composites have been used in many fields for hundreds of years and enjoyed the renaissance in the construction industry during the last century among committed architects and engineers, particularly the architect Frei Otto (Sei09). They are also widely used as structural components in aerospace, automotive, marine structures, civil, chemical processing equipments, sporting, land transportation and leisure sector due to their high stiffness and strength to weight ratio, outstanding physical, good fatigue strength, excellent corrosion resistance, mechanical and thermal properties and dimensional stability (Lon05, CLJ05).

As referred to Dubrovski (Dub10), as the textile industry grows the focus is mainly on their technical performance and functional properties rather than their aesthetic or decorative characteristics, e.g. technical textiles. An understanding of the fabric mechanisms is useful for fabric design and process control. This understanding information provides the relationships between fibre properties, yarn structure, fabric construction and fabric physical properties. For instance, the constitutive laws of fabrics are widely used in clothing construction. This closely related to the low-stress mechanical responses in fabric hand, quality and performance which can be applied to quality control, process control, product development, process optimization and product specification (Jin04).

The revolutionary role of CAE and CAD tools in the textile industry is the guaranty that the final product meets the set specifications, optimizing thus the quality control procedure. Moreover, the prediction of the properties and the aesthetic features of the product before the actual fabrication can essentially benefit the textile research community (VKDP11). The combination of geometric and elastic effects in a single model, users and manufacturers can better understand the behaviour of woven fabric composites and thus make informed decisions during the design process. The relationship between woven fabric constructional parameters and their properties must be first quantitatively defined, if woven fabrics are used to fulfil the desired properties with minimum production costs. Hence, a vast attention should be devoted on woven fabric engineering, which is an important phase by a new fabric development predominantly based on the research work and also experiences.

The elastic properties of woven fabric composites depends on several factors, including fibre and matrix properties, weave structure, and relative and total fibre volume fractions. The manufacturing and properties of the fabric material have been reviewed by Hearle *et al.* (HKN72). The fabric material has more uncertain and sophisticated mechanical properties owing to the uncertainties during its manufacturing process as compared to the conventional structural material. For example, the elemental fibres have a variety of cross-section, and also numerous weaving patterns. All these variations lead to the instability of the fabric material in mechanical properties. Some fibres are very prone to be affected by environmental factors like temperature, humidity, and the aging factor, which may significantly reduce the fibre stiffness (Buc80). Twisting and bending in fibre geometries may complicate the stress-strain relations of the fibres, which influenced the mechanical behaviour. Due to dif-

ficulties in defining the load-deformation relation by conventional analysis, Jong and Postle (JP77, JP78) developed an energy optimization method to investigate the recoverable mechanisms of fabric deformation, based on the principle of minimum strain energy. The reliable prediction of mechanical properties of woven fabric is primary importance to the success of woven fabric composites (LHL$^+$01). Nevertheless, woven fabric composite models that are reported in earlier researches deal with a particular weave structure (e.g. plain weave, a rib knit). According to Lomov *et al.* (LHL$^+$01), there is a lack of generalized models of woven fabrics, that can treat the weave pattern itself as a parameter. Lee *et al.* (LBH03) also assent to the relationships among geometric parameters have not been thoroughly investigated in most published studies to accurately determine the variation of one parameter and whether its effects are interrelated with that of other design parameters. Vaidyanathan and Gowayed (VG96) utilizes Stiffness Averaging Technique for the prediction of composite elastic properties. Ivanov and Tabiei (IT01) developed a computationally efficient and simplified micro-mechanical model of woven fabric composite materials to predict their elastic properties. Yu *et al.* (YPC$^+$02) developed a non-orthogonal constitutive model for fabric reinforced thermoplastic such that the micro-structure information (i.e. the fibre angle) is incorporated into the constitutive stiffness matrix. King *et al.* (KJS05) developed a new continuum constitutive model which simulates the woven fabric as a anisotropic continuum, and takes the meso-structure behaviour into account. The macro-structural model is shown to be accurate and efficient to predict the fabric behaviours under uni-axial loads. Nevertheless, there is no verification through biaxial tension experiments. In this study, we propose a series of complex weave structures that comparable in strength and aesthetically attractive than existing woven fabric composites. We fully-utilized the advantages of EA in simulating the weave structure and the problem of predicting the optimum elastic properties is determined with no numerical averaging process.

The material properties of the meso-scale descriptions in turn depend directly on the geometry of meso-scale unit cells of the fabric and the yarn materials used. Several studies therefore focused on fitting a macro-scale continuum description on the response of meso-scale unit cell models of fabrics. Some of the earliest studies are those of Clulow and Taylor (CT63), Hearle *et al.* (HGB69), Kawabata *et al.* (KNK73a, KNK73b), Testa and Yu (TY87) and Pan (Pan96). Gasser et al. (GBH00) proposed a non-linear finite element analysis specifically for predicting the elastic properties of dry fabrics at macro-scale behaviour via meso-scale prediction. More recent studies are those of Beex *et al.* (BVP13), Buet-Gautier and Boisse (BGB01), Lomov *et al.* (LHL$^+$01), Tabiei and Yi (TY02), Cavallaro *et al.* (CSQ07), Kumazawa *et al.* (KSMK05) and Komeili and Milani (KM12). It is also noted that the woven fabric prones to behave irregularly caused by intrinsic uncertainty in the constituent material properties and fibre geometries (KM10). In fact, engagement and friction between the warp and weft yarns, which are directly related to the yarn surface configuration and fibre alignment at the intersection points, would play a role in woven fabric mechanical properties. Uncertainty analysis of moderate to complex computational models is costly due to the high number of uncertainty criteria that might be considered in the design process. Therefore, the finite element model of a woven composite is formulated based on geometrical parameters and used to predict the macroscopic response of the composite by a numerical homogenization method. Nevertheless, the previous methods encounter all imperfections as part of the numerical model and did not considering the effect

of each factor or the possible interactions between them. In view of this limitation, we adopt four meso-scale uncertainty criteria and explain their influence on the macroscopic elastic properties of dry woven fabric.

Hybrid composites offer a broad range of properties and low-cost solution to the composite structures wherein high stiffness may not be required in every lamina to meet the design criteria. The studies on hybrid composites also have shown that the hybrid composites have more flexibility in design and better mechanical properties compared to non-hybrid composites (KS11). Several researchers have tackled complex multi-objective problems by meta-heuristic algorithms like genetic algorithms (TK$^+$05, CFF$^+$04, GVH01), neuro GA-based algorithm (GE07), scatter search (RL09a, NLA$^+$08), memetic algorithm (LR10), simulated annealing (AS11, KTS05) and Ant Colony Optimization (ACO) (HFSB13) for optimal design of laminate composite structures. Extracting and modelling of individual geometrical scale levels of the composite structure by RVE is the key problem of the multi-scale approach. Thus, we present a hierarchical multi-objective optimization over multiple scales of hybrid laminated composites. This study adopts EA and ACO because of the natural evolution of EA and the decision making process in ACO that provides solutions to the multi-objective optimization problem via artificial intelligence algorithm of a group of virtual ants. The key issue in this approach is the misalignment of yarn interactions developed between these weave structures in mesoscopic level.

1.1.1 Summary of study in textile composites

The first mechanical modelling of woven fabric mechanics published by Haas and Dietzius (HD18) for an airship report of National Advisor Committee for Aeronautics in 1918. Their work remained unknown even though it comprised the theoretical and practical components while the study of Peirce (Pei37) has been considered as the pioneer (Jin04, VKDP11). His model has been greatly used and modified by other researchers such as Painter (Pai52) and Love (Lov54). Hearle *et al.* (HGB69) also gives a vast contribution to the maturity of textile mechanics. The field of textile mechanics is booming when the Kawabata Evaluation System (KES) is introduced for fabric testing. A lot of empirical investigations have been produced to evaluate the relationship between the parameters obtained from the KES and characteristics such as fabric handle and tailorability. Further developments are explained in literature review on each chapter. Conclusively, the prominence of this field can be outlined into three categories as follows (Jin04);

(a) **Component-oriented**. The main focus is to determine the mechanical responses of fabrics by combining the properties of yarns, interactions between the yarns and fabric structure by manipulating the mathematical concepts and a set of assumptions. Hearle *et al.* (HGB69), Grosberg (Gro66) and Postle (PKN83) have been the pioneer in this matter.

(b) **Phenomena-oriented**. Investigate the fabric responses due to the loading condition on rheological models wherein representing the general relationships of stressstrain.

(c) **Results-oriented**. Observations are made based on experimental works and numerical methods which allow estimations of purely mathematical operations and theoreti-

cal background, thus avoiding many subjective assumptions that may be misleading. More effective and realistic approach may be developed from this.

1.1.2 Mechanical behaviour of textile composites

According to Vassiliadis *et al.* (VKDP11), an integrated textile modelling concepts comprised of three modelling levels: (i) micro-level modelling of yarns; (ii) meso-level modelling of fabric unit cell and (iii) macro-level modelling of the fabric sheet.

In the first modelling level, the fibre properties and the yarn structure (i.e. yarn type, number of fibres and fibre orientations) are introduced as the input parameters for the mechanical analysis and yarn property predictions. The yarn properties are then transferred into the meso-level modelling wherein the homogenization approaches are implemented to correlate the two levels. In meso-level modelling, the woven fabric structure is introduced which representing the yarns as the continuum structures and predictions are made based on the unit cell of the fabric. As for the macro-level, a simplified structure is developed and the mechanical behaviour is determined according to the deformation of continuum materials.

These three modelling levels have classified the analytical and numerical analysis of textile composites wherein the purpose of these investigations are focused on the responses of textile composites with respect to a certain deformation. For instance, the work by Backer (Bac52), Platt *et al.* (PKH59), Freeston and Schoppee (FS75), Choi and Tandon (CT06) and Park and Oh (PO06) are focused on the micro-level modelling of tensile, bending and torsional behaviour using the force, stress-analysis and energy methods.

Meso-level modelling which involving the simple deformations can be retrieved in Dastoor *et al.* (DGBH94), Kemp (Kem58), Olofsson (Olo64), Freeston *et al.* (FPS67), Grosberg and Kedia (GK66), Grosberg (Gro66), Huang (Hua79a, Hua79b), Kawabata *et al.* (KNK73a) and Ozgen and Gong (OG11) whilst the complex deformations are carried out by Behre (Beh61), Dahlberg (Dah61), Lindberg *et al.* (LBD61), Abbott *et al.* (AGL71), Shanahan *et al.* (SLH78), Amirbayat and Hearle (AH89) and Lo *et al.* (LHL02).

Many researchers also studied and reported the macro-level modelling for complex deformations such as Konopasek (Kon80a, Kon80b, Kon80c), Lloyd *et al.* (LMH96), Postle and Postle (PP96) and Stump and Fraser (SF96). Vassiliadis *et al.* (VKDP11) added that a systematic method is derived from the modular modelling which minimizing the complexity of the mechanical structure and the nature of the material involved. A global evolution of the modelling approaches has contributed to the likely way of computational aided environment.

1.2 Aim and research questions

Practically, what occurs to a fabric during its production or handling process can induce some flaws into the material (KM10). For instance, skewness takes place through the mechanism of fabric shear as the warp and weft yarns rotate at intersections from a right angle position to form an obtuse or acute angle. Skewness can be defined as misalignment of yarn angles in the warp and weft directions during relaxation, although they are straight. Naturally, yarns get closer to each other and the free spaces between the yarns became limited after relaxation due to the force contraction in warp and weft yarns. The weave

structures have a significant affect to skewness (AY04). However, few studies have reported on skewness in woven fabrics which considering complex weave structures as weave structure variables. For single-objective optimization task, the first goal is to optimize the elastic properties of proposed complex weave structure under unit cells basis based on periodic boundary conditions. We predict the geometric characteristics towards skewness of woven fabric composites via Evolutionary Algorithm (EA) and a parametric study. We also demonstrate the effect of complex weave structures on the fray tendency in woven fabric composites via tightness evaluation. We utilize a procedure which does not require a numerical averaging process for evaluating the elastic properties of woven fabric composites. The fray tendency and skewness of woven fabrics depends upon the behaviour of the floats which is related to the factor of weave (AY04). Results of this study may suggest a broader view for further research into the effects of complex weave structures or may provide an alternative to the fray and skewness problems of current weave structure in woven fabric composites.

A significant amount of study on meso-scale modelling considering with and without material flaws of woven fabrics composites done by previous researchers (KM10). Yet, none of the researchers reported on complex weave structure under uncertainties consideration. While most of the models in previous studies are designed with a combinatorial system of matrix and yarns, in many situations the designers have to, instead, deal with dry fabrics (KM10, AHW$^+$12). Dry fabric refers to a bundle of fibres with no matrix that bond them together. This makes the dry fabric in highly non-linear and strain dependent transverse stiffness condition and no shear stiffness values in their constitutive models. Respectively, the study of dry fabric elastic properties necessitates modified approaches for adequate prediction. A comprehensive study is developed on the complex weave structure model which adopts the dry woven fabric of the most potential pattern in single-objective optimization incorporating the uncertainties parameters of woven fabric composites. The comprehensive study covers the regression-based and variance-based sensitivity analyses. The second task goal is to introduce the fabric uncertainties parameters and elaborate how they can be incorporated into finite element models on macroscopic material parameters such as elastic modulus and shear modulus of dry woven fabric subjected to uni-axial and biaxial deformations. Significant correlations in the study, would indicate the need for a thorough investigation of woven fabric composites under uncertainties parameters. The study describes here could serve as an alternative to identify effective material properties without prolonged time consumption and expensive experimental tests.

Since the laminate composites are aesthetically attractive and preferable to fibrous composites because of their uniform properties in the plane of the sheet, the multi-scale optimization of weave structure is presented as our third task. In all applications, there are three characteristics (strong, lightest and most economical structures) that considered as epitome, normally contrary to each other and may come in compromise with the presence of hybridization of composite laminates (HFSB13). Hybridization of composite yields a synergistic effect of properties wherein each structure contributes its properties to the behaviour of a structure with better properties than those of each component (FS11). From theoretical considerations, it may be expected that the mechanical properties of micro-laminate composites would follow an adaptation of the well-known HallPetch relationship wherein correlation between the characteristic micro-structural parameter such as yarn diameter, fibrous

diameter, or lamina thickness is well elaborated in this study. In structural optimization, the design functions can be global as the weight, the stiffness, the vibration frequencies, the buckling loads, or local as strength constraints, strains and failure criteria. Although many studies have been done on optimization of woven fabric composites, little literature is available on complex woven fabric structure (AT09, RL09b, RL11, AS11, HFSB13). In light of this, a hierarchical stochastic multi-scale optimization approach (fine-scale and coarse-scale optimizations) under geometrical uncertainties parameters for hybrid composites considering complex weave structure is presented. The fine-scale optimization is to determine the best lamina pattern that maximizes its macroscopic elastic properties, conducted by EA under the following uncertain mesoscopic parameters: yarn spacing, yarn height, yarn width and misalignment of yarn angle. The coarse-scale optimization has been carried out to optimize the stacking sequences of symmetric hybrid laminated composite plate with uncertain mesoscopic parameters by employing the Ant Colony Algorithm (ACO). The objective functions of the coarse-scale optimization are to minimize the cost and weight of the hybrid laminated composite plate considering the fundamental frequency and the buckling load factor as the design constraints.

1.3 Research overview

1.3.1 A Single Objective Optimization - Evolutionary Algorithm

Predictions of geometric characteristics and elastic properties of patterns in woven fabric composites are proposed based on unit cells. This study addresses the optimization of the elastic properties within woven fabric composite unit cells with multiple designs based on periodic boundary conditions and EA.

Furthermore, the study permits a reliable prediction of mechanical behaviour of woven fabric composites unit cells in which the weave patterns are the variables. The models are treated as a lamina for each weave pattern embedded in a matrix pocket. The analysed weave patterns are created by TexGen, the simulation is done with ABAQUS. At the unit cell level, effective elastic properties of the yarn are estimated from Finite Element (FE) simulations using periodic boundary conditions. Periodic boundary conditions have been designed from translational symmetry transformation whilst the application of loads are described in terms of macroscopic stresses or strains to the woven fabric unit cells. Consequently, the elastic properties of woven composites can be calculated in a standard and simple procedure without implementing the numerical averaging process (LW04).

The EA is adopted in optimizing the elastic properties of woven fabric composites with recombination and mutation operators. The EA is a subset of evolutionary computation and a population-based stochastic meta-heuristic for optimization, where evolutionary programming is introduced by Fogel *et al.* (FOW66) in the United States. The EAs are based on the collective learning process within a population of individuals, each of which represents a search point in the space of potential solutions to a given problem. The population is arbitrarily initialized, and it evolves towards better and better regions of the search space by means of randomized processes of selection in which could be deterministic in some algorithms, with biologically-inspired operators like mutation, and recombination that are possible to be completely omitted in some algorithmic realizations. The environment deliv-

ers fitness value about the search points, and the selection process favours those individuals of higher fitness to reproduce more often than those of lower fitness. The recombination mechanism allows the mixing of parental information while passing it to their offspring, and mutation introduces innovation into the population (ES03, BS93). The optimization process shares similarities with the natural evolution of populations of individuals that adapt to their environment. The details of components involved in EAs are explained in Section 2.6.

We present a parameter study to investigate the effect of various geometric parameters. The parametric study is conducted by preparing a set of parameters, and to vary each parameter independently while keeping the others at their initial values. A set of parameters has been selected which greatly affects the fabric geometry or the elastic property of woven fabric composites. The gap length, yarn thickness and bundles sizes, effect of shape factor and material constituents are the parameters that evaluate the elastic properties of the optimized woven fabric composites. By examining this optimized unit cell model through the pre-determined parameters as mentioned above, an optimal parameter set for composites performance can be properly selected.

1.3.2 A Sensitivity Analysis on Material Properties

According to Saltelli (Sal08), sensitivity analysis is a useful technique on how different values of an independent variable impacts a particular dependent variable under a given set of assumptions. It helps to build confidence in the model by considering the uncertainties that are often associated with variable in models. Robust uncertainty criteria able to capture the non-linear behaviours (contact descriptions, material parameters, geometric definitions) and a large number of parameters involved lead to complex sensitivity studies. Hence, it is essential to consider input parameters of stochastic nature which requires a robust evaluation of the simulation models.

Some models represent variables that are very difficult, or even impossible to measure to a great deal of accuracy in the real world. It allows to determine what level of accuracy is necessary for a variable to make the model sufficiently useful and valid. If the model is insensitive, then it may be possible to use an estimate rather than a value with greater precision. Sensitivity analysis can also indicate which variable values are reasonable to use in the model. Experimenting with numerous of values can offer insights into behaviour of a system in extreme situations.

A leverage point can be determined when the system behaviour greatly changes for a change in a parameter value in which this point is a parameter whose specific value can significantly influence the behaviour mode of the system (BC01). Based on sensitivity analysis, we determine the key meso-scale uncertain input variables that influence the macro-scale mechanical response of a dry textile subjected to uni-axial and biaxial deformations. The dry woven fabric is assumed to behave in a transversely isotropic fashion at the macro-scale.

The regression-based and variance-based methods are utilized in defining the sensitivity analysis of material properties. The sensitivity of four meso-scale uncertain input parameters on the macro-scale response are investigated; i.e. the yarn height, the yarn spacing, the yarn width and the friction coefficient. The Pearson coefficients are adopted to measure the effect of each uncertain input variable on the structural response. Due to computational effectiveness, the sensitivity analysis is based on response surface models. The Sobol's

variance-based method which consists of first-order and total-effect sensitivity indices are presented. The sensitivity analysis utilizes linear and quadratic correlation matrices, its corresponding correlation coefficients and the coefficients of determination of the response uncertainty criteria. The correlation analysis, the response surface model and Sobol's indices are presented and compared by means of uncertainty criteria influences on *MataBerkait*-dry woven fabric material properties.

To anticipate, it is observed that the friction coefficient and yarn height are the most influential factors with respect to the specified macro-scale mechanical responses.

1.3.3 Multi-Objective Optimization - Ant Colony Optimization

Optimization is a method of defining and comparing feasible solutions until no better solution can be determined. According to Deb (Deb01), the presence of multiple conflicting objectives (for instance simultaneously minimizing the cost and maximizing the strength performance of products) is common in many problems and makes the optimization problem more complicated to solve. Due to no one solution can be determined as an optimum solution to multiple conflicting objectives, the resulting multi-objective optimization problem resorts to a number of trade-off optimal solutions. This study applies the meta-heuristic method of ACO to an established set of uncertain multi-plies, fibre reinforced and hybrid laminates of woven fabric composites. The idea is inspired by the behaviour of real ants, related to their ability to find the shortest path between the nest and the food source by pheromone tracks. The procedure simulates the decision making processes of any colonies as they search for food and likely similar to other adaptive learning and artificial intelligence approaches such as simulated annealing and genetic algorithms.

This study presents a hierarchical multi-objective optimization over multiple scales of hybrid laminated composites. The fine-scale optimization problem is treated as a meso-level single-ply RVE problem or lamina wherein the weave pattern is embedded in a matrix pocket. The weave pattern is the design variable of the first task considering the stochastic effects under uncertainties wherein four uncertain mesoscopic parameters are investigated: yarn spacing, yarn width, yarn height and misalignment in yarn angle. The fine-scale objective functions are to maximize the macroscopic elastic properties of lamina with periodic boundary conditions and optimize the pattern arrangement using evolutionary algorithm. The fine-scale optimization problem is done for a selected set of uncertainties by utilizing Latin Hypercube Sampling. The coarse-scale optimization problem is presented as the stacking sequence optimization of hybrid fibre-reinforced composite plate with two non-linear objectives and two design constraints. The coarse-scale optimization goals are to minimize the cost and weight of the laminated plate with constraint on the first fundamental frequency and the buckling load factor.

A multi-plyed, fibre reinforced and hybrid laminated composites are reconsidered with respect to the optimized macroscopic elastic properties of lamina in the fine-scale optimization problem. The investigated lamina is made of Alumina Oxide-Aluminum ($Al_2O_3 - Al$) and Silicon Carbide-Aluminum ($SiC - Al$) plies to combine the toughness and economical attributes. The ACO is utilized to formulate the Pareto-optimal solutions by optimizing a convex combination of the two non-linear objectives, weight (W) and cost (C) based on a series of multiplier values (α). Simultaneously, the latter task could be simplified into

a single-objective optimizer by employing the concept of weighted sum method. Conclusively, the best hybrid laminated composites based on the series of multiplier values are presented in the coarse-scale optimization problem.

1.4 Thesis Structure

Chapter 2 addresses the optimization of elastic properties within woven fabric composite unit cells with multiple designs based on periodic boundary conditions and EA has been chosen as an optimization strategy. It comprises an introduction to the subject of optimization and the current state of the art in giving the work some context and defining some concepts from data analysis and statistics that are central to our algorithm. Furthermore, a parametric study has been conducted to investigate the effect of various geometric parameters of optimized woven pattern on the elastic properties of the composite. Theoretical background and detail flows are provided to give a brief explanation of the whole process.

Chapter 3 presents two different global sensitivity analysis approaches i.e. regression-based and variance-based methods with particular consideration of the influences of four uncertainty criteria on *MataBerkait*-dry woven fabric material properties. They are presented in order to quantify the significant factor that influenced *MataBerkait*-dry woven fabric material properties under uni-axial and biaxial loadings. There are four uncertainty criteria highlighted as mentioned above. Practically, the global sensitivity analysis may improve the understanding of the model behaviour and may clarify the interactions among the input variables. A brief overview on correlation analysis, response surface method and Sobol's sensitivity indices is given in this chapter. Comparisons and discussions are made based on the results obtained in order to quantify the significant and insignificant variables.

Chapter 4 discusses the novel numerical approaches of EA and ACO procedures for multi-objective optimization of hybrid laminates. The EA and ACO fitness assignment procedures are described in a step-by-step algorithm and reliable results are presented. The mathematical formulation of the fundamental frequency and buckling load factor for hybrid laminated composites are derived. The applications adopted in the study could serve as the basis comparison for a study of multi-objective optimization with several objective functions. The idea of this work is motivated from the study of Hemmatian *et al.* (HFSB13), Ilyani *et al.* (BKBR13) and Tahani and Abachizadeh (AT09).

Chapter 5 contains the summary of conclusions of each chapter, and recommendations are made for further consideration.

Chapter 2

Optimization of Elastic Properties and Weaving Patterns of Woven Composites

This chapter represents the analysis of optimization in predicting the geometric characteristics and elastic properties of patterns in woven fabric composites based on unit cells. It addresses the single objective optimization of the elastic properties within woven fabric composite unit cells with multiple weave pattern based on periodic boundary conditions and evolutionary algorithms. An evolutionary algorithm is delineated and a parameter study is presented to investigate the effect of various geometric parameters on the optimized weave pattern.

2.1 Literature review

Woven fabrics generally consist of two sets of yarns that are interlaced and laid orthogonal to each other. The textile fabrics form a system from woven yarns, which are arrayed orthogonally under unstressed condition and compose of threads that are paralleled or twisted together. The symmetrically structured raw fabric is coated with special glue mixtures and the surface is tempered to protect it from external influences (Sei09). The yarns that run along the length of the fabric are known as warp ends whilst the threads that run from one side to the other side of the fabric, are weft picks (HA00).

In general, weave patterns are defined by a number notation such as 4X4, 5X3, and 2X2. The first number in the notation indicates the number of yarns that crossed "over", known as warp direction before it changes direction or known as weft direction (perpendicular yarns). A fundamental weave is made of basis weaves that served as a starting point for creating complex weave patterns and commonly are classified into 3 different basic styles; (a) Plain weave (the simplest and closest crossing of warp and weft), (b) Twill weave and (c) Harness- Satin weave, see (Fig. 2.1). A plain weave is defined as a 1X1 weave which are commonly used in fabrics manufacturing for membrane construction and a twill weave is defined as a set of identical number of weave both under and over such as 2X2 and 4X4 twill weaves. A Harness-Satin is referred as Harness, Satin, or Crowfoot, which refers to any number larger than 1, followed by X, and another larger number larger than 1. The most common satin harness used are Harness-Satin $8(8HS)$ and Harness-Satin $5(5HS)$. A common used materials for textile composites in construction are polyester fabrics with a

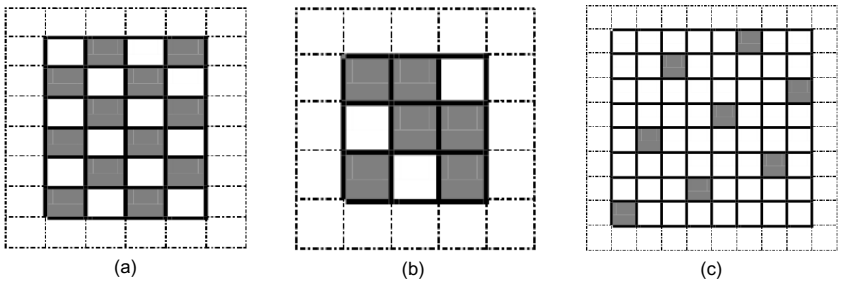

Figure 2.1: Fundamental weaves: (a) Plain weave, (b) Twill weave and (c) Harness- Satin weave

PVC coating and glass fibre high-strength fabric with PTFE coating.

Technically, the fabric mechanical behaviour is a complex and multi-scale problem due to the intricate interactions of the yarns and fibres. The macroscopic behaviour is very dependent on the interactions of yarns at the meso-scale and at the micro-scale level of the fibres constituting yarns. Regardless of various studies in the field, there is no widely accepted model that accurately describes all the main aspects of a composite woven mechanical behaviour (Boi10). As a result, the micro- and macro-structure of a manufactured preform may deviate from those of the designed/optimized model, leading to uncertainties in performance predictions (QWK$^+$15).

Large variability already exists in the fibres and yarns, and their composites could have much higher probabilistic properties. Crimp-interchange with visco-elastic yarn leads to a complicated structural performance (e.g stress-strain relationship) when dealing with loads. Therefore, the probabilistic investigation and analysis of coated woven fabric must allow for its highly non-linear and inelastic mechanical behaviour with the environment aspects (e.g. thermal effect). The crimp interchange also complicates the load-deformation relations especially when carrying various loads in biaxial directions. The simulation of the meso-structure of the crimp is very important in predicting the mechanical behaviours of the fabric under different loads. A lots of researchers like Peirce (Pei37) and Kawabata *et al.* (KNK73a, KNK73b) proposed their models, amongst which, the truss model based on the lattice formation of the fabric is found to be effective and accurate for both uni-axial and biaxial loadings (Zha10a). Zhang (Zha10a) added that the review of the nature of coated woven fabrics demonstrates that high mechanical non-linearity, variability and complexity are the basic characteristics for the fabric as a composite made of woven yarns and coatings. The analysis of the tensile behaviour of plain woven fabric is taken by Leaf (LK80) with one (1) small strain and two (2) large strain approaches. According to Leaf (LK80), assuming circular yarn cross-section in the fabric analysis is not realistic, because the compression from the transverse yarns impose on them certainly change the geometry. On the other hand, Vaidyanathan (VG96) stated that the elastic behaviour of woven fabric composites depends on a number of factors, including fibre and matrix properties, fabric architecture and relative and total fibre volume fractions (i.e. volume proportion of fibres in yarns).

As a composite of yarns and coating materials, fabric materials are initially modelled as bundles of yarns, and their probabilistic properties are often estimated based on the as-

sumption of yarn distribution (SS89). However, it is found that the mechanical performance of single yarns is significantly different from that in coated woven fabrics, because of yarn-to-yarn frictions especially for biaxial loading. The simulation of realistic yarns structural behaviour can be estimated using reduced yarn lengths which vary with different fabric types (VKDP11). This simulation lacks on the theoretical support. A lot of numerical and analytical models have been proposed to represent the mechanical behaviour of the meso-structure of the woven fabric. Most of them do not account for the interaction between yarns like crimp interchange, locking and relative yarn rotation, and the implementation of these meso-structural models is shown to be difficult for more general load cases (KJS05). The unit cell approach is employed in the analysis of most material models of woven composite structures. The composite structure is divided into repeated cells, representing the properties and the behaviour of the whole lamina.

The classical 1-D models of Ishikawa and Chou (IC82a, IC82b) are extended to 2-D elastic models by Naik and Shembekar (NS92b). Naik and Ganesh (NG96) considered the failure in the weft yarn direction of loading only. They divided the sub-cells of their representative volume cell (RVC) into many slices. They used different failure criteria for the different constituents: Tsai-Wu failure criterion for the fill strand, maximum strain criterion for the warp strand and maximum stress criterion for the pure matrix material. After the matrix material failure in the "gap" region, the fill strand is modelled as a curved cantilever slender beam. Naik (Nai95) developed 3-D micro-mechanical material models of woven and braided fabric composite materials with failure. Ivanov and Tabiei (IT01) developed a simplified micro-mechanical model of woven fabric composite materials which satisfying the lack of RVC discretization and good elastic property prediction. The choice of the RVC is intended to account for geometrical non-linearity and simple and efficient technique for fibre reorientation was incorporated in the model of Tabiei and Ivanov (TI03).

Yu *et al.* (YPC$^+$02) developed a non-orthogonal constitutive model for fabric reinforced thermoplastic which capable in predicting the angle change of the composite under the loading draping. Tabiei *et al.* (TSJ03) suggested a micro-mechanical material model of woven fabric composite materials to simulate the progressive failure. The quarter sub-cell of the RVC is divided in many blocks. Micro-mechanical failure criteria for each constituent material in the block and corresponding stiffness degradation are adopted in this matter. The material shear non-linearity described by Hahn and Tsai is included in the model.

Yi *et al.* (YDC06) stated that the uni-axial and biaxial elastic models of the fabric material are dependent, and the uni-axial loading state can be considered as one special type of uni-axial state with zero stress along one direction. The stress-strain relationship under the biaxial loads with different loading ratios can be approximately estimated based on the uni-axial deformation properties obtained from uni-axial tension tests. However, the accuracy of this estimation is easy to be justified because of the highly non-linear mechanical performance of woven fabrics. As a woven composite material, fabric exhibits highly non-linear mechanical behaviour owing to the visco-plastic nature of its fibre elements. The material failure mode and ultimate strength of the fabric are shown to be related to the micro-structure form of the matrix (AT07). Potluri and Thammandra (PT07) had simulated the meso-structure of the fabric crimp under uni-axial and biaxial loadings using a finite element model indicates the uni-axial loading increases the elastic properties along the tension direction and significantly reduces the stiffness in the transverse. In contrast, biaxial

loading increases the stiffness in both directions as the result of crimp reduction. Many of these models have been reviewed by Byun and Chou (BC89) and Tan *et al.* (TTS97) for 2D and 3D woven fabric composites, and Ayranci and Carey (AC08) for 2D woven fabric (braided) composites. Lomov *et al.* (LPI$^+$10) delineated the modelling of 3D woven fabrics with the aid of WiseTex software (AXC11).

Hence, we can conclude that the mechanical properties of woven fabrics are governed by: (a) weave parameters such as an architecture pattern, yarn size, yarn spacing length, fibre crimp angle and volume fraction of fibre bundles, see Fig. 2.2; and (b) laminate parameters such as stacking orientation and overall fibre volume fraction (LBH03). The mechanical performance could be determined either via experimental work or simulations; the latter is a less costly approach commonly used in determining the mechanical properties of woven fabrics.

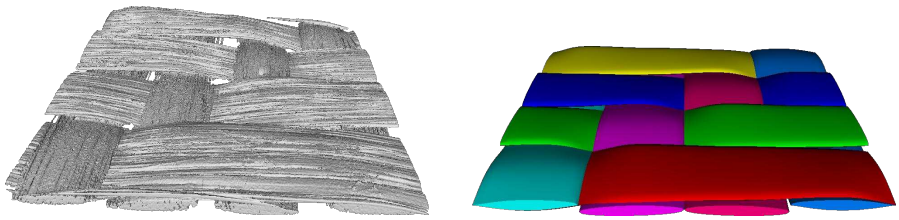

(a) (b)

Figure 2.2: fibres in a yarn. Reproduced by (Lon11).

2.2 Malaysian's weave patterns

In Malaysia (and other similar countries in South East Asia) weaving used to be a leisure activity of village women in rural coastal areas. Material used is *Pandanus* leaves or called *mengkuang* by the locals which after being stripped of thorns and split into strands, are soaked, dried, dyed and then woven according to the desired patterns. The weave patterns are inspired from nature usually from surrounding flora, fauna and carry the name of their creator (MHD89).

Fig. 2.3 depicts elements of woven fabric composite pattern used for weave classification. Referring to Long (Lon05), the pattern is represented with black squares corresponding to crossovers where the warp yarn is on top and the minimum repetitive element is called a *repeat*. The *repeat* can have different number of warp (N_{Wa}) and weft (N_{We}) yarns. *Weft float* (f_{We}) describes the length of a weft yarn on the face of the fabric, measured in number of intersections. The *warp float* (f_{Wa}) is defined similarly since the number of white squares between black squares are equal in fundamental weaves. The distance between white and black squares, measured in number of squares is called *move or step* (s) in which this characterizes the shift of the weaving pattern between two weft insertions. They are characterized by a square repeat with $N_{Wa} = N_{Wa} = N$. Each warp/weft yarn has only one weft/warp crossing with $f = 1$ for warp/weft. The pattern of adjacent yarns is regularly shifted with s being a constant.

The chosen weaves are based on aesthetics, complexity of curves, and the weight of the fabric needed in an application. In general, the looser the fabric, the more likely the fabric

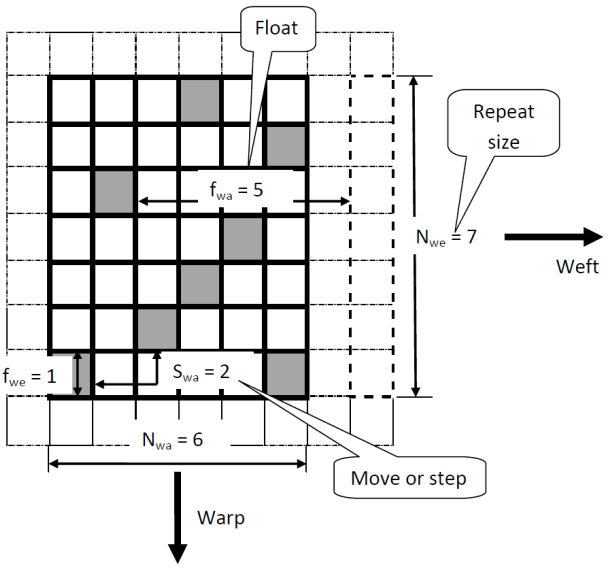

Figure 2.3: Elements of a typical weave. Reproduced by (Lon05).

will fray at the ends and create spaces in the fabric when bent around complex curves. A loose fabric fits around complex curves much better than a tighter weave fabric. A plain weave has the tightest criteria among the fundamental weaves. Since a plain weave is tight, it is the least likely to fray at the ends. Unlike plain weaves, a twill weave is much easier to bend around complex curves because its weave is looser. The Harness-Satin weave performs the best in catering for complex curves and bends compared to plain or twill weaves. This is because the fibre crimp in the geometry of Harness-satin that allows it to cater for the complexness of the curves but it tends to fray at the ends.

Normally, the plain weave is chosen if the aesthetic value is neglected. If aesthetics are very important, generally a twill weave is selected, but for a sophisticated look a Harness-Satin 8 $(8HS)$ is often used and it is the best choice for complex curves as well. The study has focused to the modified and complex weaves in which the aim is to combine the advantage criteria in fundamental weaves with some modifications that existed in Malaysian's weaves as illustrated in Fig. 2.4, Fig. 2.5, and Fig. 2.6, respectively. The designs are inspired by the secular Malaysian's weaving industry. There are 51 patterns as reported by Malaysian Handicraft Development Corporation (M.H.D.C.) (MHD89) and Chee (Che98) elaborates more on the patterns selection, however only repetitive patterns are adopted for this study.

2.3 Elasticity behaviour of woven fabric composites

According to Seidel (Sei09), textiles are anisotropic materials. Thus, physical or numerical tests must be performed in multiple directions to obtain the associated stiffnesses and strengths. The application of elasticity to woven composites is complex. Long (Lon05) explicates that at the microscopic level, woven composites (irrespective of their fibre archi-

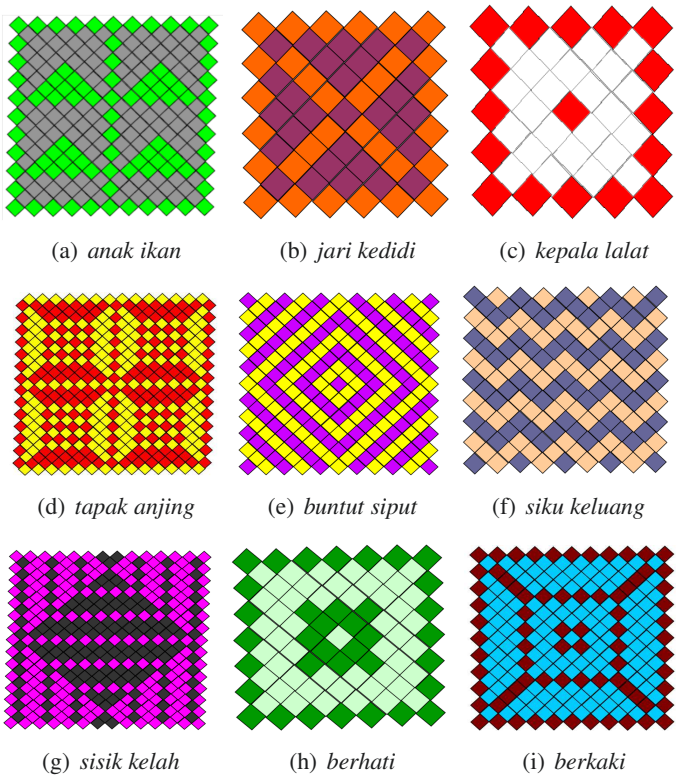

(a) *anak ikan* (b) *jari kedidi* (c) *kepala lalat*

(d) *tapak anjing* (e) *buntut siput* (f) *siku keluang*

(g) *sisik kelah* (h) *berhati* (i) *berkaki*

Figure 2.4: Selected weave patterns inspired by fauna.

tecture) are assembled from bundles of parallel fibres embedded in a matrix material that is usually polymeric and has a much lower modulus, and is usually assumed to be homogeneous and isotropic.

Consequently, the structure will have stiffness and strength properties which are much greater in the direction of the fibre rather than in any perpendicular direction. The elastic behaviour (i.e. the relationship between stresses and strains in the three principal directions) of a material possessing three such planes of symmetry is characterized by an orthotropic constitutive model. We consider orthotropic woven fabric composites with three elastic moduli E_x, E_y and E_z, three independent Poisson's ratios ν_{xy}, ν_{yz} and ν_{zx} and three shear moduli G_{xy}, G_{yz} and G_{zx}. Theoretically, the Poisson's ratios $(\nu_{yx}, \nu_{zy}, \nu_{xz})$ are related to the aforementioned moduli and Poisson's ratios as described in Eq. (2.1)

$$\nu_{yx} = \nu_{xy}\frac{E_y}{E_x}; \quad \nu_{zy} = \nu_{yz}\frac{E_z}{E_y}; \quad \nu_{xz} = \nu_{zx}\frac{E_x}{E_z}; \tag{2.1}$$

The elastic behaviour may be expressed via Hooke's law for orthotropic materials as

$$\begin{aligned}
\epsilon_x &= \tfrac{1}{E_x}\left(\sigma_x - \nu_{xy}\sigma_y - \nu_{xz}\sigma_z\right); \\
\epsilon_y &= \tfrac{1}{E_y}\left(\sigma_y - \nu_{yx}\sigma_x - \nu_{yz}\sigma_z\right); \\
\epsilon_z &= \tfrac{1}{E_z}\left(\sigma_z - \nu_{zx}\sigma_x - \nu_{zy}\sigma_y\right); \\
\gamma_{xy} &= \tfrac{\tau_{xy}}{G_{xy}}; \quad \gamma_{yz} = \tfrac{\tau_{yz}}{G_{yz}}; \quad \gamma_{xz} = \tfrac{\tau_{xz}}{G_{xz}}.
\end{aligned} \tag{2.2}$$

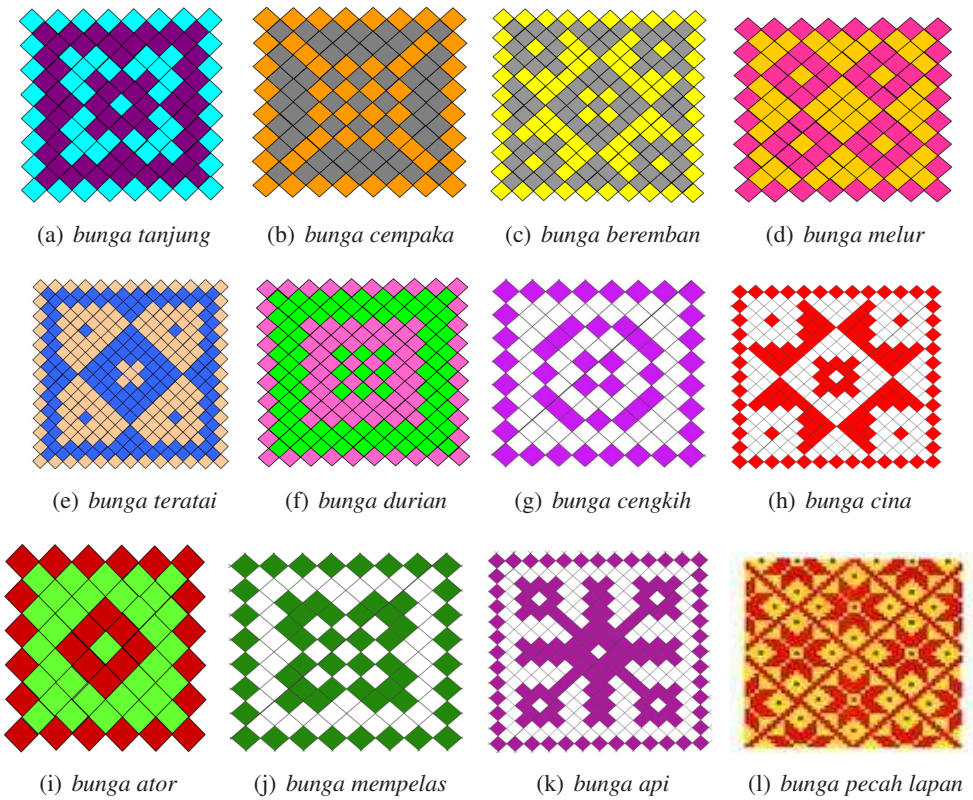

(a) *bunga tanjung* (b) *bunga cempaka* (c) *bunga beremban* (d) *bunga melur*

(e) *bunga teratai* (f) *bunga durian* (g) *bunga cengkih* (h) *bunga cina*

(i) *bunga ator* (j) *bunga mempelas* (k) *bunga api* (l) *bunga pecah lapan*

Figure 2.5: Selected weave patterns inspired by flora.

Simplified, the woven fabric composite can be modelled under plane-stress conditions, reducing Eq. (2.2) yielding to Eq. (2.3)

$$\begin{bmatrix} \epsilon_x \\ \epsilon_y \\ \gamma_{xy} \end{bmatrix} = \begin{bmatrix} \frac{1}{E_x} & -\frac{\nu_{xy}}{E_x} & 0 \\ -\frac{\nu_{yx}}{E_y} & \frac{1}{E_y} & 0 \\ 0 & 0 & \frac{1}{G_{xy}} \end{bmatrix} \times \begin{bmatrix} \sigma_x \\ \sigma_y \\ \tau_{xy} \end{bmatrix}. \tag{2.3}$$

Therefore only four independent constants (E_x, E_y, G_{xy} and either of the Poisson's ratios) are needed to define the in-plane elastic behaviour of a lamina which in agreed with Long (Lon05).

2.4 Unit cell designation in TexGen

Apart from the analytical models, several commercial computational tools are available, such as TechText CAD, WeaveEngineer, ScotWeave and WiseTex (LZS$^+$12). Table 2.1 delineates the comparison of computational tools that available in current. TexGen has been chosen due to its suitability towards this study. TexGen (LB11) is an open source software developed by University of Nottingham which offers a modelling processor for various textiles applications. The geometry of the woven fabric unit cell is produced in a generic way by independent specification of yarn path and yarn cross-sections which

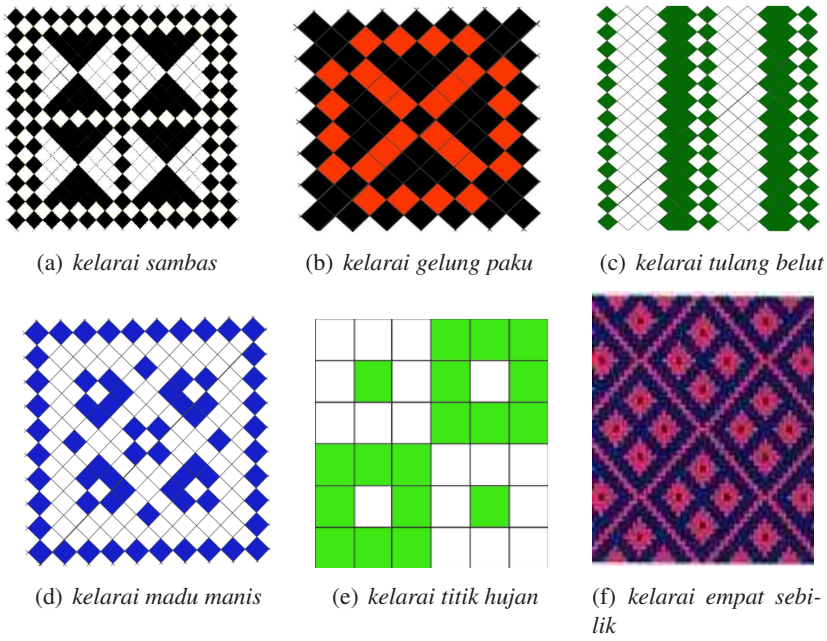

(a) *kelarai sambas* (b) *kelarai gelung paku* (c) *kelarai tulang belut*

(d) *kelarai madu manis* (e) *kelarai titik hujan* (f) *kelarai empat sebilik*

Figure 2.6: Selected abstract patterns.

produced by Lin *et al.* (LBL11). TexGen has been used extensively for prediction of textile reinforced composite mechanical properties. For some time, TexGen has been employed to generate geometric models of textile reinforcements to permit finite element (FE) analysis of the repeating unit cell in order to determine the effective macroscopic properties of the as-manufactured composite. A comprehensive description on theoretical background can be retrieved from Sherbun (She07).

2.4.1 Yarn path

The Malaysian's weave unit cells are generated using the TexGen package for the woven fabric composite unit cells. The modelling procedure starts with determining the yarn path of the unit cells. The yarn path is modelled by defining its centerline which positioning the three dimensional space as a function of the distance along the yarn. The yarn path is represented by a Bezier spline and determined by the yarn cross section, yarn spacing and fabric thickness adopted in the study. Practically, the yarns are initially modelled as a symmetrical and constant cross section with a well-defined central line. Then, the yarn cross section is modified locally based on experimental images wherein the centreline is maintained as a convenience reference line (LBL11). The master nodes in a unit cell are defined as the smallest repeatable section of the yarn or by means a series of points along its length with an interpolation function to contribute the exact path between those nodes. The interpolation function must give at least C^1 continuity function and no gaps are allowed in the nodes.

Table 2.1: Commercial computational tools for textile composite (LZS$^+$12)

Computational tool	Attributes
TechText	The software has the ability to predict the uniaxial and biaxial stress-strain curves of fabric for 2D woven and weft-knitted fabrics based on an energy method using the yarn mechanical properties.
WeaveEngineer	Built to design the 3D woven textile structures with both solid and hollow architectures and non-crimp composite reinforcements. No features for predicting the mechanical properties available.
ScotWeave	Features are more suitable for weave designers rather than for research.
ScotWeave Technical Weaver	Aim specifically at modelling technical textiles at the mesoscopic scale.
WiseTex	Capable in modelling a variety of fabric structures incorporated physical properties of the yarns. Modelling fabric physical properties, including resistance to tension, compression, shear and bending.
TexGen	A modelling pre-processor for textiles simulation for a variety of applications in solid mechanics, fluid dynamics and thermodynamics.

2.4.2 Yarn cross section

As for yarn cross-sections, they are defined as 2D-woven solid volumes where the cross-sections are approximated to be the smallest region that encompasses all of the fibres within the yarns. We should recall that woven fabrics are divided into 2D- and 3D-wovens wherein the 2D- and 3D-wovens are defined as the interlacement of two- and three- orthogonal sets of yarns, respectively. There are five options given in cross-section shape: Ellipse, power ellipse, lenticular, hybrid and polygon. Interpolations between yarn sections are set into constant to minimize the computational time in the unit cell models. TexGen models a yarn as a series of individual sections defined at each control node along the yarn path. These sections are composed of separate upper and lower curves to improve conformance to the geometry. The yarn cross section that implemented in TexGen is defined as the 2D parameter equation of the form $C(v)$. The ellipse form is given by Eq. (2.4)(LBL11).

$$\begin{array}{ll} C(v)_x = \frac{w}{2}\cos(2\pi v) & 0 \leq v \leq 1 \\ C(v)_y = \frac{h}{2}\sin(2\pi v) & 0 \leq v \leq 1 \end{array} \tag{2.4}$$

where w is the width o the yarn cross section and h is the height of the yarn cross section.

A power ellipse is described as

$$C(v)_x = \frac{w}{2}\cos(2\pi v) \qquad 0 \leq v \leq 1 \tag{2.5}$$

$$C(v)_y = \left\{ \begin{array}{ll} \frac{h}{2}\sin\left(2\pi v\right)^n & 0 \leq v \leq 0.5 \\ -\left(\frac{h}{2} - \sin(2\pi v)\right)^n & 0.5 \leq v \leq 1 \end{array} \right\} \tag{2.6}$$

where n is power index $(0, 1, 2, ...)$.

The lenticular cross sectional is defined as an intersection of two circles of radii r_1 and r_2 offset vertically by distances o_1 and o_2, respectively (see, Fig. 2.7(b)). The above parameters can be calculated from the desired width w, height h and distortion d of the lenticular section as expressed in Eq. (2.7)(LBL11):

$$\begin{array}{ll} r_1 = \frac{w^2+(h-2d)^2}{4(h-2d)}, & r_2 = \frac{w^2+(h+2d)^2}{4(h+2d)} \\ o_1 = -r_1 + \frac{h}{2}, & o_2 = r_1 - \frac{h}{2}. \end{array} \tag{2.7}$$

Correspondingly, the lenticular section is calculated by

$$C(v)_x = \begin{cases} r_1 \cos\theta + o_1 & 0 \leq v \leq 0.5 \\ -r_2 \cos\theta + o_2 & 0.5 \leq v \leq 1 \end{cases} \tag{2.8}$$

$$C(v)_y = \begin{cases} r_1 \sin\theta + o_1 & 0 \leq v \leq 0.5 \\ -r_2 \sin\theta + o_2 & 0.5 \leq v \leq 1 \end{cases} \tag{2.9}$$

where

$$\theta = \begin{cases} (1-4v)\sin^{-1}\left(\frac{w}{2r_1}\right) & 0 \leq v \leq 0.5 \\ (-3+4v)\sin^{-1}\left(\frac{w}{2r_2}\right)_2 & 0.5 \leq v \leq 1 \end{cases} \tag{2.10}$$

The lenticular shape has been assumed as the cross-sectional shape of a yarn. It is a realistic assumption due to the interlocking and compression of over- and under-laid warp yarns, see Fig. 2.7(a) in which the imperfection of interlacement in composite process will lead to yarn flattening as observed by (VIV96).

By taking the cross-sectional shape factor, AR_i, as the yarn width, b_i, divided by the yarn thickness, d_i, the cross sectional area, A_i, of the weft yarn is given by Eq. (2.11) and Eq. (2.12)(LBH03)

$$r_i = \frac{d_i}{4}(1 + AR_i^2); \quad \alpha_i = 2\sin^{-1}\left[\frac{2 \times AR_i}{1 + AR_i^2}\right] \quad (i = \text{warp(w)}, \text{weft(f)}), \tag{2.11}$$

$$A_i = r_i^2\,(\alpha_i - \sin\alpha_i) \quad (i = \text{warp(w)}, \text{weft(f)}), \tag{2.12}$$

where r_i is the radius value, α_i is the inner angle and subscript i indicates the warp and weft yarn.

The cross-sectional area of a yarn also can be calculated from the manufacturer specifications data via Eq. (2.13) (AXC11, Wu09)

$$A_i = \frac{T_i}{\rho_i \beta_i} \quad (i = \text{warp(w)}, \text{weft(f)}), \tag{2.13}$$

where T_i is the yarn linear density, ρ_i is the volumetric density of yarn and β_i is the yarn packing factor which depends on the layout of circular fibres within the yarn cross-section and referring to two different arrangements:(a) rectangular packing array and (b) hexagonal packing array. Since the fibres within the yarn cannot be 100% packed without gaps between them, the yarn packing factor β_i is expressed as: $\beta_i \leq \dfrac{\pi}{4} = 0.7854$ (For a rectangular

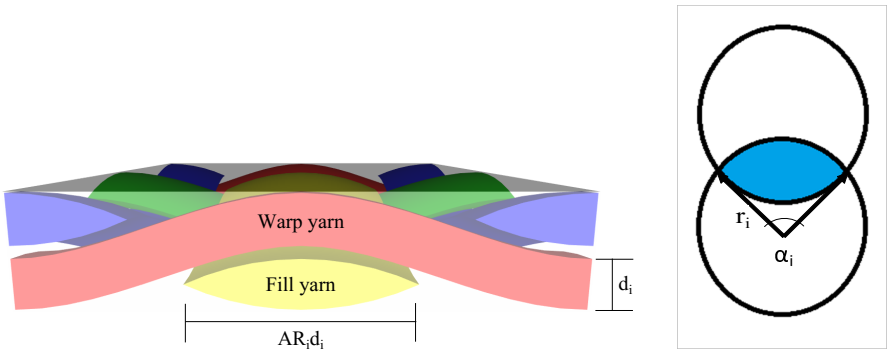

(a) (b)

Figure 2.7: Yarn cross-sectional shape of woven fabric composites (d_i = the thickness of warp/weft yarns; r_i = the radius of yarn; AR_i = the cross-sectional shape factor; α_i = the inner angle of warp/weft direction).

packing array) and $\beta_i \leq \dfrac{\pi/2}{\sqrt{3}} = 0.9069$ (For a hexagonal packing array) in which the values are as reported by Ansar *et al.* (AXC11). For a particular yarn shape, the yarn thickness d_i has been found a function (fn) of yarn linear density (T_i), yarn density (ρ_i), yarn aspect ratio $(AR_i = b_i/d_i)$ and yarn packing factor (β_i), as given in Eq. (2.14)(AXC11, QMM03)

$$d_i = fn\frac{T_i}{\rho_i \beta_i AR_i} \quad (i = \text{warp(w), weft(f)}). \tag{2.14}$$

Ansar *et al.* (AXC11) and Quinn *et al.* (QMM03) also added that the width, b_i, of warp and weft yarn is expressed as Eq. (2.15)

$$b_i = AR_i \times d_i \quad (i = \text{warp(w), weft(f)}). \tag{2.15}$$

2.4.3 Unit cell and weave pattern

A 2D binary matrix is used to represent the proposed patterns. Each interlacing is represented by an element in the 2D binary matrix, and elements in the array can only have one of the two values: 1 and 0. 1 means that the warp yarn is over the weft yarn at the crossover and 0 indicates the vice-versa situation. The method of modelling unit cells used in TexGen can lead to yarn intersections (i.e. part of one yarn volume intersecting with/ penetrating either a crossing or parallel yarn volume). A robust approach is available in TexGen to encounter the yarn intersection identifications and modification of the unit cells to reduce the intersections to an acceptable level.

2.4.4 Yarn material orientation

It is noted that the yarns are highly anisotropic material thus, the stress and strain components will be defined in the local orientation. A local (Gauss-point level) orthogonal coordinate system is defined for material properties. TexGen defines material orientation for each element. In this manner, the mechanical constitutive behaviour of yarns is fully defined at

each element. Hence all stresses, strains and state variables are defined with respect to local material axes and these axes rotate with material deformation (LBL11). Yarn properties are assigned to each yarn as follows: Youngs modulus, shear modulus and Poisson's ratio.

2.4.5 Mesh generation

The geometrical woven fabric composite unit cell modelled by TexGen package is shown in Fig. 2.8.

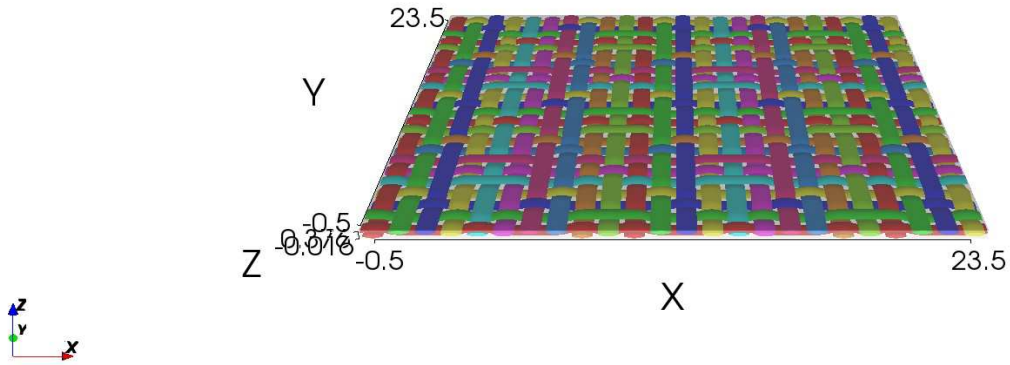

(a) Overall dimensions of unit cell created in TexGen packages.

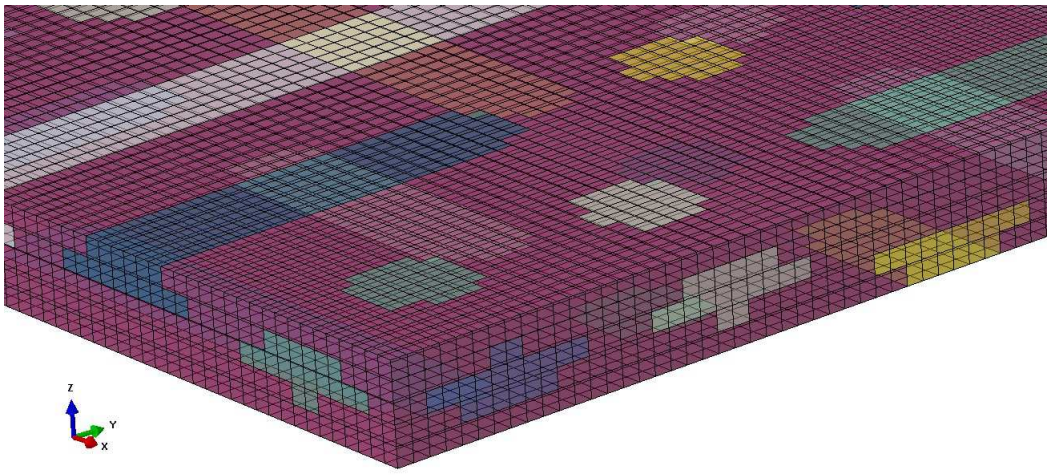

(b) A sample FE-discretization of unit cell in TexGen.

Figure 2.8: Unit cell designation in TexGen.

The unit cell undergone a discretization process before being imported to an input files. A simple mesh generator has been implemented in TexGen to discretize yarns. In TexGen, the unit cells are meshed with two steps. The first mesh step is to mesh the cross sections in two dimensions, ensuring that the cross-section meshes are compatible. It is then simply necessary to link adjacent cross-section meshes together to form 3D elements. The four corners of the grid contain triangular elements to avoid highly distorted elements, which are undesirable in numerical simulations. Secondly, a number of equi-spaced meshed cross

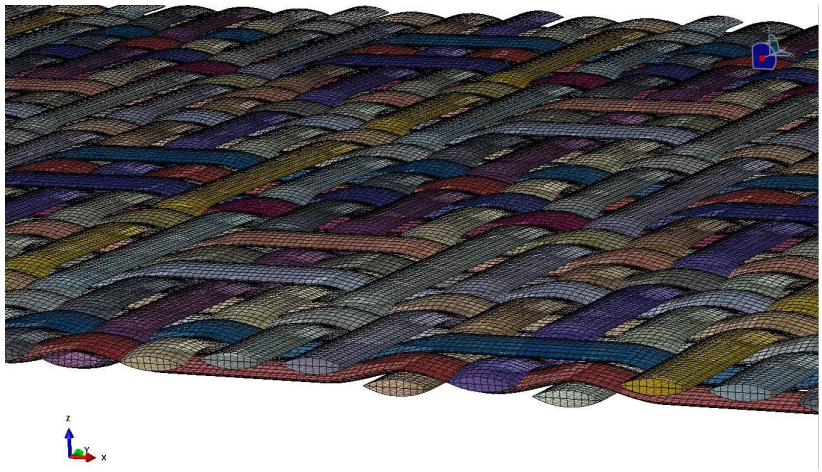

Figure 2.9: Meshed yarn in TexGen using continuum three-dimensional eight-node brick elements (hexahedral element) for the yarn main body and continuum three-dimensional six-node tetrahedral elements (wedge element) for the edges.

sections are created along the length of the yarn path and the number of columns and rows are the same for each cross section along the length of the yarn. Consecutive cross sections are linked together to form 3D volume elements. In order to link two cross sections together, the meshes must be compatible, that is, each element from one cross section must map to an element on the other cross section. In this way, pairs of triangles can be linked together to form six-noded wedge elements and pairs of quadrilaterals can be linked together to form eight-noded hexahedral elements, as shown in Fig. 2.9. TexGen ensures that the degrees of freedom of each node lying on the boundary of the unit cell are linked to the degrees of freedom of a corresponding node on the opposite side of the unit cell. In essence these pairs of nodes represent identical positions in the unit cell and as such cannot have different displacements or slope. This is important for the application of periodic boundary conditions to the unit cell in order to represent the repeating nature of fabrics and correspondingly to the extraction of unit cell material properties (She07).

2.4.6 Contact algorithm

Creating the contacts between yarns are the major challenge in textile structures modelling. Corresponds to this, the explicit finite element system is always preferable over an implicit one. Contact algorithms in an implicit system are extremely complicated and memory intensive compared to those of an explicit system. For the complicated contacts involved with textile fabrics, it is impractical to use implicit contact algorithms as these tend not to behave in a stable manner. As a further complication, the repeating nature of the problem requires special contact code to deal with repeated unit cells (She07). TexGen creates an upper and lower surface for each yarn and defines contacts between the lower and upper surface of two yarns when they are directly or potentially in touch with each other using master and slave contact techniques for finite element analysis.

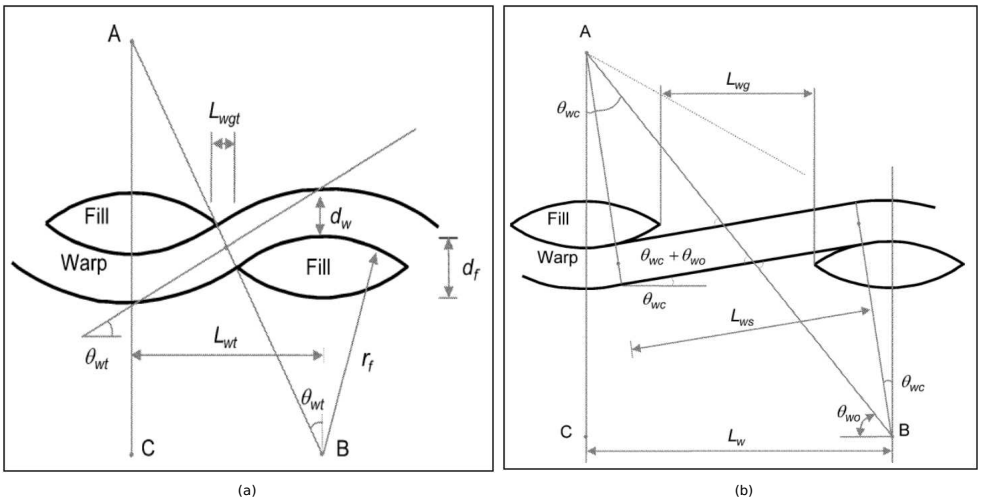

Figure 2.10: Yarn configuration in geometric model (a) for tight configuration (L_{wgt} = gap length; L_{wt} = yarn-to-yarn distance; d_w,d_f = thickness of warp and weft yarns respectively; r_f = the radius of warp yarn undulation on a weft yarn; θ_{wt} = crimp angle of warp yarn) (b) for general configuration (L_{wg} = gap length; L_w = yarn-to-yarn distance; L_{ws}=length of straight part of warp yarn; θ_{wc} = crimp angle). Reproduced by (LBH03).

2.4.7 General and tight configuration

Woven fabric composites can have a tight or loose configuration depending on the flexibility of the fibres, the yarn-to-yarn distance and the yarn cross-sectional shape. Theoretically, maximum fibre volume fraction can be achieved under a tight configuration when the yarn-to-yarn distance is minimum. The crimp angle, θ_{wt} for the warp yarn is calculated via Eq. (2.16)

$$\theta_{wt} = \cos^{-1}\left(\frac{2r_f + d_w - d_f}{2r_f + d_w}\right). \tag{2.16}$$

The gaps still exist even in a tight configuration, see Fig. 2.10(a). Thus, the expression of tight configuration gaps between the warp and weft direction can be defined by Eq. (2.17)

$$L_{wgt} = (2r_f + d_w)\sin\theta_{wt} - AR_f d_f. \tag{2.17}$$

The yarn crimp angle varies with respect to the yarn thickness, yarn-to-yarn distance and aspect ratio of a yarn section. The space between yarns is also depends on the number of warp and weft in the unit length and width. Fig. 2.10(b) depicts a straight portion of yarn can exist, which leaves larger open space in the fabric unit cells. The yarn-to-yarn distance of general configuration, L_w is expressed in terms of yarn width and gap length of general configuration, L_{wg} in Eq. (2.18)

$$L_w = AR_f d_f + L_{wg}, \tag{2.18}$$

where L_{wg} is a measured parameter in this study. The value of L_{wg} should be greater than yarn spacing in the tight configuration. The equations provided under this subsection is attributing to Lee *et al.* (LBH03).

2.4.8 Fibre volume fraction

The fibre volume of a woven fabric composite may be determined by chemical matrix digestion, in which the matrix is dissolved and the fibres weighed and calculated from substituent weights and densities or a photomicrography technique may be used in which the number of fibres in a given area of a polished cross section is counted and the volume fraction determined as the area fraction of each constituent. Chua (Chu11) expounded that the number of fibres is determined by the volume of a yarn, i.e a higher yarn volume represents higher number of fibres and vice versa. This gives a major impact on the yarn packing factor which depends on the layout of circular fibres within the yarn cross-section. In this study, the yarn packing factor has been taken as the fibre volume fraction in a yarn section and a hexagonal packing factor ($\beta = 0.9069$) has been chosen for both yarns. The cross-sectional area and yarn packing factor are assumed to be constant throughout the fabric. Knowing the respective values of yarn length (L_i) and yarn cross-sectional area (A_i), the volume (V_i) of each yarn can be calculated as Eq. (2.19) which referring to Ansar *et al.* (AXC11)

$$V_i = L_i A_i \quad (i = \text{warp(w)}, \text{weft(f)}). \tag{2.19}$$

Thus, the total volume of fibre in the unit cell can be expressed by

$$V = \Sigma V_i \quad (i = \text{warp(w)}, \text{weft(f)}). \tag{2.20}$$

Overall fibre volume fraction (V_f) and thickness, (H) are important preform parameters for both manufacturers and designers. These preform parameters are provided at the unit cell level. The dimensions of the unit cells are illustrated in Fig. 2.8 and the volume of the unit cell, V_u is calculated using the following equation

$$V_u = L_x \times L_y \times H_u, \tag{2.21}$$

where L_x, L_y = length of unit cell in x and y directions and H = thickness of the unit cell. Finally, the fibre volume fraction in yarn section,v_f, and total fibre volume fraction, V_f, of multiple woven pattern composites, a useful parameters for both manufacturers and designers V_f are obtained by

$$\begin{aligned} V_f &= V/V_u \\ v_f &= V_f \times \beta_i, \end{aligned} \tag{2.22}$$

where β_i = yarn packing factor.

2.4.9 Yarn Repeats and Domain

The patterns in unit cells are repeated by assigning the repeat vectors in the Modeller tree. The domain is specified after yarn repeats have been specified, so that the unit cell can be

constrained to a specific region. In most cases the domain will correspond to the unit cell of the textile but maintaining a distinction between the two gives added flexibility. TexGen allows the users to specify the domain either a bounding box (requires the minimum and maximum x, y, z values for bounding box) or planes (requires number of planes) domains.

The domain is specified by planes where the space on the negative side of the plane is considered to be outside of the domain. Each plane is defined as: $Ax + By + Cz + D = 0$. The vector (A, B, C) represents the unit normal to the plane, and D represents the distance from the plane to the origin. In order to specify an axis aligned bounding box with minimum of $(x1, y1, z1)$ and maximum of $(x2, y2, z2)$, six planes P need to be defined.

2.4.10 Save and Export Data

Patterns in unit cells are saved in TexGen $.tg3$ format and exported in voxel mesh format as an ABAQUS file which includes the periodic boundary conditions. All ABAQUS exports include additional $.ori$ and $.eld$ files containing element orientation, fibre volume fraction and yarn information.

2.5 Numerical computational of woven fabric composite unit cells

2.5.1 Displacement and periodic boundary conditions for unit cells

The displacement boundary conditions for the unit cell have been defined following the procedures asserted by Li and Wongsto (LW04) in Section 4.2 of their study. They have treated the unit cells by using translational symmetry transformation alone neglecting the involvement of reflectional or rotational symmetry transformations. Stresses, strains and displacements are transformed as the images of one cell to any other cells in the unit cell under translational symmetry transformations. This leads to a relation between the macroscopic strains and the relative displacements at a point Q in the unit cell to those at Q' in another unit cell as expressed in Eq. (2.23)

$$\begin{aligned} u\text{'} - u &= \left(x' - x\right)\epsilon_x^0 + \left(y' - y\right)\gamma_{xy}^0 + \left(z' - z\right)\gamma_{xz}^0 \\ v\text{'} - v &= \left(y' - y\right)\epsilon_y^0 + \left(z' - z\right)\gamma_{yz}^0 \\ w\text{'} - w &= \left(z' - z\right)\epsilon_z^0, \end{aligned} \tag{2.23}$$

where x, y and z are the coordinates of Q, u, v, and w are the displacements at this point and ϵ_x^0, ϵ_y^0, ϵ_z^0, γ_{yz}^0, γ_{xz}^0, γ_{xy}^0 are the macroscopic strains. Quantities with a prime are associated with point Q' which denote the image of point Q. Three rigid body translations are eliminated by constrained the displacements at any arbitrary point which given as in Eq. (2.24)

$$u = v = w = 0. \tag{2.24}$$

The rotations of the coordinate axes are constrained. The macroscopic strains ϵ_y^0, ϵ_z^0, γ_{yz}^0, γ_{xz}^0, γ_{xy}^0 in Eq. (2.23) are treated as six extra degrees of freedom through which loads

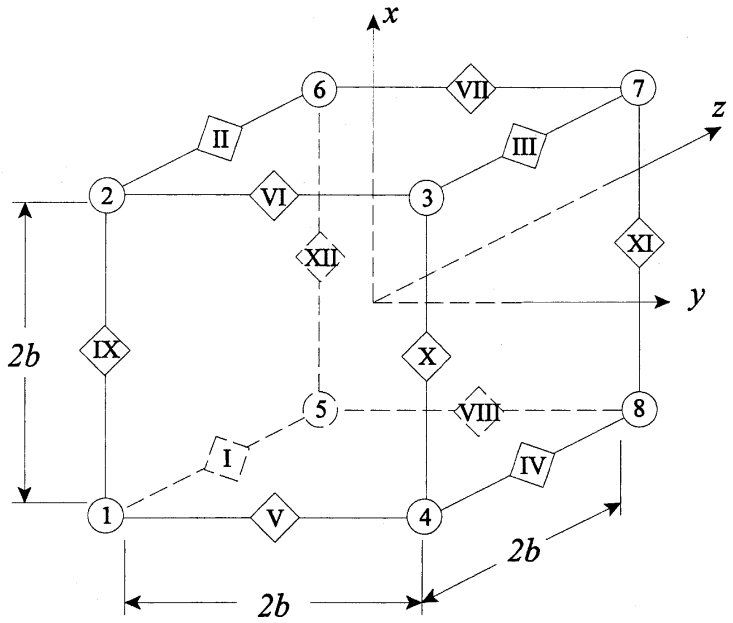

Figure 2.11: Faces, edges and vertices involved in the unit cell for the displacements and boundary conditions. Reproduced by (LW04).

to the unit cell can be prescribed as Eq. (2.25)

$$\frac{\partial w}{\partial x} = \frac{\partial w}{\partial y} = \frac{\partial w}{\partial z} = 0 \qquad \text{at } x = y = z = 0. \tag{2.25}$$

The coordinates between the two points, Q'(x', y', z') and Q(x, y, z) under a translational symmetry transformation are related to each other as Eq. (2.26), see Fig. 2.11 for notations

$$\left(x', y', z'\right) = \left(x + 2ib, y + 2jb, z + 2kb\right), \tag{2.26}$$

where i, j and k denotes the translational symmetry transformation defined in Eq. (2.27).

The two faces in each of the three pairs of faces of the unit cell as shown in Fig. 2.11 are transformed from one to another by

$$\begin{aligned} x = \pm b \ \ (+ \text{ for face A and } - \text{ for B}) : \\ (i = 1, j = 0, k = 0), \\ y = \pm b \ \ (+ \text{ for face C and } - \text{ for D}) : \\ (i = 0, j = 1, k = 0), \\ z = \pm b \ \ (+ \text{ for face E and } - \text{ for F}) : \\ (i = 0, j = 0, k = 1). \end{aligned} \tag{2.27}$$

The three equations in 2.27 are the displacement boundary conditions for 4 pairs of faces of the unit cell. The complete list of pairs are given by Eq. (2.28)

$$\begin{aligned}
(u\mid_{x=b} - u\mid_{x=-b})\mid_{y,z} &= 2b\epsilon_x^0 \\
(v\mid_{x=b} - v\mid_{x=-b})\mid_{y,z} &= 0 \\
(w\mid_{x=b} - w\mid_{x=-b})\mid_{y,z} &= 0 \\
\text{abbreviated as } U_A - U_B &= F_{AB} \\
(u\mid_{y=b} - u\mid_{y=-b})\mid_{x,z} &= 2b\gamma_{xy}^0 \\
(v\mid_{y=b} - v\mid_{y=-b})\mid_{x,z} &= 2b\epsilon_y^0 \\
(w\mid_{y=b} - w\mid_{y=-b})\mid_{x,z} &= 0 \\
\text{abbreviated as } U_C - U_D &= F_{CD} \\
(u\mid_{z=b} - u\mid_{z=-b})\mid_{x,y} &= 2b\gamma_{xz}^0 \\
(v\mid_{z=b} - v\mid_{z=-b})\mid_{x,y} &= 2b\gamma_{yz}^0 \\
(w\mid_{z=b} - w\mid_{z=-b})\mid_{x,y} &= 2b\epsilon_z^0 \\
\text{abbreviated as } U_E - U_F &= F_{EF}.
\end{aligned} \tag{2.28}$$

For the edges parallel to the x-axis, y- and z-axis, respectively, the displacement at these edges can be obtained, i.e for x-axis, when edge I is considered as the images of eges II, III and IV under symmetry transformations ($i = 1, j = 0, k = 0$), ($i = 1, j = 1, k = 0$) and ($i = 0, j = 1, k = 0$), respectively, three sets of relations can be obtained as in Eq. (2.29), see Fig. 2.11

$$\begin{aligned}
U_{II} - U_I &= F_{AB} \\
U_{III} - U_I &= F_{AB} + F_{CD} \\
U_{IV} - U_I &= F_{CD},
\end{aligned} \tag{2.29}$$

where F_{AB} and etc. are defined in Eq. (2.28) yielding to Eq. (2.30)

$$\begin{aligned}
U_{VI} - U_V &= F_{AB} \\
U_{VII} - U_V &= F_{AB} + F_{EF} \\
U_{VIII} - U_V &= F_{EF} \\
U_X - U_{IX} &= F_{CD} \\
U_{XI} - U_{IX} &= F_{CD} + F_{EF} \\
U_{XII} - U_{IX} &= F_{EF}.
\end{aligned} \tag{2.30}$$

The vertices are numbered with circles as Eq. (2.31)

$$\begin{aligned} U_2 - U_1 &= F_{AB} \\ U_3 - U_1 &= F_{AB} + F_{CD} \\ U_4 - U_1 &= F_{CD} \\ U_5 - U_1 &= F_{EF} \\ U_6 - U_1 &= F_{AB} + F_{EF} \\ U_7 - U_1 &= F_{AB} + F_{CD} + F_{EF} \\ U_8 - U_1 &= F_{CD} + F_{EF}. \end{aligned} \tag{2.31}$$

The traction boundary conditions are defined in terms of stresses in a similar way by Eq. (2.32)

$$\begin{aligned} (\sigma_x \mid_{x=b} - \sigma_x \mid_{x=-b}) \mid_{y,z} &= 0 \\ (\tau_{xy} \mid_{x=b} - \tau_{xy} \mid_{x=-b}) \mid_{y,z} &= 0 \\ (\tau_{xz} \mid_{x=b} - \tau_{xz} \mid_{x=-b}) \mid_{y,z} &= 0 \\ (\tau_{xy} \mid_{y=b} - \tau_{xy} \mid_{y=-b}) \mid_{x,z} &= 0 \\ (\sigma_y \mid_{y=b} - \sigma_y \mid_{y=-b}) \mid_{x,z} &= 0 \\ (\tau_{yz} \mid_{y=b} - \tau_{yz} \mid_{y=-b}) \mid_{x,z} &= 0 \\ (\tau_{xz} \mid_{z=b} - \tau_{xz} \mid_{z=-b}) \mid_{x,y} &= 0 \\ (\tau_{yz} \mid_{z=b} - \tau_{yz} \mid_{z=-b}) \mid_{x,y} &= 0 \\ (\sigma_z \mid_{z=b} - \sigma_z \mid_{z=-b}) \mid_{x,y} &= 0. \end{aligned} \tag{2.32}$$

Periodic boundary conditions are applied in the form of equations for all the unit cells that can be implemented using 'Equation' option in ABAQUS. It is developed based on voxel-based meshing using 8 node 3D linear brick elements.

2.5.2 Computational of elastic properties

The work done by the force can be expressed by Eq. (2.33)

$$W = \frac{1}{2} F_x \epsilon_x^0. \tag{2.33}$$

The strain energy can be written as in Eq. (2.34)

$$E = \frac{1}{2} \int_V \sigma_x^0 \epsilon_x^0 dV = \frac{1}{2} V \sigma_x^0 \epsilon_x^0, \tag{2.34}$$

where V is the volume of the unit cell. Equating W to E yields a relationship between the concentrated forces and the macroscopic stress applied as in Eq. (2.35)

$$\begin{aligned} \sigma_x^0 = F_x/V, \quad \sigma_y^0 = F_y/V, \quad \sigma_z^0 = F_z/V, \\ \tau_{yz}^0 = F_{yz}/V, \quad \tau_{zx}^0 = F_{zx}/V, \quad \tau_{xy}^0 = F_{xy}/V. \end{aligned} \tag{2.35}$$

Eventually, the elastic properties are then obtained by Eq. (2.36)

$$
\begin{aligned}
E_x^0 = \sigma_x^0/\epsilon_x^0 = F_x/V\epsilon_x^0 \text{ when } F_y = F_z = F_{yz} = F_{zx} = F_{xy} = 0 \\
\nu_{xy}^0 = -\epsilon_y^0/\epsilon_x^0 \text{ when } F_y = F_z = F_{yz} = F_{zx} = F_{xy} = 0 \\
\nu_{xz}^0 = -\epsilon_z^0/\epsilon_x^0 \text{ when } F_y = F_z = F_{yz} = F_{zx} = F_{xy} = 0 \\
E_y^0 = \sigma_y^0/\epsilon_y^0 = F_y/V\epsilon_y^0 \text{ when } F_x = F_z = F_{yz} = F_{zx} = F_{xy} = 0 \\
\nu_{yx}^0 = -\epsilon_x^0/\epsilon_y^0 \text{ when } F_x = F_z = F_{yz} = F_{zx} = F_{xy} = 0 \\
\nu_{yz}^0 = -\epsilon_z^0/\epsilon_y^0 \text{ when } F_x = F_z = F_{yz} = F_{zx} = F_{xy} = 0 \\
E_z^0 = \sigma_z^0/\epsilon_z^0 = F_z/V\epsilon_z^0 \text{ when } F_x = F_y = F_{yz} = F_{zx} = F_{xy} = 0 \\
\nu_{zx}^0 = -\epsilon_x^0/\epsilon_z^0 \text{ when } F_x = F_y = F_{yz} = F_{zx} = F_{xy} = 0 \\
\nu_{zy}^0 = -\epsilon_y^0/\epsilon_z^0 \text{ when } F_x = F_y = F_{yz} = F_{zx} = F_{xy} = 0 \\
G_{yz}^0 = \tau_{yz}^0/\gamma_{yz}^0 = F_{yz}/V\gamma_{yz}^0 \text{ when } F_x = F_y = F_z = F_{zx} = F_{xy} = 0 \\
G_{zx}^0 = \tau_{zx}^0/\gamma_{zx}^0 = F_{zx}/V\gamma_{zx}^0 \text{ when } F_x = F_y = F_z = F_{yz} = F_{xy} = 0 \\
G_{xy}^0 = \tau_{xy}^0/\gamma_{xy}^0 = F_{xy}/V\gamma_{xy}^0 \text{ when } F_x = F_y = F_z = F_{yz} = F_{zx} = 0.
\end{aligned} \tag{2.36}
$$

More details can be found in (LW04).

2.5.3 Extraction of material properties using voxel-based meshing and ABAQUS

Voxel-based meshing creates an ABAQUS input file by producing a mesh of regularly shaped hexahedral voxel elements for a unit cell produced by TexGen. The periodic boundary condition equations are generated as aforementioned section. After the ABAQUS simulation has been run, the material properties are extracted by running a script, provided in the TexGen download, which interrogates the ABAQUS $.odb$ file. The procedure is described as follows (LB11);

i. **Create Textile** - Once the unit cell geometries are created in TexGen, the unit cell geometries containing the yarns and solid domain (matrix) volumes are exported into ABAQUS input files for further analysis.

ii. **Create ABAQUS voxel file** - The ABAQUS files for the voxel mesh are created in a script. The number of voxels in the x, y and z directions are specified and the element type, boundary conditions and geometries of yarn and matrix are exported. Three files are generated: (a) the $.inp$ file containing the nodes, elements, boundary conditions, load cases and material definitions; (b) the $.eld$ file containing the element data (yarn index, location, volume fraction and distance from surface of yarn) and (c) the $.ori$ file containing the yarn orientation vectors. The yarn data for the elements is calculated at the centre point of each element. The element is assigned to either the appropriate yarn or matrix based on this centre point. It may be necessary to perform a sensitivity study in order to assess the best number of voxels for the particular simulation.

iii. **Run ABAQUS simulation** - The ABAQUS simulation is then run from the ABAQUS Command Line. The $.inp$ is loaded into ABAQUS CAE as it uses equations in the

boundary conditions which match multiple node sets together. The orientation file is read in correctly when run from the command line. The job is ran and produced a number of files including a *.odb* file. If there are errors in the job analysis, then the *.dat* file should give some indication of the cause.

iv. **Extract material properties from** *.odb* **file** - The material properties are extracted using the python script ($dataHandling.py$, $dataHandlingInPlane.py$ and $effective-MatPropRVE.py$) downloaded in the TexGen package.

2.6 Evolutionary algorithm technique

Evolutionary algorithms (EA) are stochastic search methods that mimic natural biological evolution. According to Yu and Gen (YG10), EAs have three main characteristics:

a. **Population-based**: An EA employs a population of candidate solutions. The optimization process is based on parallelism, which is a basic principle of evolutionary processes, and is in particular interesting for parallel computing.

b. **Fitness-oriented**: A candidate solution in the population (called individual) is represented as gene, and is evaluated by a fitness function. The foundation of the optimization process is based on the survival of the fittest solutions.

c. **Variation-driven**: Individuals will undergo a number of variation operations to mimic genetic gene changes, which is fundamental to searching in the solution space.

The most important components in evolutionary algorithms are:

i. **Individuals / Representation**

ii. **Fitness function / objective function**

iii. **Population**

iv. **Parent selection mechanism**

v. **Variation operators**

vi. **Survivor selection mechanism**

The algorithm in Fig. 2.12 illustrates the evolutionary algorithm in pseudo-code that is adopted in our experimental study. For a detailed introduction to evolutionary computation we refer to Eiben and Smith (ES03), Beyer and Schwefel (BS02).

The fitness evaluation of a candidate solution is based on a simulation of a given woven fabric composite. It is implemented in the software TexGen, which is part of ABAQUS, forming a geometrical and meshing preprocessor in voxel meshing basis. Fig. 2.13 shows the structure of the optimization flow, where A, B, and C are sets of populations, s stands for the current generation of the evolutionary process, and x_i, $i = 1, \ldots,$ is a single individual from the population.

```
1   Start
2     initialize solutions x_i of population P
3     evaluate solutions x_i of P
4     Repeat
5       For i = 1 To λ
6         select ρ parents from P
7         create x_i by recombination
8         mutate x_i
9         evaluate x_i → f(x_i)
10        add x_i to P'
11      Next
12      select μ parents P from P'
13    Until termination condition
14  End
```

Figure 2.12: Pseudo-code of a general evolutionary algorithm ($\mathcal{P}$ = initial population; $\mathcal{P}'$ = new population).

The goal of the evolutionary optimization process is to find a set of optimal weave pattern parameters given a certain norm. Fig. 2.13 explains how the initial population is produced. For this sake, a number of patterns x_i in population $A(0)$ are randomly initialized. The fitness function $\Phi(x_i)$ (a weave pattern simulation run per individual) is evaluated for each pattern, $x_i \in A(0)$. If the termination condition has not been reached the creation of a new generation starts. Then, the evolutionary process begins: The patterns are sorted with respect to their fitness, and the best patterns x_i are selected from the population $A(s)$ as population of parents $B(s)$ for the following generation. We employ a method called Fitness Proportional Selection that selects individual x_i with probability P_i that is proportional to its fitness $\Phi(i)$ for the following generation. Parents in $B(s)$ are recombined to form the population $C(s)$. The offsprings in $C(s)$ are either imperfect clones of the parents or a melange of multiple parents and inherit some attributes of the parents. Mutation operators are also implemented and include swap and insert mutations. The fitness of the offspring is then computed. The offsprings are inserted into the population replacing the parents, producing a new generation, $A(s+1) = C(s)$. This cycle is repeated until the maximization is met. In the case of woven fabric composites, the algorithm stops, if the composite pattern maximizes its elastic properties, i.e., to an upper bound on the total number of fitness evaluations, E and G conducted by EA.

2.6.1 Fitness function evaluation

A weighted sum fitness function is utilized in this study in order to maximize an equally weighted average of the elastic properties of a carbon/polyester composite. The elastic properties of carbon fibre and polyester are shown in Table 2.2. The design problem is

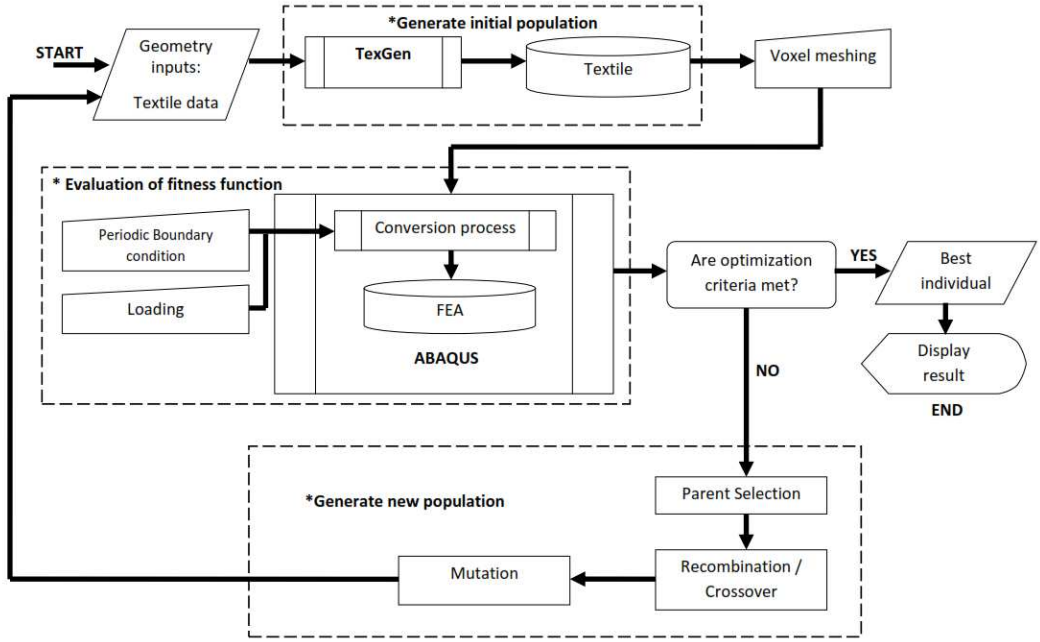

Figure 2.13: The scheme of optimization flow with TexGen-ABAQUS integration of woven fabric composite unit cells

represented by the following optimization problem, see Eq. (2.37)

$$\textbf{max } \left(0.333 \cdot E_x + 0.333 \cdot E_y + 0.333 \cdot G_{xy}\right), \tag{2.37}$$

subject to multiple weave patterns preform.

2.6.2 Parent Selection

The selection operator selects the offspring population for the following generation. The first step is fitness assignment as shown in Fig. 2.15. Each pattern in the population receives a reproduction probability depending on their own objective value, and the objective value of all other individuals in the selection pool. Fitness proportional selection, also known as Roulette-wheel selection has been chosen for this purpose. The advantage of this method is that it gives every member of the population a chance to become a parent (i.e., a non-extinctive breeding procedure) as defined by Soremekun (Gra97). Before the process of parent selection begins, all pattern populations must be ranked from the best to the worst according to the value of each pattern's fitness value. A Roulette wheel is implemented where the i^{th} ranked pattern in the population is given an interval $[\phi_{i-1}, \phi_i]$, whose size depends on the population size, P, and its rank, i, in the population as expressed in Eq. (2.38)

$$\phi_i = \phi_{i-1} + \frac{2(P-i+1)}{P(P+1)}, \tag{2.38}$$

where ϕ_o = 0, and i = 1,...,P. Conceptually, a proportion of the wheel is assigned to each of the possible selections based on their fitness value. This can be achieved by dividing the fitness of a selection by the total fitness of all the selections, thereby normalizing them to 1. Then, a random selection is made similar to how the roulette wheel is rotated. For example, if there are 51 fitness values in a population, the Roulette-wheel is divided into 51 pieces with the best fitness value taking 2% of the wheel, the second best taking 2% and the poorest taking 1%, see the algorithm as described in Fig. 2.14 and Fig. 2.16 for Roulette-wheel distribution corresponds to Fig. 2.15.

```
1   Start
2     initialize λ = random number; where 0 ≤ λ < 1
3     sum:=0;
4     Repeat
5       For i = 1 To λ
6         evaluate sum:= sum + P(choice=i);
7         if λ < sum
8       return i = 1
9   End
```

Figure 2.14: Pseudo code of a Roulette-wheel selection

2.6 Evolutionary algorithm technique

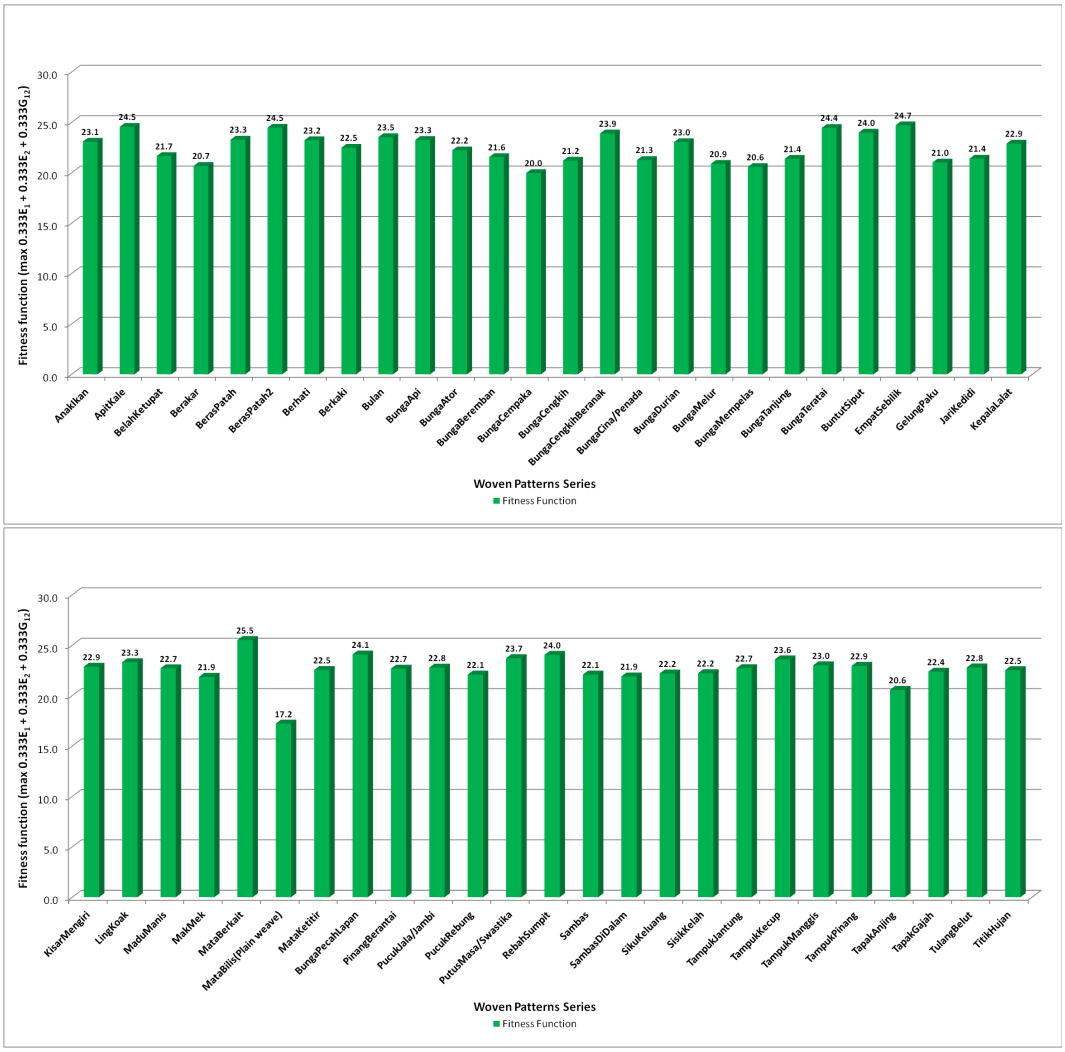

Figure 2.15: Fitness values of initial generation

2. OPTIMIZATION OF ELASTIC PROPERTIES AND WEAVING PATTERNS OF WOVEN COMPOSITES

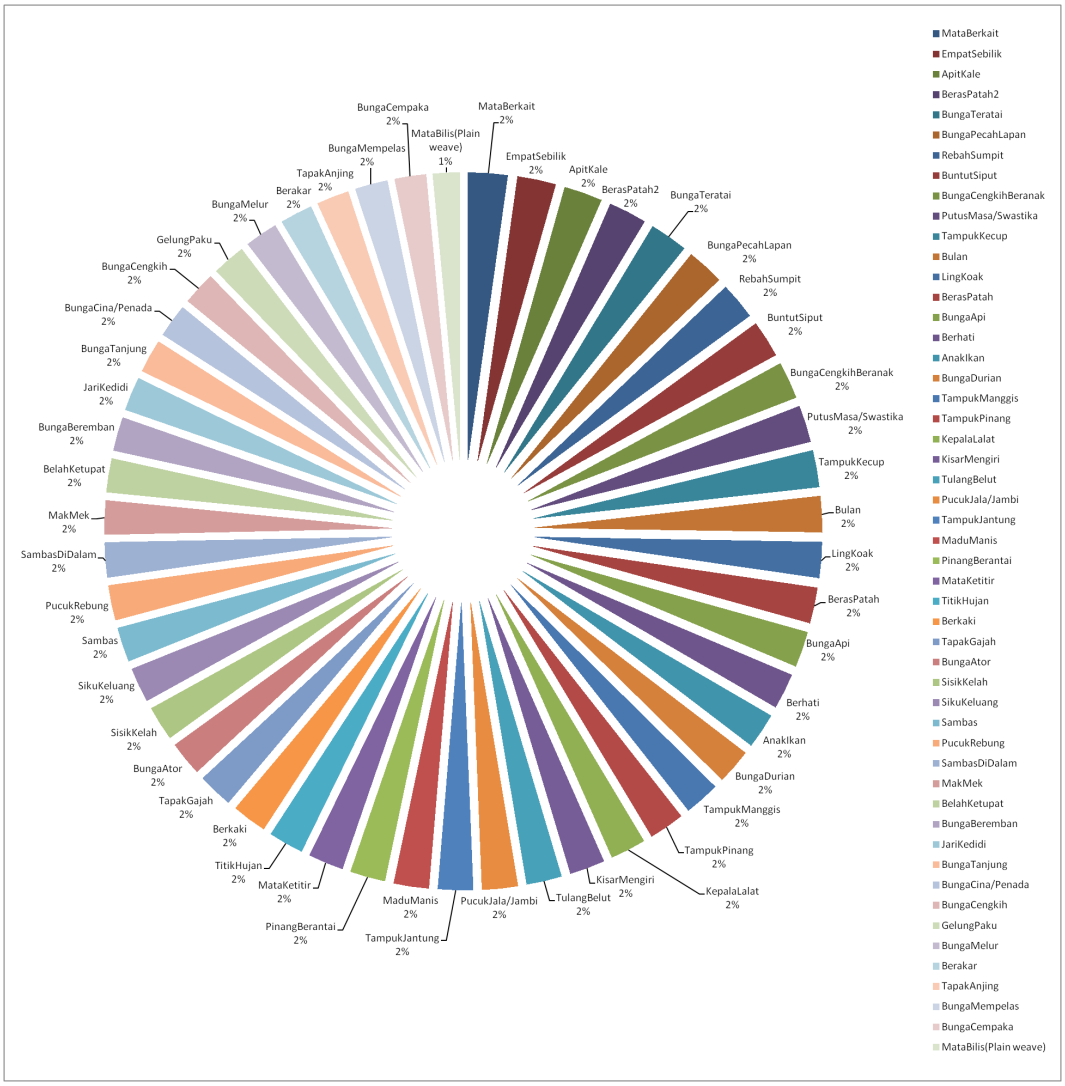

Figure 2.16: Roulette wheel distribution for initial generation

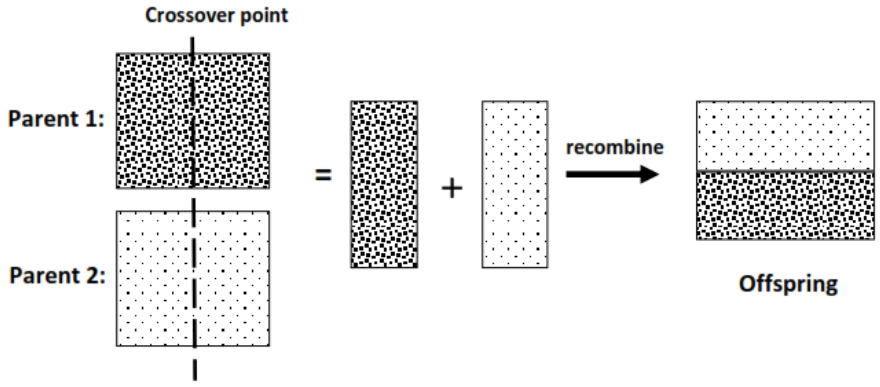

Figure 2.17: One-point crossover scheme

2.6.3 Recombination/Crossover

Recombination, also known as crossover, is a process in producing new individuals by combining the characteristics of two or more solutions. Offsprings are created by combining a portion of each parent's genetic string in an operation called one-point crossover. One-point crossover is based on choosing the random point, r, in the range $[1, l-1]$ (with l the length of the encoding), then splitting both parents at this point and creating the two children by exchanging the substrings. The random crossover point is restricted to fall in unequal region string on both parents to ensure that the offspring pattern is unique, see Fig. 2.17. Thus, the integer ceiling value of this pattern determines the crossover point. The left piece from parent 1 and the right piece from parent 2 are combined to form an offspring pattern. The crossover process is repeated as many times as necessary to create a new population of patterns.

2.6.4 Mutation

For permutation representations, it is relatively easy to perform mutation operators. Mutation generates randomized changes to individuals as stated by Eiben and Smith (ES03) and the purpose of mutation is preserving and introducing diversity. Usually, offsprings are mutated after being created by recombination. Insert and swap mutation are done simultaneously on created offsprings. Conceptually, insert mutation selects the genes at random and inserts them in a random position. When a pattern is added, a uniform random number is chosen to determine the position of the pattern. Whilst, swap mutation works by picking the two positions of genes in the string and swapping their genes. Furthermore, when genes are switched in the swap operator, the both patterns are swapped randomly with a uniform random number of positions. Fig. 2.18 depicts the implementation of swap mutation, and the scheme of insert mutation.

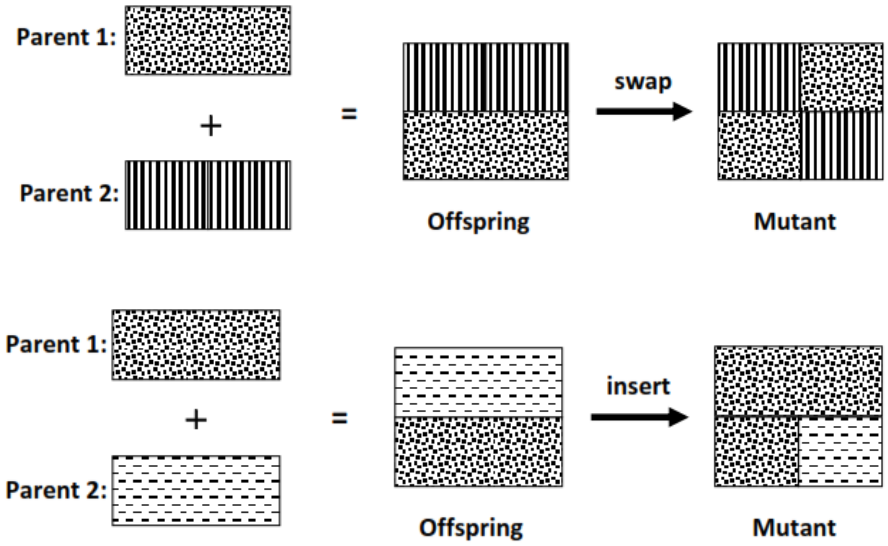

Figure 2.18: Swap and insert mutation scheme

2.7 Numerical results

The geometric input data of unit cells designation and material properties of the fibre and matrix are summarized in Table 2.2. This data is utilized in the calculation of the mechanical properties of the woven fabric composites from the micro-mechanics expressions. The data is obtained from the literature and has been applied to all the samples accordingly.

Table 2.2: Geometric input of unit cells designation and mechanical properties of constituent models

Geometric input	Mechanical input(LB11, PT07)	
	Carbon fibre	Polyester (Matrix)
$d_w = d_f = 0.18$	E_x = 200 GPa	
	$E_y = E_z$ = 10 GPa	E = 2.50 GPa
$AR_w = AR_f = 4.44$	G_{xy} = 5 GPa	ν = 0.35
	$G_{yz} = G_{xz}$ = 5 GPa	
$\beta_w = \beta_f = 0.9069$	ν_{xy} = 0.3	
	$\nu_{xz} = \nu_{yz}$ = 0.4	

2.7.1 Woven Fabric Composite Optimization

The selection of weave patterns is made corresponding to the best performance of elastic properties as stated in Section 2.6. The best weave is optimized with respect to the following input parameters: gap length, shape of yarn section, yarn thickness and the bundle size as

well as the constituent materials. The calculations of engineering constants are based on the equations described in Section 2.5.2. We first study the influence of the mesh refinement on the macroscopic material properties. There is a clear difference between the mesh 1(coarse) and other four meshes, however mesh 3 and 4 show very similar results, see Fig. 2.19. It can be concluded that the mesh 3 is the best number of voxels due to the convergence of line between mesh 2 and 4, correspondingly sufficient to provide the accurate results.

Table 2.3: Mesh statistics of woven fabric RVE

Mesh	**Number of nodes**	**Number of elements**	**DOF**	**Relative CPU time** (sec)
1 $(coarse)$	204310	151875	612918	114.10
2	453011	360000	1359021	421.97
3	689532	571220	2068584	1160.90
4	848262	703125	2544774	1585.60
5 $(fine)$	1423813	1215000	4271427	3785.10

It is noted that the chosen weaves are based on aesthetics, complexity of curves and the weight of the fabric as well as the weave tightness or connectivity ensuring the fabric strength. The weave tightness is defined by the weave pattern and the ability of yarns to move freely, it characterizes the weave pattern, providing an indication on fabric properties as a function of weave type. In order to determine the weave tightness, Eq. (2.39) is applied which is similarly to the practice by (Lon05)

$$Tightness = \frac{N_{liaision}}{2N_{Wa}N_{We}}, \tag{2.39}$$

in which $N_{liaison}$ is the number of transitions of warp/weft yarns from one side of the fabric to another and the denominator is multiplied by 2 so as to have a value of 1 for plain weaves. The N_{Wa} and N_{We} are the number of warp and weft respectively. Besides, it can also be calculated by using Eq. (2.40)

$$Tightness = \frac{2}{f_{Wa} + f_{We}}, \tag{2.40}$$

where f_{wa} and f_{we} are the warp float and weft float respectively.

Lower weave tightness values indicate less fixation of the yarns in a fabric and less fabric stability. A low tightness also allows to accommodate a better fabric drapability, whilst, higher tightness values create higher crimp which is known to deteriorate the fabric strength. Plain weaves are the tightest weaves. Twill weaves show a similar weave tightness. The best woven patterns should be able to cater for complex curves and bends and fray moderately at ends due to the tightness values. The best woven patterns can be summarized by tightness and elastic properties as shown in Fig. 2.20 and Tab. 2.4, respectively. This study shows that the fray tendency and skewness of woven fabrics depends upon the behaviour of the floats (which is related to the factor of weave). It is also proven that by increasing the

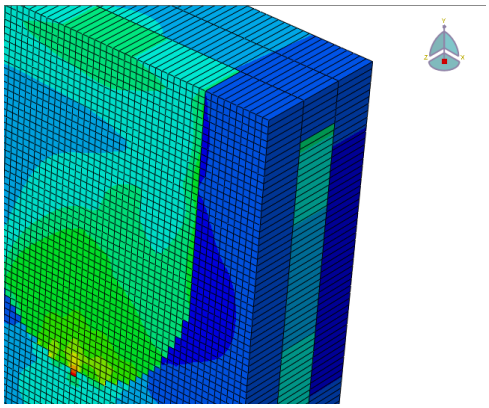

(a) Mesh 1 (Coarse)

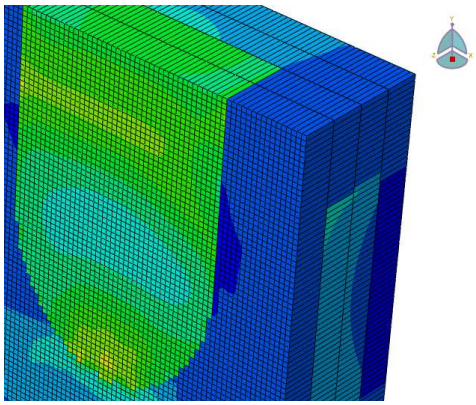

(b) Mesh 2

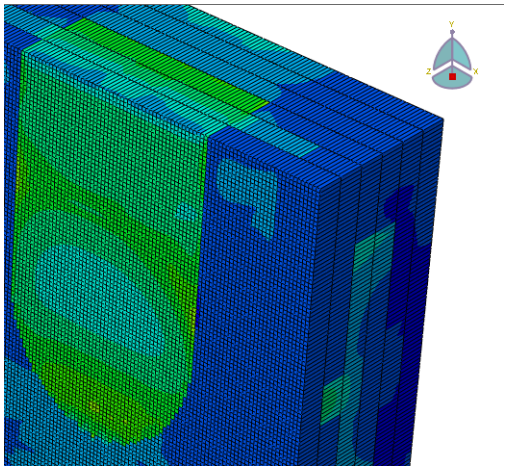

(c) Mesh 3

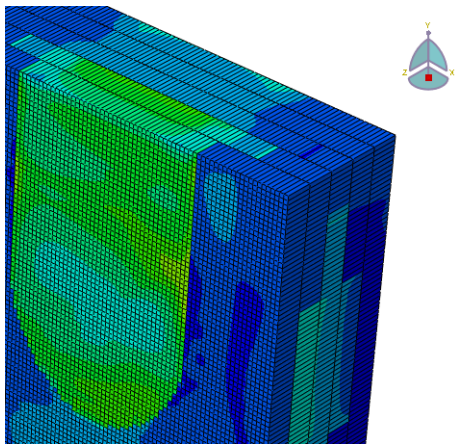

(d) Mesh 4

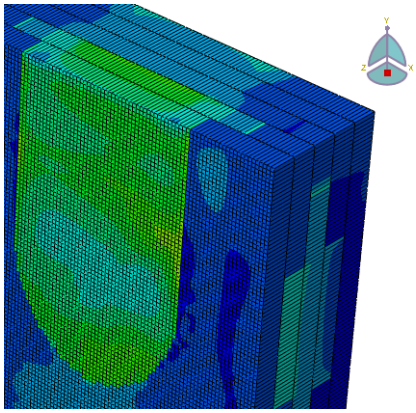

(e) Mesh 5 (fine)

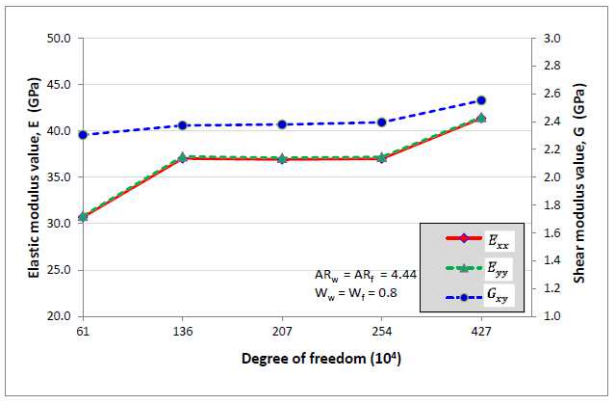

(f) Relationship graph between Young's moduli and DOF

Figure 2.19: Mesh sensitivity on homogenized properties.

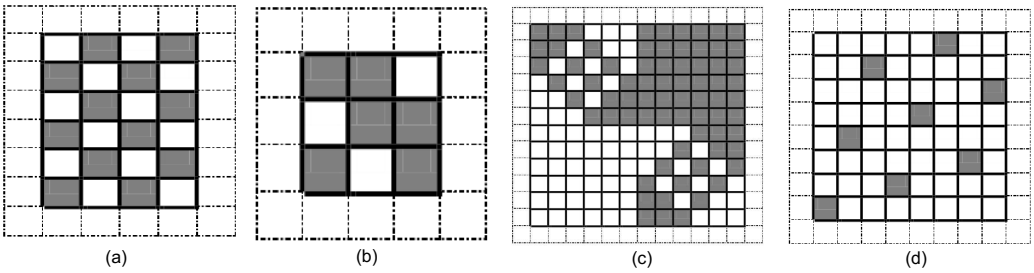

Figure 2.20: Best Malaysian's woven fabric pattern and fundamental weaves, *from left*: (a) Plain weave, (b) Twill weave, (c) Best weave (*Mata Berkait*) and (d) Satin weave

weft density, free spaces between the floats is reduced, shortens the float length and raises the shearing rigidity of the fabric. Thus, the probability of the warp floats in-plane lever to move and skew is lowered. The most potential pattern of woven fabric composites is chosen based on the optimized mechanical properties and the weave tightness value and compared to existing woven fabric composites.

Table 2.4: Comparison of best Malaysian's woven pattern with fundamental weaves

Engineering Constants	**Plain weave**	**Twill weave**	**Best weave**	**Satin weave**
E_x (GPa)	24.7	29.7	37.2	40.0
E_y (GPa)	24.7	29.7	37.2	40.0
E_z (GPa)	6.0	5.9	5.9	5.8
G_{xy} (GPa)	2.4	2.3	2.3	2.3
G_{yz} (GPa)	2.0	2.0	1.8	1.8
G_{zx} (GPa)	2.0	2.0	1.8	1.8
ν_{xy}	0.23	0.17	0.10	0.10
ν_{yz}	0.43	0.46	0.50	0.48
ν_{zx}	0.43	0.46	0.50	0.48
Tightness	1	0.67	0.38	0.25

2.7.2 Parametric study

Analyses have been performed in an endeavour to establish the consequences of various geometric parameters on the elastic properties of selected woven fabric composites. The format of the parametric study is to ascertain a set of parameters, and to vary each parameter independently while keeping the others at their original values. A set of parameters has been selected which greatly affect the fabric geometry or the elastic property of woven fabric composites. A tow packing factor, β, of 0.9069 is used in all cases of the parametric study.

Yarn spacing effect on woven fabric composites

The yarn spacing has been varied with fixed values of yarn thickness and width. As the yarn spacing increases the adjacent yarns distance becomes large, thus significantly reducing the fibre volume fraction, see Fig. 2.21(a). Fig. 2.21(b) depicts the variation of moduli when the yarn spacing in the warp and weft directions are changed at an equally rate. It can be observed that the Young's and shear moduli show a reduction corresponding to yarn spacing changes. Fig. 2.21(c) and Fig. 2.21(d) show the relative variation of Young's moduli in both directions when yarn spacing in the weft direction changes while the spacing in the warp direction is fixed and vice versa. The values of E_x and E_y start at the same point and show gradual discrepancy as the yarn spacing increases. Increasing the yarn spacing in the weft direction, the warp yarn volume fraction and Poisson's ratio values within the unit cell decrease steeply. In correlation to that, E_x reduces in great magnitude and E_y slightly enhances.

As to the shear modulus, it shows that the G_{xy} values gradually decreases in both cases as yarn spacing increases. These results are in a good agreement with Naik and Shembekar (NS92a) and Lee *et al.* (LBH03) who highlighted that an optimum spacing between adjacent yarns gives higher Young's moduli.

Variation in yarn thickness and bundle sizes

Slight changes in the total fibre volume fraction can occur when the yarn thickness varies while keeping its width and the adjacent yarn distance fixed. Fig. 2.22(a) shows that the total fibre volume fraction and Poisson's ratio significantly increase with the increase in yarn thickness. The variation of elastic and shear moduli with respect to yarn thickness is shown in Fig. 2.22(b). It is noted that the maximum values of total fibre volume fraction does not guarantee the highest moduli in the $x-$ and $y-$directions. Bundle sizes are referring to number of strands in a yarn. It ranges from 1K to 48K which K $(K = thousand)$ is the unit used. Bundle sizes showing a good relation on total fibre volume fraction and Poisson's ratio however the increment of bundle sizes shown in Fig. 2.23(a) and Fig. 2.23(b) deteriorate the elastic properties of woven composites.

Effect of yarn aspect ratio variation on yarn sections

Yarn aspect ratio variations have been carried out with the variation of yarn width sizes and fixed values on spacing and depth of yarns as well as the choices of the shape of the yarn. Lenticular, ellipse and power ellipse have been chosen for this purpose. The yarn aspect ratio results illustrate the elastic and shear moduli greatly increase with an increase in the yarn aspect ratio, AR, as shown in Fig. 2.24(b) and in all three shape choices, see Fig. 2.24(a), and Fig. 2.24(c). The total fibre volume fraction increases steeply whilst, Poisson's ratio decreases with increased yarn width. Based on this results, it can be concluded that the total fibre volume fraction influences the values of elastic and shear moduli differently depending on the yarn aspect ratios.

2.7 Numerical results

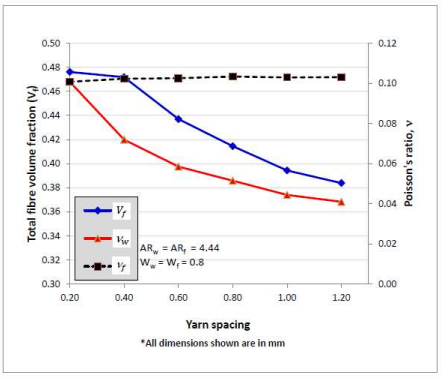

(a) Total fibre volume fraction and Poisson's ratio results to the variation of yarn spacing in weft directions

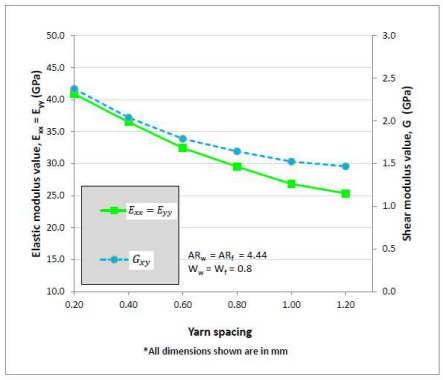

(b) A result of yarn spacing variation in warp and weft directions with an equal rate of changes

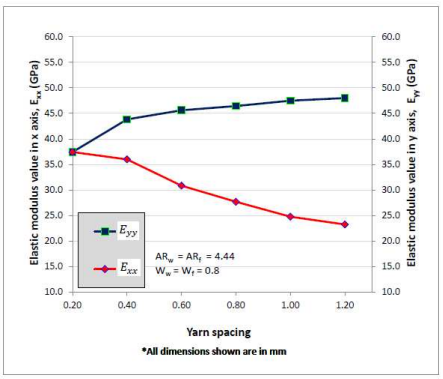

(c) Variation of moduli as a function of the yarn spacing in weft directions for the case of fixed yarn spacing in warp direction

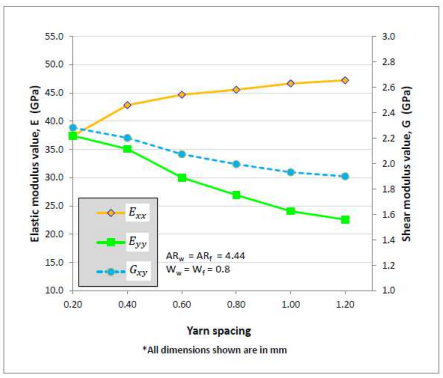

(d) Variation of moduli as a function of the yarn spacing in warp directions for the case of fixed yarn spacing in weft directions

Figure 2.21: Results of variation in yarn spacing (w = yarn width; AR = yarn aspect ratio; subscripts w and f refer to warp and weft yarns).

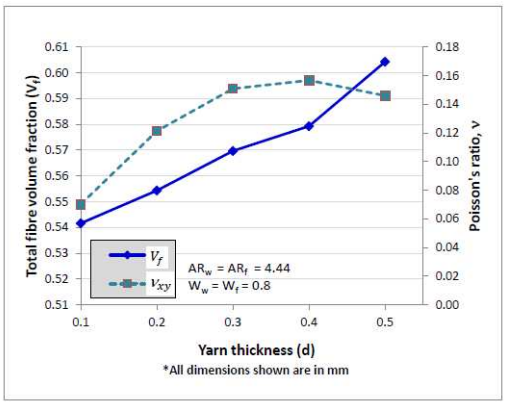

(a) Variation of fibre volume fraction in warp and weft yarns as a function of yarn thickness

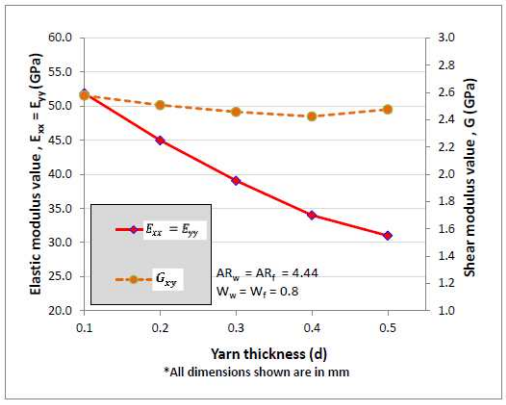

(b) Variation of moduli in warp and weft yarns as a function of yarn thickness

Figure 2.22: Results of variation in yarn thickness (w = yarn width; d = yarn thickness; l_{gp} = gap length; subscripts w and f refer to warp and weft yarns).

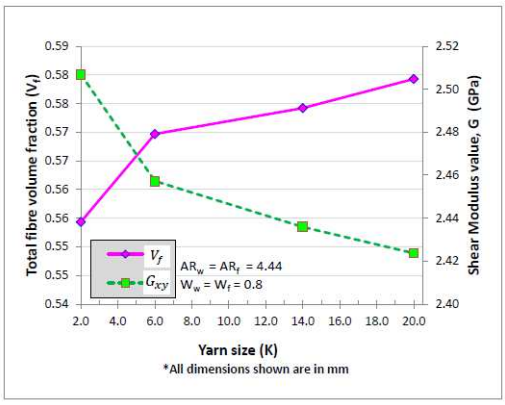

(a) Variation of fibre volume fraction and shear modulus values as a function of bundle sizes

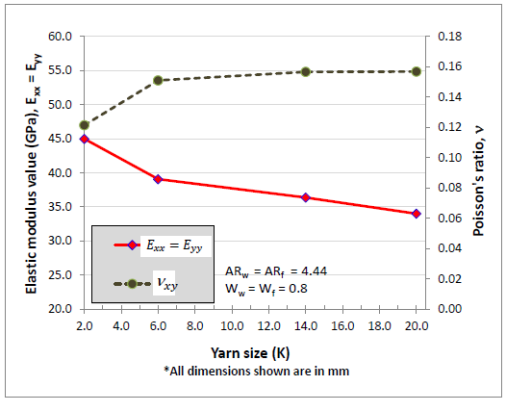

(b) Variation of moduli and Poisson's ratio values as a function of bundle sizes

Figure 2.23: Results of variation in bundle sizes.

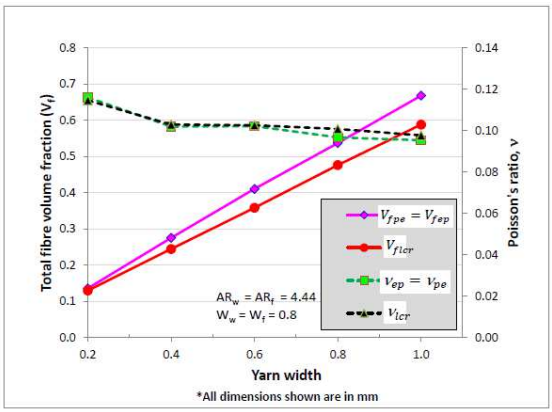

(a) Tabulation of total fibre volume fraction and Poisson's ratio with corresponds to yarn aspect ratios and shape

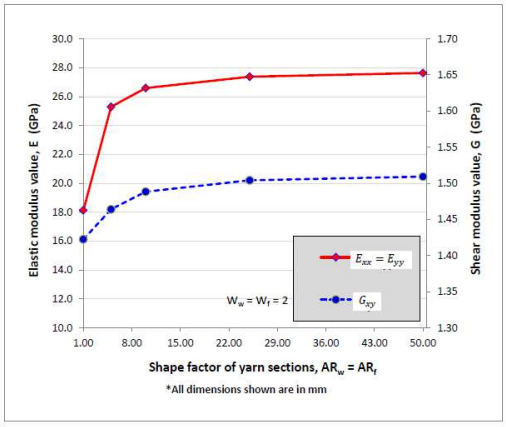

(b) Variation of moduli as a function of yarn aspect ratios and shape

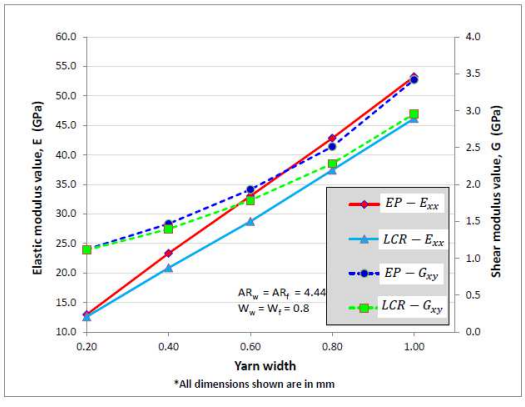

(c) Variation of moduli in a function of yarn aspect ratios and shape options

Figure 2.24: Results of variation in yarn aspect ratio on yarn sections (AR = yarn aspect ratio; d = yarn thickness; l_{gp} = gap length; subscripts w and f refer to warp and weft yarns; LCR = lenticular shape; EP = ellipse shape; PE = power ellipse).

Variation in material constituents

With a fixed geometry specification, various material constituents for fibres and matrices have been utilized. Tab. 2.5 shows the list of various fibres and matrix used. Fig. 2.25 shows that SiC(mono filament)/Al composites give the highest moduli followed by Al_2O_3/Al. In contrast to that, the E-glass/epoxy composite exhibit the lowest values of moduli among all. For the aluminum matrix systems, silicon carbide (SiC) composites have greater moduli than the other types of fibres. Since the transverse modulus of silicon carbide fibres is slightly smaller than the longitudinal modulus, the shear modulus of the composites shows significantly lower values.

Table 2.5: Material specification of various fibres and material utilized in parametric study

Properties	Material	Elastic modulus (GPa)	Poisson's ratio
fibre	Al_2O_3	380	0.26
	SiC(mono filament)	400	0.20
	Nicalon	190	0.20
	E-glass	72.5	0.22
Matrix	Cu	115	0.35
	Polyester	2.5	0.35
	Aluminum	69	0.33
	Epoxy Resin	3.5	0.35

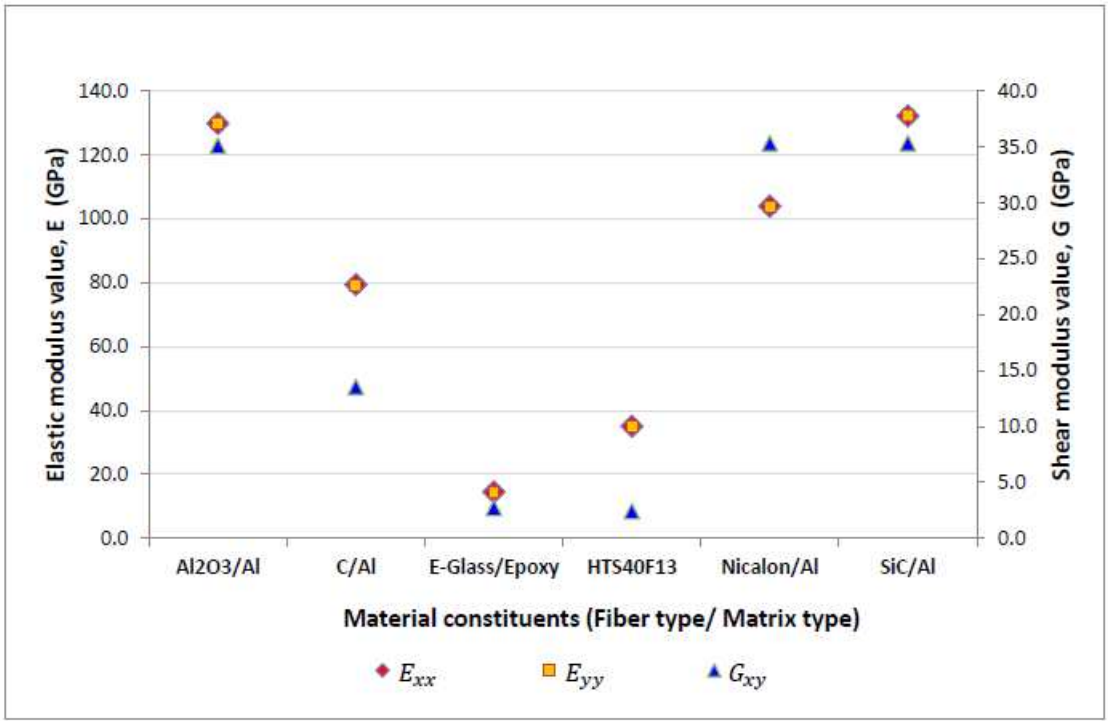

Figure 2.25: Tabulation of strength performance with various of material properties.

Chapter 3

Uncertainty Quantification of Dry Woven Fabrics: A Sensitivity Analysis on Material Properties

This chapter addresses the current and historical literature on the analysis of textile composites and the designation of *MataBerkait*-dry woven fabrics. The combination of a large search space with multidisciplinary analyses leads to a computational burden that hinders design methods in dry woven fabrics computational analysis. A pre-screening of the most important variables is required before simulation based optimization can be applied. Sensitivity analysis allows to study the impact of the variability in the inputs of the model on the outputs. It is substantiated by a comparison benchmark between the global sensitivity analysis methods on macroscopic material parameters of dry woven fabric subjected to uni-axial and biaxial deformations. This chapter elaborates with a brief outline of the global sensitivity analysis; i.e. regression-based and variance-based methods as well as the uncertainty parameters of *MataBerkait*-dry woven fabrics. The significance of sensitivity analysis on the proposed pattern also delineated here. The model incorporates the potential pattern obtained in 1^{st} task with the adopted uncertainties parameters. Numerical results based on the proposed sensitivity analysis methods are also presented.

3.1 Literature review

The mechanical behaviour of dry fabrics is important for the manufacturing process of textile composites. The first step of the manufacturing process of a textile composite is the placement of a dry woven fabric in a preform. Subsequently, resin is poured over it in order to form the solid shape of the textile composite. Any deformations and uncertainty factors during the placement possibly affect the elastic behaviour of the final textile composite. For instance, wrinkles, folds, and tearing possibly lead to unexpected mechanical behaviour of the final textile composites.

Using numerical simulation methods (SPH03), the placement of a dry fabric in a preform can be investigated. Since not all individual yarns can be incorporated at the macroscale due to the computational costs, meso-scale models are mostly used for this matter. At the mesoscopic scale, the woven fabric is seen as a set of yarns, respectively the warp and the weft (or fill) yarns in case of a woven fabric. The meso-scale modelling of dry fabrics implies that all of the mechanical properties of the meso-scale constituents must

be considered. These properties can be determined based on the micro-scale modelling of an individual yarn or by defining an appropriate constitutive model for the yarn material (KM12). A study by Komeili and Milani (KM12) presented two sets of geometrical and material-related meso-level uncertainty parameters on a glass fibre plain weave fabric using two-level factorial designs. For the geometrical uncertainty factors, the yarn spacing, yarn width, yarn thickness and misalignment of the yarns angle are investigated.

For material uncertainty parameters, the longitudinal Young's modulus, transverse Young's modulus and friction coefficient are adopted in the analysis. Gasser *et al.* (GBH00) used an inverse characterization method on experimental results (experiments performed on large pieces of fabrics) to obtain the material properties of yarns. This approach uses special material constitutive models for yarns to account for the effects of the discrete fibres at the micro-level as utilized by Sherbun (She07), which is adopted by Buet-Gautier *et al.* (BGGLB99) as well. Conversely, Peng and Cao (PC00) utilized classical elastic material properties and finite element procedures in defining the material properties. They also implemented homogenization to predict the effective non-linear elastic moduli of textile composites at the macro-scale similar to Takano *et al.* (TUKZ99) and Peng and Cao (PC02), Rabczuk *et al.* (RKSB04) and Bakhvalov and Panasenko (BP89).

In many cases, a structural response is dominated by only a few uncertainty parameters since the computational models are costly (RL08). To overcome this issue, a pre-screening of the most important variables of the problem is required before the specific strategies can be applied. The pre-screening of the most important mesoscopic uncertainty parameters relies on sensitivity analysis. Sensitivity analysis is the study of how the variation in the model output can be apportioned, qualitatively or quantitatively to variations in the model inputs. The screening of the most important effects helps the decision maker to settle on which factors will be considered. Saltelli (STC$^+$00, BBBLR13) delineates the importance of using sensitivity analysis. It allows to determine

a. if the computer model represents the system or physical processes under study,

b. the factors that contribute the most to the output variability,

c. in significant model input factors,

d. areas in the domain of variation of input factors for which the model variation is maximal,

e. if and which factors interact with each other.

There are several categories of global sensitivity analysis methods exist: the variance decomposition methods (Sobol's indices (Sob01), ANalysis Of VAriance (Gel05), Response surface model (VBLK$^+$13), differential analysis (Ram06) and linear relationship measures (Correlation Analysis (RL08), Partial Correlation Coefficients (BSS04), Standardized Regression coefficients (Fre09). In this study, we propose to compare the global sensitivity analysis methods, to their features, domain of applicability, and to apply the different methods to determine the significant and insignificant uncertainty parameters on macro-scale response of a *MataBerkait*-dry woven fabric. Correlation analysis (regression-based), Response surface models and Sobol's indices (variance-based) are the methods of global sensitivity analysis. In this study, the influence of four meso-scale uncertainty parameters

on the macro-scale response of a *MataBerkait*-dry woven fabric are investigated via these methods. The *MataBerkait*-dry woven fabric is previously generated by Ilyani Akmar *et al.* (BKBR13), and the meso-scale uncertainty parameters of interest are the yarn spacing, yarn width, yarn height and the friction coefficient between the yarns. According to previous studies, these properties have been the most important parameters in yarn designation. The geometry of the meso-scale unit cell is generated in TexGen and ABAQUS is used to discretize the unit cell with finite elements and analyses its response as a function of applied uni-axial and biaxial deformations including periodic boundary conditions.

3.2 Dry woven fabric unit cell

3.2.1 Geometry and discretization

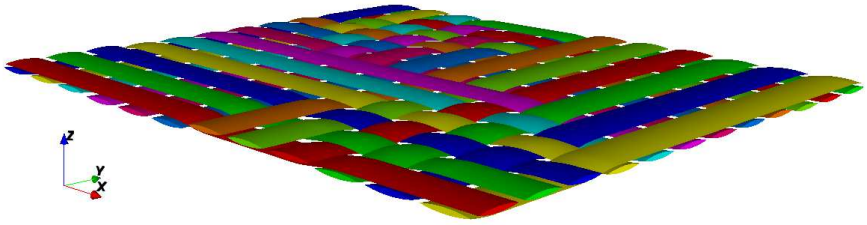

(a) An elementary pattern

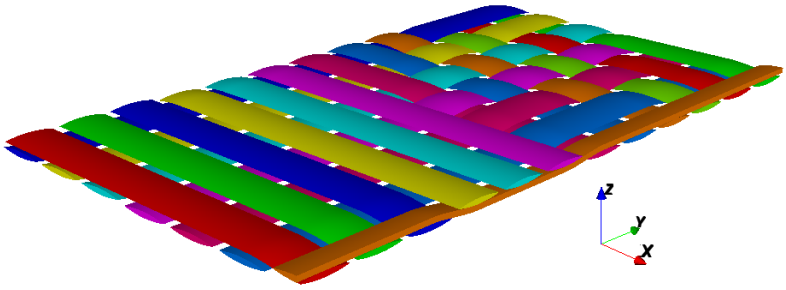

(b) The half of elementary pattern

Figure 3.1: The unit cell geometry used by Ilyani Akmar *et al.* (BKBR13).

The dry woven fabric unit cells used in this study are based on the unit cell models introduced by Ilyani Akmar *et al.* (BKBR13) and inspired by M.H.D.C. (MHD89) who adopted *Mata Berkait* as the pattern arrangement of the yarns, see Fig. 3.1. Three basic dimensional values of the yarns specified in this study are $s_y = 5.13mm$, $w_y = 4.44mm$ and $t_y = 0.5mm$ for initial yarn spacing, yarn width and yarn height, respectively. The cross-sections are assumed to have an elliptical shape. The assumption of uniform fabric deformation at the macro-scale is applied in fabric unit cell modelling and periodic boundary conditions are applied to replicate its repetitive nature, as is for instance shown by (CKG08, ZŠ07, GZŠ06). The periodic boundary conditions guarantee that macroscopic deformation modes, or a combination of them, are applied in an average sense to the meso-

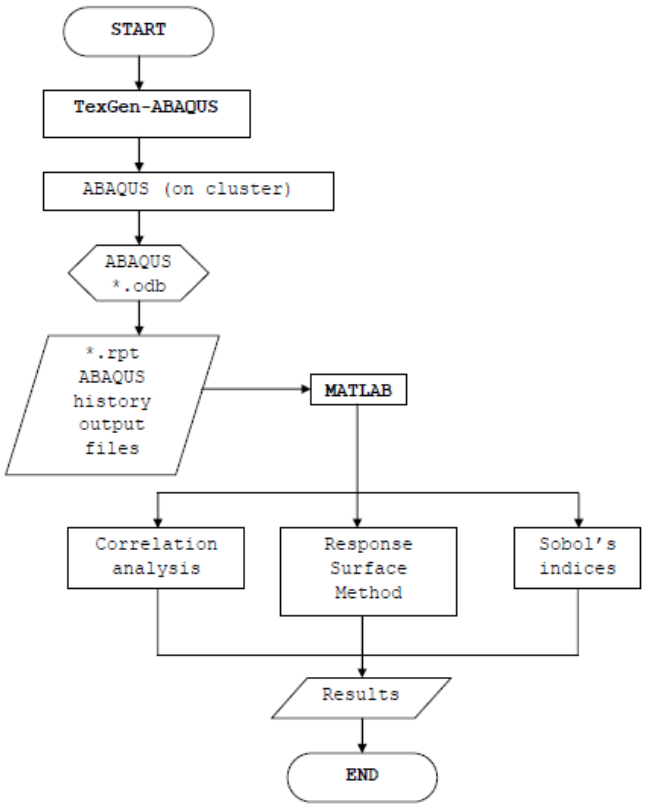

Figure 3.2: Uncertainty quantification procedures on *Mata Berkait*-dry fabric unit cell

scopic model, whilst at the meso-structure fluctuations can still occur but are limited such as if the meso-structural unit cell was to be surrounded by other unit cells.

Once a unit cell model has been specified as described above, the unit cell is imported in ABAQUS. Fig. 3.2 contains a flowchart that explains the procedures for uncertainty quantification on *Mata Berkait*-dry fabric unit cell.

3.2.2 Material properties of the yarns

It is essential to have a detailed study of the fabric behaviour at the meso-scale to determine its equivalent material properties for macro-scale models. The meso-scale modelling of dry fabrics implies that an appropriate constitutive description is formulated for the meso-scale constituents (the yarns and the interactions between them in this study). The material properties of the yarns are obtained from Peng and Cao (PC02), see Tab. 3.1 in which the materials used are pure E-Glass and Polypropylene.

3.2.3 Macro-scale response

At the macro-scale, the out-of-plane response is assumed to be negligible compared to the in-plane responses. For this reason, we focus on the in-plane responses and no loading is

Table 3.1: Material Properties of E-Glass/Polypropylene fibrous composite predicted by (PC02).

Mechanical Inputs	Values
Longitudinal stiffness, E_l	51.92 GPa
Transverse stiffness, E_t	21.97 GPa
Longitudinal Poisson's ratio, ν_{lt}	0.2489
Transverse Poisson's ratio, ν_{tt}	0.2143
Longitudinal shear stiffness, G_{lt}	8.856 GPa
Transverse shear stiffness, G_{tt}	6.250 GPa

imposed in the z-direction. This condition is crucial in the absence of a resin or matrix. Furthermore, yarns in dry fabrics can easily slide over each other which results in a substantial decrease of the shear modulus and transverse Young's modulus. It has been assumed that the longitudinal stiffness and shear moduli are given by Hooke's law

$$\begin{aligned} E_x &= \tfrac{\sigma_x}{\varepsilon_x} \\ G_{yz} &= \tfrac{\sigma_{yz}}{2\varepsilon_{yz}} \\ G_{xz} &= \tfrac{\sigma_{xz}}{2\varepsilon_{xz}} \\ G_{xy} &= \tfrac{\sigma_{xy}}{2\varepsilon_{xy}}. \end{aligned} \tag{3.1}$$

A postulation is made on the stiffness functions due to the lack of a comprehensive and consistent source of data/benchmark for the material properties of fabric yarns at meso-level. Constitutive models of yarns can also be estimated based on physical observations of yarn characteristics. For instance, due to the absence of a matrix, it is apparent that there are zero or quasi zero stiffness values in the constitutive model of yarn materials due to the fibrous nature in the fabric. The negligible longitudinal compressive response of yarns is in agreement with this observation. For the same reason, Gasser *et al.* (GBH00) has introduced the crushing law in modelling the transverse behaviour of fibres. As mentioned by Komeili and Milani (KM12), this law is developed based on the observations that the more compression is applied to the fibres, the stiffer it becomes. With respect to the crushing law, the transverse modulus of yarns is a function of contact conditions between yarns. Conversely, Kawabata *et al.* (KNK73a, KNK73b, KNK73c) defined the transverse modulus as a function of contact force. Other crushing functions in obtaining the transversal behaviour can be retrieved in Badel *et al.* (BVSB08). In this study, Gasser's approach is adopted as similar to Komeili and Milani's implementation. Gasser *et al.* (GBH00) defined that the transversal stiffness which related to transversal behaviour of yarns is a function of both longitudinal and transverse strain using Eq. (3.2) by taking direction 1(x-direction for the present work) as the longitudinal axis

$$E_i = E_0|\varepsilon_{ii}^n|\varepsilon_{xx}^m \quad [i = y, z], \tag{3.2}$$

where E_0, n and m are constants that can be determined using an inverse identification method; ε_{xx} is the strain in x-direction. Eventually, the elastic moduli, E and shear moduli,

G, are summarized in Eq. (3.3) wherein the other material properties due to the Poisson's ratios' effect are zero leading to the following stiffness matrix

$$C = \begin{bmatrix} E_x & 0 & 0 & 0 & 0 & 0 \\ 0 & E_y & 0 & 0 & 0 & 0 \\ 0 & 0 & E_z & 0 & 0 & 0 \\ 0 & 0 & 0 & G_{yz} & 0 & 0 \\ 0 & 0 & 0 & 0 & G_{zx} & 0 \\ 0 & 0 & 0 & 0 & 0 & G_{xy} \end{bmatrix}. \tag{3.3}$$

3.3 Sensitivity analysis: Material properties of woven fabric unit cells

A sensitivity analysis is performed to determine the influence of uncertain input variables on the elastic macro-scale mechanical response of *MataBerkait*-dry woven fabrics. The correlation analysis (regression-based), the response surface model (variance-based) and Sobol's indices (variance-based) (Sob01) are used. The Anthill-Plots are presented to describe the correlation between the uncertainty parameters and their influences on the material properties of *MataBerkait*-dry woven fabrics.

3.3.1 Uncertainty parameters

The four uncertainty parameters of interest in this study are:

a. **Yarn spacing,** s_y

b. **Yarn width,** w_y

c. **Yarn height,** t_y

d. **Friction coefficient,** μ**.**

Yarn spacing primarily relates to the fabric arrangement and has a major influence on fabric macro-scale mechanical properties. Here, the yarn spacing is defined as the distance between the right-hand edges of the picks in woven fabric. The geometrical designation of basic yarn is given in Fig. 3.3.

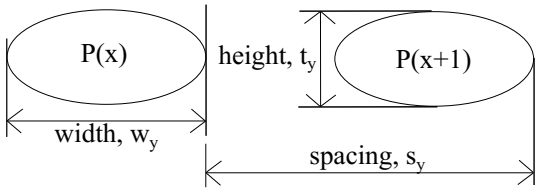

Figure 3.3: Geometrical designation of basic yarn.

The yarn width w_y, has an inter-related correlation with the yarn height, t_y. Both of these uncertainty parameters are commonly used to identify the yarn cross-sectional aspect ratio,

AR_y, as given in Eq. (3.4) (BKBR13). Here, AR_y is not necessarily constant because the t_y and w_y are the uncertainty parameters

$$w_y = AR_y t_y. \tag{3.4}$$

In textile manufacturing, the yarn height, t_y or thickness of yarns refers to the yarn weight of fabrics. The identification of the fabric height is classified as from super fine to super bulky. Varying the yarn weights can have a significant impact on the finished fabrics. The higher the yarn weight, the heavier the yarn.

Frictional properties are dependent on the composition of the material, the surface of the yarns, pressure between the yarn surfaces, temperature and relative humidity. Yarns experience friction either between themselves or against metallic surfaces where both yarn-to-yarn and yarn-to-metal friction play a significant role in textile manufacturing. The friction response appears to be significantly sensitive to the relative positioning and orientation of the dry woven fabrics during manufacturing due to the highly non-linear behaviour of woven fabrics. It can also lead to manufacturing defaults such as unweaving or wrinkles (AHW$^+$12). Further research on the friction coefficient of woven fabrics can be found in studies such as Virto and Naik (VN00), Lima *et al.* (LVSC09), Jeddi *et al.* (JSNS03), Gupta and Mogahzy (GM91), Ajayi and Elder (AE97) and Gupta (Gup08). Tab. 3.2 shows the tolerances of the four uncertainty parameters used in the analysis.

Table 3.2: Uncertainty parameters

Uncertainty parameters	**Lower bound**	**Upper bound**	**Data sources**
Yarn spacing, s_y	-2.5 %	2.5 %	Peng and Cao (PC02)
Yarn width, w_y	-3.55 %	3.55 %	Peng and Cao (PC02)
Yarn height, t_y	-4.0 %	4.0 %	upper estimation Komeili and Milani (KM12)
Friction coefficient, μ	0	0.5	modified estimation of Lin *et al.* (LZS$^+$12)

3.3.2 Correlation analysis (regression-based method)

A correlation analysis is commonly measured in terms of a correlation coefficient ρ. It quantifies the strength and direction of a linear/quadratic correlation between the output (the macro-scale mechanical response) and an uncertain variable, i.e. the input (e.g. the friction coefficient). The best known correlation coefficient is the Pearson correlation coefficient. It is derived by dividing the covariance of the two uncertainty parameters by the product of their standard deviations. The format of the correlation analysis is to ascertain a set of variables, and to vary each variable independently while keeping the others at their original values. The correlation coefficient, $\rho_{X,Y}$ can be expressed according to Eq. (3.5)(RL08) where $E(\cdot)$ denotes the expected value for correlation coefficient $\rho_{X,Y}$ between 2 random

variables X and Y

$$\rho_{X,Y} = \frac{E(XY) - E(X)E(Y)}{\sqrt{E(X^2) - E^2(X)}\sqrt{E(Y^2) - E^2(Y)}}. \tag{3.5}$$

Since the correlation coefficient $\rho_{X,Y}$ can be written as the Pearson correlation coefficient in estimating the correlation of X and Y, Eq. (3.5) can be expressed in terms of the Pearson correlation coefficient as follows

$$r_{x,y} = \frac{\sum_{i=1}^{N}(x_i - \bar{x})(y_i - \bar{y})}{\sqrt{\sum_{i=1}^{N}(x_i - \bar{x})^2 \sum_{i=1}^{N}(y_i - \bar{y})^2}}, \tag{3.6}$$

where N is the sample size, $\bar{x}$ and $\bar{y}$ are the mean of the x_i and y_i values, respectively. The coefficients resulting from Eq. (3.5) and Eq. (3.6) are located at the interval [-1,1] where the values between the investigated uncertainty parameters X and output response, Y are categorized as follows: ± 0.8 and above (strong correlation), $\pm 0.5 - 0.79$ (moderate correlation) and ± 0.49 and below (weak correlation). The $+1$ and -1 indicate the perfect positive and perfect negative correlations, respectively. Perfect positive correlation defines that as one variable moves, either up or down, the other variable will move in locksteps, in the same direction. Alternatively, perfect negative correlation implies that if one variable moves in either direction the variable that is perfectly negatively correlated moves in the opposite direction.

The Pearson correlation coefficient is associated with the regression coefficient derived by linear regression analysis. A linear regression as shown in Eq. (3.7) is modelled for n data inputs with one independent variable x_i, two uncertainty parameters $\hat{a}$ and $\hat{b}$ and one error term, ϵ_i

$$y_i = \hat{a} + \hat{b}x_i + \varepsilon_i, \tag{3.7}$$

where the uncertainty parameters $\hat{a}$ and $\hat{b}$ are estimated via least squares fittings

$$\hat{b} = \rho \frac{\sum_{i=1}^{N}(x_i - \bar{x})(y_i - \bar{y})}{\sum_{i=1}^{N}(x_i - \bar{x})^2}, \tag{3.8}$$

$$\hat{a} = \bar{y} - \hat{b}\bar{x}. \tag{3.9}$$

The interrelation between linear regression and the Pearson correlation coefficient is given by (RL08)

$$\hat{b} = r_{x,y}\frac{s_y}{s_x} \tag{3.10}$$

where s_x and s_y are the standard deviations of the respective data.

The proportion of variability in the investigated data through the linear regression is defined by the coefficient of determination, R^2. The variability of the data is measured via the residuals as follows

$$\hat{u}_i = y_i - (\hat{a} + \hat{b}x_i). \tag{3.11}$$

In the case of linear regression R^2 is the square of the Pearson correlation coefficient. The coefficient of determination R^2 is given by

$$R^2_{x,y} = 1 - \frac{\sum_{i=1}^{N} \hat{u}_i^2}{\sum_{i=1}^{N} (y_i - \bar{y})^2}, \tag{3.12}$$

and interprets the accuracy of the regression fit.

3.3.3 Response surface model

Response surface modelling is a method used in the empirical study of the correlation between the output response and a number of input uncertainty parameters. It is typically used to find the optimal setting for the input uncertainty parameters that maximize (or minimize) the predicted response (Khu06, Chapter 4). This method is based on the development of a response surface approximation of the unit cell model response. This approximation is then used as a surrogate for the original model in uncertainty and sensitivity analysis. Sensitivity measures for the uncertainty parameters are derived from the constructed response surface. This surface plays the same role in a response surface methodology as the Taylor series in a differential analysis. Due to its advantage in minimizing the numerical effort, a response surface model (MR03) is implemented to evaluate the effects of uncertainty parameters on material properties of *MataBerkait*-dry woven fabric.

The response surface model is constructed using Latin Hypercube Sampling (LHS) in order to quantify the regression coefficient, coefficient of determination, R^2 and adjusted coefficient of determination, R_{adj}. R^2 is often interpreted as the proportion of response variation as explained by the regression mode in the model. R_{adj} is derived as an alternative approach of regression evaluation in which it penalizes the statistic as extra variables are included in the model. In comparison to Monte-Carlo sampling (MCS) e.g., using LHS can significantly reduce the number of required dry woven fabric unit cell samples because LHS is not depending on the dimension of the random vectors as well as the number of random variable (Kei11, VBLK$^+$13). By using LHS, the computational cost can be reduced due to the dense stratification across the range of each dry woven fabric unit cell samples (HD03).

Based on a linear polynomial, the response of the meso-scale unit cell model (here, in terms of the elastic meso-scale properties), $\mathbf{Y}(N \times 1)$, as a function of the uncertain input uncertainty parameters, $\mathbf{X} = (\mathbf{X}_1, \mathbf{X}_2, \ldots, \mathbf{X}_k)(N \times 1)k$ is approximated as

$$\hat{\mathbf{Y}} = \beta_0 + \beta_1 \mathbf{X}_1 + \beta_2 \mathbf{X}_2 + \ldots + \beta_k \mathbf{X}_k + \varepsilon = \mathbf{X}\boldsymbol{\beta} + \mathbf{e}, \tag{3.13}$$

where N is the number of samples, k is the input uncertainty variables, $\boldsymbol{\beta}$ is the regression coefficient vector $(k \times 1)$ and the error between the real models, $\hat{\mathbf{Y}}$ and $\mathbf{Y}$ is $\mathbf{e}$ as Eq. (3.14). Consequently, the sum squared errors, SS_E can be calculated as Eq. (3.15)

$$\mathbf{e} = \mathbf{Y} - \hat{\mathbf{Y}}, \tag{3.14}$$

$$SS_E = \mathbf{e}^T \mathbf{e}. \tag{3.15}$$

By substituting Eq. (3.14) into Eq. (3.15), SS_E can be written as

$$SS_E = \sum_{i=1}^{N} \left(\mathbf{Y} - \hat{\mathbf{Y}}\right)^T \left(\mathbf{Y} - \hat{\mathbf{Y}}\right). \tag{3.16}$$

Minimizing SS_E with respect to $\boldsymbol{\beta}$ yields the regression coefficient, $\hat{\boldsymbol{\beta}}$ as

$$\hat{\boldsymbol{\beta}} = \left(\mathbf{X}^T\mathbf{X}\right)^{-1}\mathbf{X}^T\mathbf{Y}. \tag{3.17}$$

Hence, the coefficient of determination, R^2 and the total variation, SS_T can be approximated by

$$R^2 = 1 - \frac{SS_E}{SS_T}, \quad 0 \leq R^2 \leq 1; \tag{3.18}$$

$$SS_T = V(\mathbf{Y}) = (\mathbf{Y} - \overline{\mathbf{Y}})^T(\mathbf{Y} - \overline{\mathbf{Y}}), \tag{3.19}$$

where $\overline{\mathbf{Y}}$ is the mean value of Y_i expressed by Eq. (3.20)

$$\overline{\mathbf{Y}} = \frac{1}{N}\sum_{i=1}^{N}(Y_i). \tag{3.20}$$

By substituting Eq. (3.16), Eq. (3.19) and Eq. (3.20) into Eq. (3.18), R^2 can be simplified by

$$R^2 = 1 - \frac{\sum_{i=1}^{N}(Y_i - \hat{Y}_i)}{\sum_{i=1}^{N}(Y_i - \overline{Y_i})}. \tag{3.21}$$

The adjusted coefficient of determination R^2_{adj} is given by

$$R^2_{adj} = 1 - \frac{N-1}{N-k}\left(1 - R^2\right). \tag{3.22}$$

It is desirable that the coefficient of determination (C.O.D.), R^2 is greater than 0.8 reflecting a strong correlation. For large N values, R^2 is equivalent to R^2_{adj}. Higher order approaches are also carried out in the analysis as such quadratic without mixed terms

$$\hat{\mathbf{Y}} = \beta_0 + \beta_1\mathbf{X}_1 + \beta_2\mathbf{X}_2 + \ldots + \beta_{kN}\mathbf{X}_{kN} + \beta_{11}\mathbf{X}_1^2 + \beta_{22}\mathbf{X}_2^2 + \ldots + \beta_{kN}\mathbf{X}_{kN}^2 + \mathbf{e}, \tag{3.23}$$

and fully quadratic terms as follows

$$\begin{aligned}\hat{\mathbf{Y}} =& \beta_0 + \beta_1\mathbf{X}_1 + \beta_2\mathbf{X}_2 + \ldots + \beta_{kN}\mathbf{X}_{kN} + \beta_{11}\mathbf{X}_1^2 + \beta_{22}\mathbf{X}_2^2 + \ldots + \beta_{kNkN}\mathbf{X}_{kN}^2 \\ &+ \beta_{12}\mathbf{X}_1\mathbf{X}_2 + \ldots + \beta_{kN-1kN-1}\mathbf{X}_{kN-1}\mathbf{X}_{kN} + \mathbf{e}.\end{aligned} \tag{3.24}$$

3.3.4 Sensitivity indices / Sobol's indices (variance-based method)

We apply the variance-based sensitivity methods for arbitrary complex computational models. The estimation of the sensitivity indices is based on the effect of the random input variables on the model output ('the macro-scale material parameters'). The "first-order sensitivity index", S_i also known as "main effect index" is defined as a direct variance-based measure of sensitivity. However, when the number of variables becomes large, the "total-effect index" or "total-order sensitivity index", S_{Ti} gives an exclusive and residual influence (Sob01, GI12). 10000 sampling points are generated to quantify the sensitivity indices of uncertainty parameters where the regression coefficient adopted are based on the values obtained in the response surface model. This subsection provides a short elaboration for computing the full set of first-order and total-effect indices for a model of k-factors (Sal08).

(a) A (N,2k) matrix of random numbers is generated where k is the number of inputs and two matrices of data (**A** and **B**) are defined which contain half of the sample. N is the number of sample which varies from few hundreds to few thousands.

$$\mathbf{A} = \begin{bmatrix} x_1^{(1)} & x_2^{(1)} & \dots & x_i^{(1)} & \dots & x_k^{(1)} \\ x_1^{(2)} & x_2^{(2)} & \dots & x_i^{(2)} & \dots & x_k^{(2)} \\ \dots & \dots & \dots & \dots & \dots & \dots \\ x_1^{(N-1)} & x_2^{(N-1)} & \dots & x_i^{(N-1)} & \dots & x_k^{(N-1)} \\ x_1^{(N)} & x_2^{(N)} & \dots & x_i^{(N)} & \dots & x_k^{(N)} \end{bmatrix} \tag{3.25}$$

$$\mathbf{B} = \begin{bmatrix} x_{k+1}^{(1)} & x_{k+2}^{(1)} & \dots & x_{k+i}^{(1)} & \dots & x_{2k}^{(1)} \\ x_{k+1}^{(2)} & x_{k+2}^{(2)} & \dots & x_{k+i}^{(2)} & \dots & x_{2k}^{(2)} \\ \dots & \dots & \dots & \dots & \dots & \dots \\ x_{k+1}^{(N-1)} & x_{k+2}^{(N-1)} & \dots & x_{k+i}^{(N-1)} & \dots & x_{2k}^{(N-1)} \\ x_{k+1}^{(N)} & x_{k+2}^{(N)} & \dots & x_{k+i}^{(N)} & \dots & x_{2k}^{(N)} \end{bmatrix} \tag{3.26}$$

(b) A matrix $\mathbf{C}_i$ is defined by taking all columns of **B** except the ith column which taken from **A** as

$$\mathbf{C}_i = \begin{bmatrix} x_{k+1}^{(1)} & x_{k+2}^{(1)} & \dots & x_i^{(1)} & \dots & x_{2k}^{(1)} \\ x_{k+1}^{(2)} & x_{k+2}^{(2)} & \dots & x_i^{(2)} & \dots & x_{2k}^{(2)} \\ \dots & \dots & \dots & \dots & \dots & \dots \\ x_{k+1}^{(N-1)} & x_{k+2}^{(N-1)} & \dots & x_i^{(N-1)} & \dots & x_{2k}^{(N-1)} \\ x_{k+1}^{(N)} & x_{k+2}^{(N)} & \dots & x_i^{(N)} & \dots & x_{2k}^{(N)} \end{bmatrix}. \tag{3.27}$$

(c) The model output is computed for all the input values in the sample matrices **A**, **B** and $\mathbf{C}_i$ which yields three vectors of model outputs of dimension $N \times 1$

$$\mathbf{y}_A = f(\mathbf{A}), \quad \mathbf{y}_B = f(\mathbf{B}), \quad \mathbf{y}_C = f(\mathbf{C}_i). \tag{3.28}$$

These vectors are needed in computing the first-order and total-effect indices, S_i and S_{Ti}, for a given factor X_i. Since there are the k-factors, the cost of this approach is $N + N$ runs of the model for matrices A, B, plus $k \times N$ to estimate k-times the output vector corresponding to matrix C_i (Sal08). The first-order sensitivity index S_i can be written as

$$S_i = \frac{V\left(E\left(\mathbf{Y}|X_i\right)\right)}{V(\mathbf{Y})} = \frac{(1/N)\sum_{j=1}^{N} \mathbf{y}_A^{(j)} \mathbf{y}_{C_i}^{(j)} - f_0^2}{(1/N)\sum_{j=1}^{N} (\mathbf{y}_A^{(j)})^2 - f_0^2}, \tag{3.29}$$

where $V(E(\mathbf{Y}|X_i))$ is the variance of the expected value of $\mathbf{Y}$ under the condition that X_i is kept fixed. X_i and $V(\mathbf{Y})$ is the unconditional variance of $\mathbf{Y}$. The f_0^2 is given by

$$f_0^2 = \left(\frac{1}{N} \sum_{j=1}^{N} y_A^{(j)} \right)^2. \tag{3.30}$$

The high and low values of y_A and y_{Ci} are randomly associated if X_i is non-influential parameter. Contradictorily, if X_i is influential, then high (or low) values of y_A will be preferentially multiplied by high (or low) values of y_{Ci} increasing the value of the resulting scalar product. Note that the accuracy of both f_0 and $V(Y)$ can be improved by using both y_A and y_B points rather than y_A only. The accuracy of the estimation for S_i and S_{Ti} is obtained with respect to the above condition, although the factors ranking remains unchanged (Sal08).

The index S_i is a measure for the exclusive influence of an uncertainty criterion, X_i. If the sum of all S_i is close to one, the model is additive, and no interaction of the uncertainty parameter exists. In complex engineering problems, interactions between input variables may exist, thus, higher order sensitivity indices are needed (KKL$^+$11). Each of Sobol's (Sob01) indices represents a sensitivity measure that describes which amount of each variance is caused due to the randomness of the single random input variables and its mapping onto the output variables (RL08). The total-effect index S_{Ti} is used to present the total contribution of the uncertainty criterion, X_i to the output, i.e. first order effects in addition to all higher order effects and the expression of S_{Ti} is defined by

$$S_{Ti} = 1 - \frac{V\left(E\left(\mathbf{Y}|X_i\right)\right)}{V(\mathbf{Y})}. \tag{3.31}$$

Due to the mutual interaction of the uncertainty parameters, the total-effect index of a parameter in uncertainty parameters increases, therefore ΣS_{Ti} will always be constant (on top of $\Sigma S_{Ti} \geq 1$). The difference of $S_{Ti} - S_i$ measures the numbers of interactions that X_i has with other input variables in the uncertainty parameters (KKL$^+$11). In addition, S_i and S_{Ti} demand a large number of samples which leads to an expensive computational analysis.

The sensitivity indices S_i and S_{Ti} shown in Eq. (3.29) and Eq. (3.31) are reduced by the coefficient of determination as follows

$$\begin{aligned} \hat{S}_i &= R^2 S_i \\ \hat{S}_{Ti} &= R^2 S_{Ti}. \end{aligned} \tag{3.32}$$

3.4 Numerical results

In this section, we quantify the main parameters and their interactions that play an important role in influencing the fabric material properties. It is obligatory for a significantly statistic analysis to represent the design space equally which corresponds to an equal representation of the upper and lower bounds of the variables. In this case, the Latin Hypercube Sampling (LHS) is used as a random sample parameter distribution into equal probability intervals (IC80). This method represents the design space equally by minimizing the variation vectors. Each variable is assumed to be uniformly distributed due to insufficient information with respect to the meso-scale uncertain input parameters.

3.4.1 Correlation analysis

The scatter plots in Fig. 3.4, Fig. 3.5 and Fig. 3.6 show the influence of different input variables on the mechanical properties for uni-axial loading. The scatter plots for biaxial loading are depicted in Fig. 3.7, Fig. 3.8 and Fig. 3.9. The ranking of the uncertainty parameters can be gained from the Ant-hill plots where 100 sampling points for each pair-wise uncertainty parameters are used. Based on the scatter plots, we can preliminarily predict the influences of uncertainty parameters (friction coefficient, yarn height, yarn width and yarn spacing) on material properties (E_{xx}, E_{yy}, E_{zz}, G_{xy}, G_{xz} and G_{yz}).

The changes of the Young's moduli with respects to the input parameters are very small due to the sample size of the unit cells (meso-scale analysis). It is shown that E_{xx} and E_{zz} either under uni-axial or biaxial loadings, increase gradually with an increasing friction coefficient. In addition, E_{yy} decreases with an increase of friction coefficient under both loading cases. This behaviour is expected since there is no loading imposed in z-direction in all cases and the direction of loading in x- and y-directions in the biaxial case. Consequently, the behaviour of E_{zz} is mainly affected by the weave arrangement and its undulation. The decrement in E_{yy} is also correlated to the yarn height which is significantly influenced by the ratio of height and width of the yarns. The friction shows an important role through the external forces imposed at the contact surfaces on moving yarns.

As for the yarn height, a decrease of elastic moduli can be observed as the yarn height variation becomes higher. Theoretically, the results from yarn height variation can be correlated with the results obtained in yarn width variation because they are inter-related by yarn aspect ratio as derived in Eq. (3.4). Nevertheless, E_{xx} decreases gradually with the varying of yarn height. The decrement in E_{xx} is due to greater yarn surfaces as the yarn height varies. A contradiction also occurred for the variation of yarn width since E_{yy} and E_{zz} show a significant increase whilst E_{xx} is gradually decreased with an increasing yarn width.

However, yarn spacing variation increases the values of E_{xx} and E_{yy} for both loading cases. The shear moduli components are presented in the correlation analysis summary. A summary of correlation analysis is carried out by identifying the strong/poor correlation between the inputs (uncertainty parameters) and the *MataBerkait*-dry woven fabric response (material properties) to give a clear observation based on the scatter plots. Tab. 3.3 shows the summary of the correlation analysis under both loading conditions.

According to Tab. 3.3, it is observed that friction coefficient and yarn height have the strongest correlations on elastic moduli whilst a weak correlation on shear moduli of

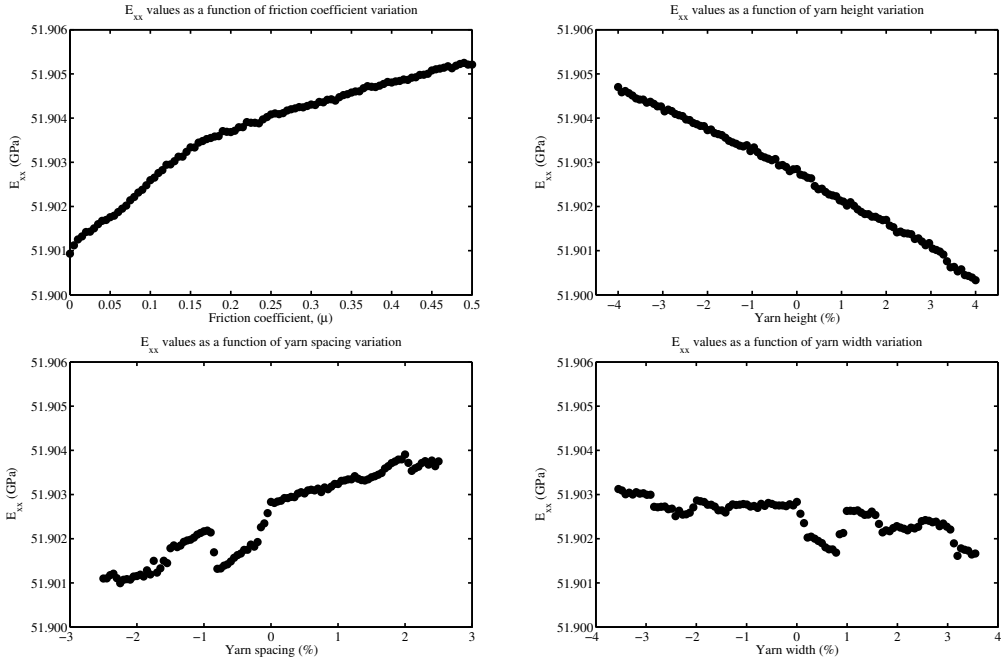

Figure 3.4: Effects of friction coefficient, yarn height, yarn spacing and yarn width variations on E_{xx} under uni-axial loading in X-direction for *MataBerkait*-dry woven fabric.

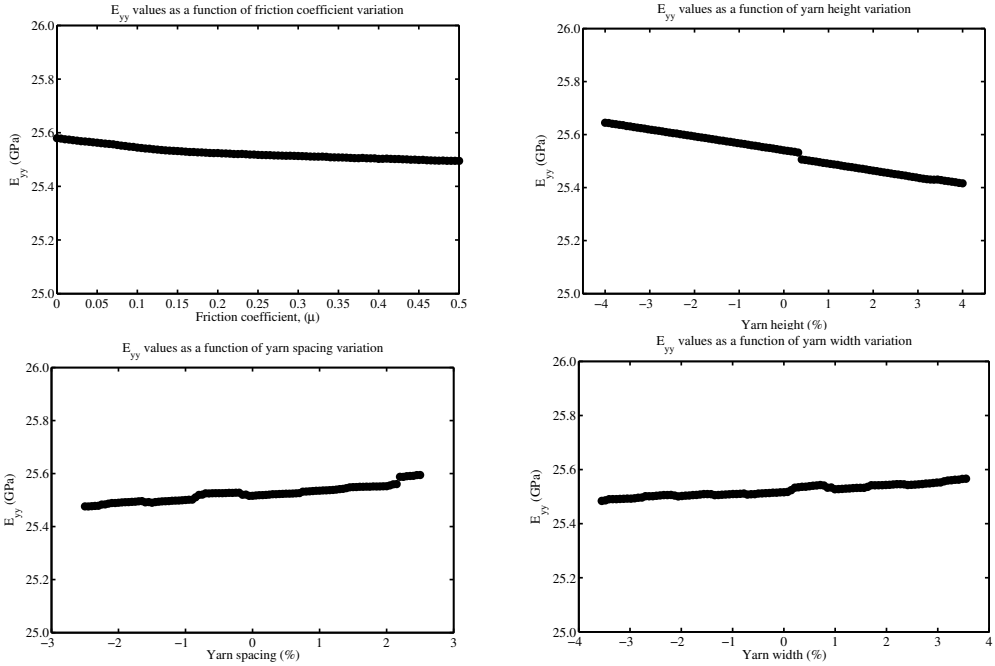

Figure 3.5: Effects of friction coefficient, yarn height, yarn spacing and yarn width variations on E_{yy} under uni-axial loading in X-direction for *MataBerkait*-dry woven fabric.

Table 3.3: Correlation coefficient for four uncertainty parameters under uni-axial and biaxial loadings (± 0.8 and above: strong correlation, $\pm 0.5 - 0.79$: moderate correlation and ± 0.49 and below: weak correlation).

Uni-axial mode	**Correlation coefficient**, ρ					
Variables	E_{xx}	E_{yy}	E_{zz}	G_{xy}	G_{xz}	G_{yz}
C. Friction	0.97 (strong)	-0.96 (strong)	0.95 (strong)	-0.07 (weak)	-0.09 (weak)	0.02 (weak)
Yarn height	-0.99 (strong)	-0.99 (strong)	-0.99 (strong)	-0.3 (weak)	-0.01 (weak)	-0.07 (weak)
Yarn width	-0.77 (moderate)	0.97 (strong)	0.99 (strong)	0.15 (weak)	0.11 (weak)	-0.18 (weak)
Yarn spacing	0.96 (strong)	0.95 (strong)	0.95 (strong)	-0.04 (weak)	-0.27 (weak)	-0.27 (weak)
Biaxial mode	**Correlation coefficient**, ρ					
Variables	E_{xx}	E_{yy}	E_{zz}	G_{xy}	G_{xz}	G_{yz}
C. Friction	0.99 (strong)	-0.99 (strong)	0.96 (strong)	-0.05 (weak)	-0.06 (weak)	-0.1 (weak)
Yarn height	-0.99 (strong)	-0.99 (strong)	-0.97 (strong)	0.53 (moderate)	0.01 (weak)	-0.18 (weak)
Yarn width	-0.09 (weak)	0.95 (strong)	0.99 (strong)	0.25 (weak)	-0.12 (weak)	0.20 (weak)
Yarn spacing	0.99 (strong)	0.95 (strong)	-0.59 (moderate)	0.31 (weak)	-0.04 (weak)	-0.12 (weak)

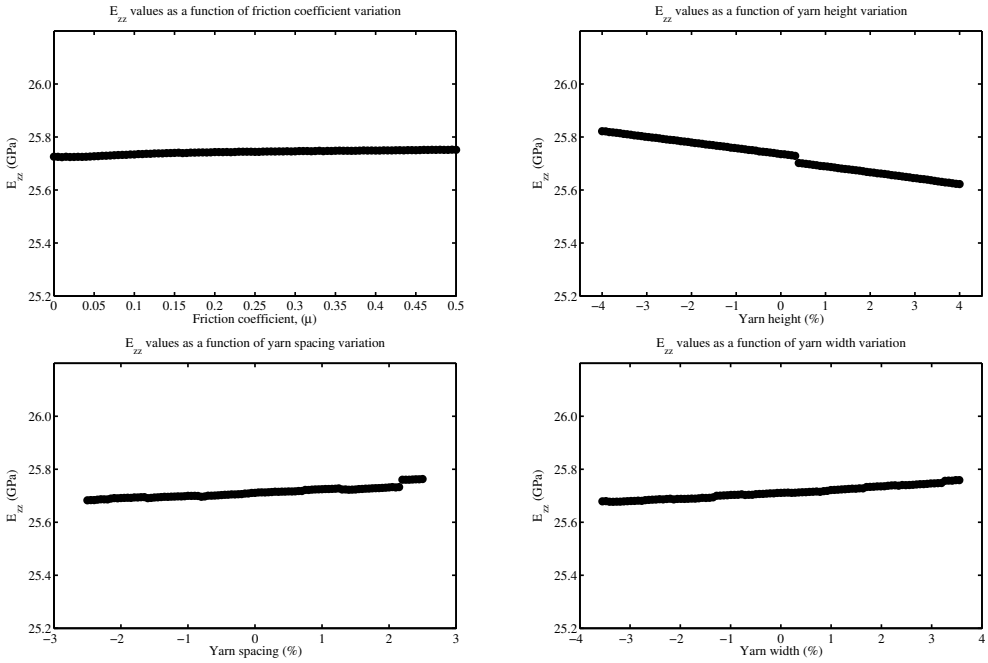

Figure 3.6: Effects of friction coefficient, yarn height, yarn spacing and yarn width variations on E_{zz} under uni-axial loading in X-direction for *MataBerkait*-dry woven fabric.

Table 3.4: Coefficient of determination, R^2 of correlation analysis

Uniaxial mode	Coefficient of determination, R^2					
Variables	E_{xx}	E_{yy}	E_{zz}	G_{xy}	G_{xz}	G_{yz}
C. Friction	0.94	0.92	0.90	0.005	0.008	0.0004
Yarn height	0.98	0.98	0.98	0.09	0.0001	0.005
Yarn width	0.59	0.94	0.98	0.02	0.01	0.03
Yarn spacing	0.92	0.90	0.90	0.002	0.07	0.07
Biaxial mode	Coefficient of determination, R^2					
Variables	E_{xx}	E_{yy}	E_{zz}	G_{xy}	G_{xz}	G_{yz}
C. Friction	0.98	0.98	0.92	0.003	0.004	0.01
Yarn height	0.98	0.98	0.94	0.28	0.0001	0.03
Yarn width	0.008	0.90	0.98	0.06	0.01	0.04
Yarn spacing	0.98	0.90	0.35	0.10	0.002	0.01

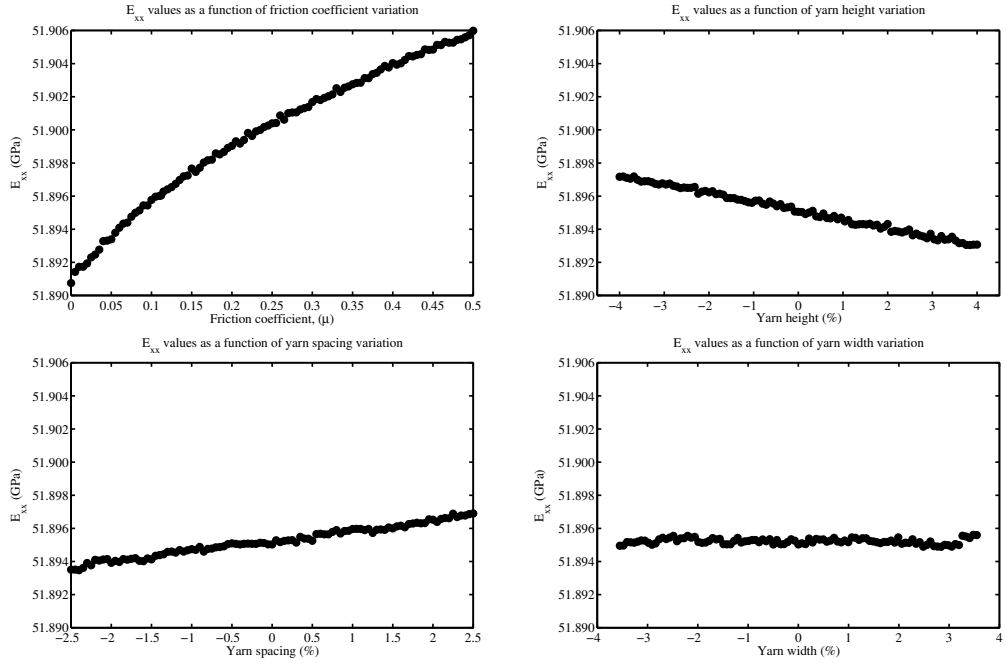

Figure 3.7: Effects of friction coefficient, yarn height, yarn spacing and yarn width variations on E_{xx} under biaxial loading in X and Y-directions for *MataBerkait*-dry woven fabric.

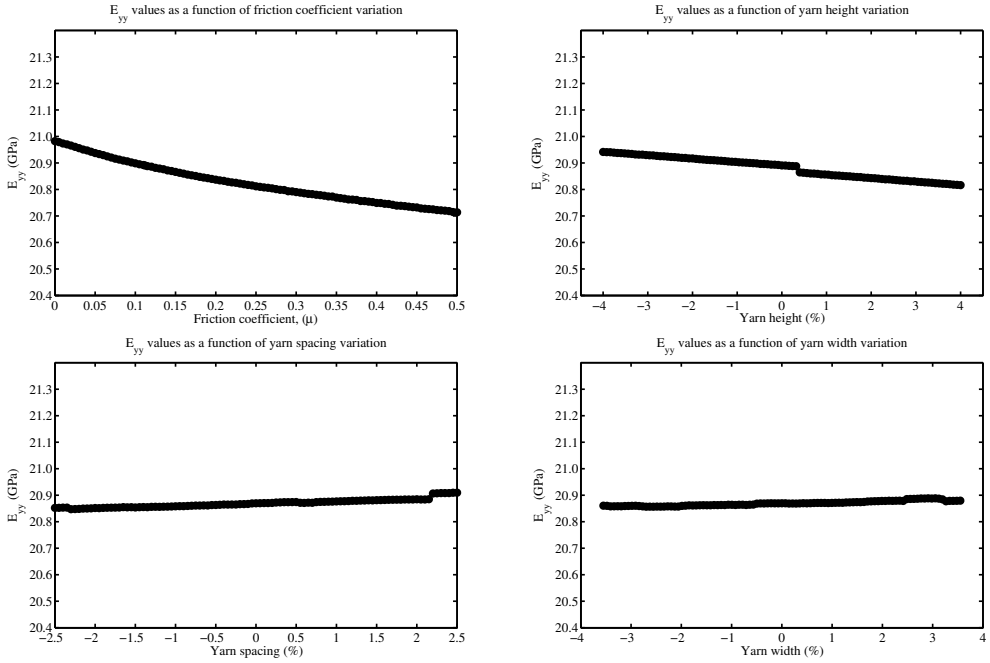

Figure 3.8: Effects of friction coefficient, yarn height, yarn spacing and yarn width variations on E_{yy} under biaxial loading in X and Y-directions for *MataBerkait*-dry woven fabric.

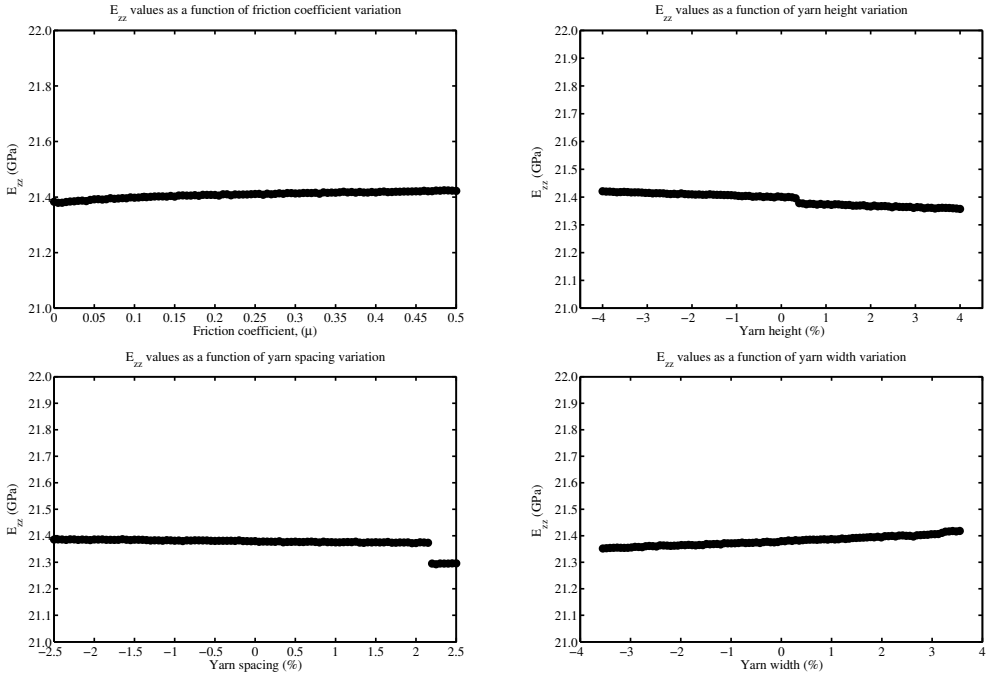

Figure 3.9: Effects of friction coefficient, yarn height, yarn spacing and yarn width variations on E_{zz} under biaxial loading in X and Y-directions for *MataBerkait*-dry woven fabric.

MataBer-kait-dry woven fabric under both loadings. It can be concluded that more than 90% of the correlation coefficient reflected by the change of the friction coefficient and yarn height for the distribution of E-moduli (E_{xx}, E_{yy} and E_{zz}). Due to the low value of R^2 for all shear moduli, it can be concluded that the shear modulus is insignificant. This is because we observed the effect of dry-woven fabric loading in a direction that is neither parallel nor perpendicular to the fibres.

If an external force is applied perpendicular to the yarns, then the E-Glass/Polypropylene fibrous composite will stretch in the same direction. Note that the stiffness of the E-Glass/Poly-propylene fibrous composite, measured perpendicular to the fibres increases much more slowly than stiffness measured parallel to the fibres as the volume fraction of fibres is increased.

Moreover, in a fibrous composite (for instance E-Glass/Polypropylene) with the applied stress aligned perpendicular to the fibres, the stress is transferred to the fibres through the fibre matrix interface and both the fibre and the matrix experience the same stress. While the rule of mixtures has proved adequate for tensile modulus (E) in the axial direction, the iso-strain rule of mixtures does not work for either the shear (G) moduli. Instead, these are dependent on the phase morphology.

Since the dry-woven fabric is used in the analysis, the strain in the yarn represents as the volume average of the strain in E-Glass/Polypropylene fibrous composite. In this study, the volume fraction of E-Glass is given by 0.70. The type of weave affects dimensional stability and the drapability of the fabric over complex surfaces. *MataBerkait* weaves, for example, exhibit good drapability. Unfortunately, good drapability and resistance to shear are mutually exclusive. Most of 2D-weaves involve two orthogonal directions of yarn, implying weak in-plane shear resistance within a single ply. Obviously, these are the reasons on why a poor shear stiffness is obtained in the analysis.

Tab. 3.4 summarizes the coefficient of determination between the inputs (uncertainty parameters) and the *MataBerkait*-dry woven fabric response (material properties). Again, the shear stiffness contributes a lower R^2 with less than 0.49. In addition to the previous elaboration, this scenario also relates to the effect of transverse pressure on the individual yarns caused by the tension of the yarn. When a yarn is subjected to such compression, the individual fibres (fibres that construct a yarn) lose contact with each other. This results in a considerable reduction in the axial stiffness of the yarn, consequently to the shear stiffness. Besides, the properties of the yarns, the properties of the fibrous composite, the orientation of the yarns, and the size and shape of the yarns also reflect to the result of R^2 in stiffness properties.

Further uncertain variables with relevant correlations are yarn spacing and yarn width variations. Yarn spacing and width are found to be important parameters in almost every elastic moduli under both loading cases. As for yarn spacing, it is noticeable that its contribution is marginal. This is because the yarn spacing is related to the undulation of yarns along the loading directions. This can be proven with the results of E_{zz} where in uni-axial case, the ρ is almost perfectly positive correlation whilst in biaxial case, the ρ is moderately negative correlation. In uni-axial loading case, the yarn spacing becomes one of the most dominant uncertain variable influencing the elastic moduli.

Theoretically, the increase in yarn height or width relates to the increase of yarn cross sectional area which acquires a greater reaction force corresponding to the stretching of the

larger yarn cross-sectional area. A wider yarn will let the side contact between the yarns becomes closer. The undulation of the yarns is also influenced by these two uncertainty parameters (height and width variations) even though the variations given for these uncertainty parameters are considerably small. This is clearly seen in the results of R^2 for E_{xx} due to yarn width and E_{zz} with respect to yarn spacing variations. Both show a poor R^2 value due to the discussed matter. A greater yarn height contributes to a curvier path line of the yarn.

Subsequently, a yarn with greater height acquires larger strain to enforce elongation in the yarn and eventually affect the reaction force of the unit cell. At certain strain level, where yarns are not in fully-tensioned, undulation and relative movements become the two dominant factors. This is when the yarns elongate correspondingly to the imposed load and friction becomes significant through the reaction forces at the contact surfaces. It is clearly shows that in any loading cases, the cross-sectional area of the yarns, yarn undulations and the friction coefficients between the moving yarns certainly influence the strains in each axes.

Consequently, the strains are associated to the performance of elastic moduli. In practical, the cross-sectional aspect ratios of yarns are not uniform along their axes. Each yarn is subjected to irregular pressures imposed by neighbouring yarn during both manufacture of the textile preform and the consolidation process. Each yarn is pinched in different directions at different points. Indeed, all four uncertainty parameters show a reliable result that relates to the theoretical and practical issues.

However, a correlation analysis is only a preliminary analysis for a sensitivity analysis. For a more significant result, a response surface model and sensitivity indices are presented in subsection 3.4.2 and 3.4.3. The influences of each uncertainty parameters on the material properties of *MataBerkait*-dry woven fabric are clearly presented in both models.

3.4.2 Response surface model

The results are illustrated in Tab. 3.5 and Tab. 3.6 for both loading conditions with respect to the linear, quadratic without mixed terms and fully quadratic polynomial regression, respectively.

Table 3.5: Regression coefficient, coefficient of determination, R^2 (C.O.D. R^2) and adjusted coefficient of determination, R_{adj} (Adjusted C.O.D.) under uniaxial loading

Response surface method			
Regression mode	Elastic properties	Regression coefficient	Standardized regression coefficient
Linear Regression	E_{xx} C. O. D., R^2 = 0.89	β_0 = 51.898 β_1 = 0.012 β_2 = -0.003	 β_1 = 0.452 β_2 = -0.146

Continued on next page

Table 3.5 – continued from previous page

Regression mode	Elastic properties	Regression coefficient	Standardized regression coefficient
	Adjusted C. O. D., R^2_{adj} = 0.89	β_3 = -0.089 β_4 = 0.008	β_3 = -0.543 β_4 = 0.554
	E_{yy} C. O. D., R^2 = 0.82 Adjusted C. O. D., R^2_{adj} = 0.82	β_0 = 25.420 β_1 = 0.311 β_2 = 0.187 β_3 = -4.604 β_4 = -0.150	β_1 = 0.324 β_2 = 0.240 β_3 = -0.778 β_4 = -0.298
	E_{zz} C. O. D., R^2 = 0.79 Adjusted C. O. D., R^2_{adj} = 0.79	β_0 = 25.595 β_1 = 0.201 β_2 = 0.223 β_3 = -3.806 β_4 = 0.047	β_1 = 0.243 β_2 = 0.331 β_3 = -0.746 β_4 = 0.108
Quadratic without mixed terms	E_{xx} C. O. D., R^2 = 0.91 Adjusted C. O. D., R^2_{adj} = 0.90	β_0 = 51.50 β_1 = 0.101 β_2 = 0.037 β_3 = 0.230 β_4 = 0.014 β_5 = -0.009 β_6 = -0.005 β_7 = -0.319 β_8 = -0.013	β_1 = 3.814 β_2 = 1.727 β_3 = 1.405 β_4 = 1.008 β_5 = -3.370 β_6 = -1.875 β_7 = -1.945 β_8 = -0.464
	E_{yy} C. O. D., R^2 = 0.83 Adjusted C. O. D., R^2_{adj} = 0.82	β_0 = 22.235 β_1 = 2.952 β_2 = -1.587 β_3 = -3.200 β_4 = -0.256 β_5 = -0.257 β_6 = 0.200 β_7 = -1.423 β_8 = 0.212	β_1 = 3.077 β_2 = -2.034 β_3 = -0.540 β_4 = -0.509 β_5 = -2.749 β_6 = 2.273 β_7 = -0.240 β_8 = 0.218

Continued on next page

Table 3.5 – continued from previous page

Regression mode	Elastic properties	Regression coefficient	Standardized regression coefficient
	E_{zz} C. O. D., R^2 = 0.80 Adjusted C. O. D., R^2_{adj} = 0.79	β_0 = 24.701 β_1 = 1.657 β_2 = -1.269 β_3 = -1.939 β_4 = 0.112 β_5 = -0.142 β_6 = 0.168 β_7 = -1.860 β_8 = -0.130	β_1 = 2.005 β_2 = -1.889 β_3 = -0.380 β_4 = 0.259 β_5 = -1.764 β_6 = 2.219 β_7 = -0.365 β_8 = -0.155
Full Quadratic	E_{xx} C. O. D., R^2 = 0.91 Adjusted C. O. D., R^2_{adj} = 0.90	β_0 = 51.633 β_1 = 0.082 β_2 = 0.020 β_3 = 0.064 β_4 = -0.008 β_5 = -0.009 β_6 = -0.004 β_7 = -0.267 β_8 = -0.012 β_9 = 0.003 β_{10} = 0.018 β_{11} = 0.000 β_{12} = 0.003 β_{13} = 0.000 β_{14} = 0.039	β_1 = 3.074 β_2 = 0.912 β_3 = 0.392 β_4 = -0.555 β_5 = -3.429 β_6 = -1.774 β_7 = -1.630 β_8 = -0.460 β_9 = 0.845 β_{10} = 0.671 β_{11} = 0.051 β_{12} = 0.089 β_{13} = 0.121 β_{14} = 1.383
	E_{yy} C. O. D., R^2 = 0.84 Adjusted C. O. D., R^2_{adj} = 0.83	β_0 = 13.547 β_1 = 6.114 β_2 = 0.497 β_3 = -19.259 β_4 = -0.427 β_5 = -0.152 β_6 = 0.273 β_7 = 8.567 β_8 = 0.206 β_9 = -0.809 β_{10} = -1.408 β_{11} = 0.188	β_1 = 6.371 β_2 = 0.637 β_3 = -3.253 β_4 = -0.850 β_5 = -1.627 β_6 = 3.108 β_7 = 1.447 β_8 = 0.212 β_9 = -6.903 β_{10} = -1.441 β_{11} = 1.926 β_{12} = 2.845

Continued on next page

Table 3.5 – continued from previous page

Regression mode	Elastic properties	Regression coefficient	Standardized regression coefficient
		β_{12} = 2.957 β_{13} = -0.259 β_{14} = 0.727	β_{13} = -2.294 β_{14} = 0.723
	E_{zz} C. O. D., R^2 = 0.81 Adjusted C. O. D., R^2_{adj} = 0.80	β_0 = 15.085 β_1 = 4.798 β_2 = 0.709 β_3 = -12.871 β_4 = -0.600 β_5 = -0.018 β_6 = 0.233 β_7 = 8.934 β_8 = -0.132 β_9 = -0.743 β_{10} = -2.308 β_{11} = 0.131 β_{12} = 2.607 β_{13} = -0.180 β_{14} = 1.685	β_1 = 5.804 β_2 = 1.054 β_3 = -2.524 β_4 = -1.388 β_5 = -0.225 β_6 = 3.079 β_7 = 1.752 β_8 = -0.158 β_9 = -7.365 β_{10} = -2.742 β_{11} = 1.556 β_{12} = 2.911 β_{13} = -1.846 β_{14} = 1.943

Table 3.6: Regression coefficient, coefficient of determination, R^2 (C.O.D. R^2) and adjusted coefficient of determination, R_{adj} (Adjusted C.O.D.) under biaxial loading

Response surface method			
Regression mode	Elastic properties	Regression coefficient	Standardized regression coefficient
Linear regression	E_{xx} C. O. D., R^2 = 0.94 Adjusted C. O. D., R^2_{adj} = 0.94	β_0 = 51.881 β_1 = 0.009 β_2 = 0.002 β_3 = -0.093 β_4 = 0.028	β_1 = 0.151 β_2 = 0.045 β_3 = -0.247 β_4 = 0.887

Continued on next page

Table 3.6 – continued from previous page

Regression mode	Elastic properties	Regression coefficient	Standardized regression coefficient
	E_{yy} C. O. D., R^2 = 0.51 Adjusted C. O. D., R^2_{adj} = 0.51	β_0 = 20.395 β_1 = 0.274 β_2 = 0.088 β_3 = -2.545 β_4 = -0.467	β_1 = 0.202 β_2 = 0.080 β_3 = -0.304 β_4 = -0.657
	E_{zz} C. O. D., R^2 = 0.17 Adjusted C. O. D., R^2_{adj} = 0.15	β_0 = 20.738 β_1 = 0.014 β_2 = 0.240 β_3 = -1.034 β_4 = 0.102	β_1 = 0.014 β_2 = 0.297 β_3 = -0.168 β_4 = 0.196
Quadratic without mixed terms	E_{xx} C. O. D., R^2 = 0.96 Adjusted C. O. D., R^2_{adj} = 0.96	β_0 = 51.867 β_1 = 0.113 β_2 = -0.096 β_3 = -0.225 β_4 = 0.048 β_5 = -0.010 β_6 = 0.011 β_7 = 0.134 β_8 = -0.040	β_1 = 1.850 β_2 = -1.944 β_3 = -0.599 β_4 = 1.509 β_5 = -1.708 β_6 = 1.987 β_7 = 0.358 β_8 = -0.641
	E_{yy} C. O. D., R^2 = 0.54 Adjusted C. O. D., R^2_{adj} = 0.52	β_0 = -35.022 β_1 = 13.668 β_2 = 9.185 β_3 = 1.146 β_4 = -0.854 β_5 = -1.305 β_6 = -1.025 β_7 = -3.799 β_8 = 0.785	β_1 = 10.066 β_2 = 8.320 β_3 = 0.137 β_4 = -1.201 β_5 = -9.857 β_6 = -8.243 β_7 = -0.483 β_8 = 0.570
		β_0 = -24.273 β_1 = 12.630 β_2 = 6.346	β_1 = 12.682 β_2 = 7.837 β_3 = -0.732

Continued on next page

Table 3.6 – continued from previous page

Regression mode	Elastic properties	Regression coefficient	Standardized regression coefficient
	E_{zz} C. O. D., R^2 = 0.18 Adjusted C. O. D., R^2_{adj} = 0.15	β_3 = -4.497 β_4 = 0.108 β_5 = -1.230 β_6 = -0.688 β_7 = 3.416 β_8 = -0.001	β_4 = 0.208 β_5 = -12.670 β_6 = -7.546 β_7 = 0.556 β_8 = -0.001
Full Quadratic	E_{xx} C.O.D, R^2 = 0.97 Adjusted C.O.D, R^2_{adj} = 0.97	β_0 = 51.99 β_1 = 0.072 β_2 = -0.061 β_3 = -0.597 β_4 = 0.018 β_5 = 0.003 β_6 = 0.017 β_7 = 0.185 β_8 = -0.040 β_9 = -0.022 β_{10} = 0.015 β_{11} = -0.018 β_{12} = 0.052 β_{13} = 0.021 β_{14} = 0.054	β_1 = 1.188 β_2 = -1.239 β_3 = -1.591 β_4 = 0.563 β_5 = 0.474 β_6 = 2.886 β_7 = 0.492 β_8 = -0.653 β_9 = -2.905 β_{10} = 0.246 β_{11} = -2.882 β_{12} = 0.791 β_{13} = 2.988 β_{14} = 0.844
	E_{yy} C. O. D., R^2 = 0.57 Adjusted C. O. D, R^2_{adj} = 0.54	β_0 = -32.387 β_1 = 16.047 β_2 = 11.041 β_3 = -51.919 β_4 = 2.279 β_5 = -1.216 β_6 = -0.785 β_7 = 12.721 β_8 = 0.781 β_9 = -1.132 β_{10} = 3.478 β_{11} = 0.010 β_{12} = 4.109 β_{13} = -0.917 β_{14} = 1.781	β_1 = 11.818 β_2 = 10.002 β_3 = -6.197 β_4 = 3.207 β_5 = -9.186 β_6 = -6.317 β_7 = 1.519 β_8 = 0.568 β_9 = -6.831 β_{10} = 2.516 β_{11} = 0.069 β_{12} = 2.794 β_{13} = -5.727 β_{14} = 1.251

Continued on next page

Table 3.6 – continued from previous page

Regression mode	Elastic properties	Regression coefficient	Standardized regression coefficient
	E_{zz} C. O. D., R^2 = 0.23 Adjusted C. O. D., R^2_{adj} = 0.17	β_0 = -25.267 β_1 = 14.938 β_2 = 9.513 β_3 = -53.766 β_4 = 2.824 β_5 = -0.841 β_6 = -0.361 β_7 = 20.150 β_8 = -0.019 β_9 = -1.629 β_{10} = 2.092 β_{11} = -0.430 β_{12} = 4.772 β_{13} = -0.399 β_{14} = 2.549	β_1 = 14.999 β_2 = 11.749 β_3 = -8.750 β_4 = 5.419 β_5 = -8.666 β_6 = -3.955 β_7 = 3.280 β_8 = -0.019 β_9 = -13.402 β_{10} = 2.063 β_{11} = -4.243 β_{12} = 4.423 β_{13} = -3.402 β_{14} = 2.440

In this study, a response surface model is used to determine the uncertain input variables to the fabric response outputs. We establish two types of second-order regression models by separating the mixed terms (quadratic without mixed terms) and fully quadratic terms (main effect, quadratic terms and interactions terms). The response surface models are well-replicated under uni-axial loading for all output parameters while only the response surface model of E_{xx} is well-replicated under biaxial loading. This can be seen through the comparison of R^2 values obtained wherein the R^2 values are approximately greater than 0.80.

Theoretically, a higher order of the polynomials leads to the higher values of coefficient of determination and adjusted coefficient of determination. This has been proven by the results in Tab. 3.5 and Tab. 3.6, where as the polynomial order becomes higher, the R^2 value for each elastic moduli becomes larger. For example, E_{yy} in all regression modes under uni-axial loading contributed $R^2 = 0.82$ for linear regression, $R^2 = 0.83$ for quadratic without mixed terms and $R^2 = 0.84$ for full quadratic analysis. Under biaxial loading, it can be seen that the R^2 values for E_{xx} in each regression modes are higher than the R^2 values for E_{xx} under uni-axial loading.

We should recall that when loaded in the transverse direction, the fibrous composite (fibre and matrix) experience the same stress. This relates to the effect of yarn materials, the volume fraction of yarns, orientation of the yarns and loading cases. For instance, we found that E_{yy} and E_{zz} results in all regression modes under biaxial loading are low. E_{yy}

contributes 0.51, 0.54 and 0.57 whilst E_{zz} with 0.17, 0.18 and 0.23 with respect to the linear, quadratic without mixed term and full quadratic regressions, respectively. These are caused by the yarn orientation effect that behave towards the load given and other related factors as discussed previously. Contour plot is a helpful visualization of the response surface when the measured input variables are no more than three. Since the uncertain input variables are more than three, it is impossible to visualize the response surface. For that reason, in order to locate the optimum value, finding the stationary point could be the best approach.

Concerning the shear moduli, the values of R^2 are too low in order to derive a conclusion from the response surface model. Moreover, as only axial modes (uni-axial and biaxial) are considered in our studies, shear effects seem to be negligible. It is favourable to highlight that the analysis is focused on a 2D-weave only and the samples are assumed to be perfectly aligned in the arrangements. As mentioned earlier, the R_{adj} takes into account only the independent variables that assist in explaining the variation of the dependent variable. It means that the R^2 will increase if more independent variables (uncertainty parameters) are added to the regression, however the R_{adj} will only increase if the independent variables that are added to the regression affect the overall explanatory power of the regression. It is found that the values of R^2 and R_{adj} are approximately similar which reflects that a sufficient number of samples have evaluated.

Unfortunately, a high R^2 does not give any guarantee for the accuracy of the fit of the model. The reason is that a high R^2 can occur in the presence of misspecification of the functional form of a correlation. With regards to this, the evaluation of R^2 values cannot be fully taken as an evaluation of sensitivity analysis for the uncertainty parameters in which the approach does not quantify the dominant factor significantly. It is important to note that each coefficient is influenced by the other variables in a regression model. Due to the uncertainty parameters that are nearly always inter-related, two or more variables may explain the same variation in material properties.

Therefore, each coefficient does not explain the total-effect on material properties of its corresponding variable, as it would if it was the only variable in the model. Rather, each coefficient represents the additional effect of adding that variable into the model, if the effects of all other variables in the model are already accounted for. Therefore, each coefficient will change when other variables are added to or deleted from the model. As a conclusion, the response surface model is an empirical statistical modelling that is able to develop an appropriate approximating relationship between the fabric response (elastic properties) and the input variables.

3.4.3 Sensitivity indices (Sobol's indices)

Tab. 3.7 and Tab. 3.8 depict the first-order and total-effect sensitivity indices that demonstrate the influences of uncertainty parameters on material properties.

Table 3.7: Main effect and total-effects sensitivity indices of uncertainty parameters on *MataBerkait*-dry woven fabric elastic properties under uni-axial loading: 1 - yarn spacing; 2 - yarn width; 3 - yarn height; 4 - friction coefficient

Material properties	Linear regression	Quadratic without mixed term	Full quadratic
E_{xx}	Main effect indices, $\hat{S}_i$ $\hat{S}_1$ = 0.15 $\hat{S}_2$ = 0.04 $\hat{S}_3$ = 0.33 $\hat{S}_4$ = 0.37 $\sum_{i=1}^{4} \hat{S}_i$ = 0.89	Main effect indices, $\hat{S}_i$ $\hat{S}_1$ = 0.14 $\hat{S}_2$ = 0.03 $\hat{S}_3$ = 0.31 $\hat{S}_4$ = 0.43 $\sum_{i=1}^{4} \hat{S}_i$ = 0.91	Main effect indices, $\hat{S}_i$ $\hat{S}_1$ = 0.14 $\hat{S}_2$ = 0.03 $\hat{S}_3$ = 0.32 $\hat{S}_4$ = 0.42 $\sum_{i=1}^{4} \hat{S}_i$ = 0.91
	Total-effect indices, $\hat{S}_{Ti}$ $\hat{S}_{T1}$ = 0.20 $\hat{S}_{T2}$ = 0.04 $\hat{S}_{T3}$ = 0.33 $\hat{S}_{T4}$ = 0.39 $\sum_{i=1}^{4} \hat{S}_{Ti}$ = 0.96	Total-effect indices, $\hat{S}_{Ti}$ $\hat{S}_{T1}$ = 0.20 $\hat{S}_{T2}$ = 0.04 $\hat{S}_{T3}$ = 0.33 $\hat{S}_{T4}$ = 0.39 $\sum_{i=1}^{4} \hat{S}_{Ti}$ = 0.96	Total-effect indices, $\hat{S}_{Ti}$ $\hat{S}_{T1}$ = 0.21 $\hat{S}_{T2}$ = 0.04 $\hat{S}_{T3}$ = 0.33 $\hat{S}_{T4}$ = 0.39 $\sum_{i=1}^{4} \hat{S}_{Ti}$ = 0.97
E_{yy}	Main effect indices, $\hat{S}_i$ $\hat{S}_1$ = 0.07 $\hat{S}_2$ = 0.06 $\hat{S}_3$ = 0.59 $\hat{S}_4$ = 0.10 $\sum_{i=1}^{4} \hat{S}_i$ = 0.82	Main effect indices, $\hat{S}_i$ $\hat{S}_1$ = 0.08 $\hat{S}_2$ = 0.06 $\hat{S}_3$ = 0.59 $\hat{S}_4$ = 0.10 $\sum_{i=1}^{4} \hat{S}_i$ = 0.83	Main effect indices, $\hat{S}_i$ $\hat{S}_1$ = 0.08 $\hat{S}_2$ = 0.06 $\hat{S}_3$ = 0.60 $\hat{S}_4$ = 0.10 $\sum_{i=1}^{4} \hat{S}_i$ = 0.84
	Total-effect indices, $\hat{S}_{Ti}$ $\hat{S}_{T1}$ = 0.08 $\hat{S}_{T2}$ = 0.06 $\hat{S}_{T3}$ = 0.59 $\hat{S}_{T4}$ = 0.10 $\sum_{i=1}^{4} \hat{S}_{Ti}$ = 0.83	Total-effect indices, $\hat{S}_{Ti}$ $\hat{S}_{T1}$ = 0.09 $\hat{S}_{T2}$ = 0.07 $\hat{S}_{T3}$ = 0.60 $\hat{S}_{T4}$ = 0.10 $\sum_{i=1}^{4} \hat{S}_{Ti}$ = 0.86	Total-effect indices, $\hat{S}_{Ti}$ $\hat{S}_{T1}$ = 0.09 $\hat{S}_{T2}$ = 0.08 $\hat{S}_{T3}$ = 0.60 $\hat{S}_{T4}$ = 0.10 $\sum_{i=1}^{4} \hat{S}_{Ti}$ = 0.87

Continued on next page

Table 3.7 – continued from previous page

Material properties	Linear regression	Quadratic without mixed term	Full quadratic
E_{zz}	Main effect indices, $\hat{S}_i$ $\hat{S}_1$ = 0.05 $\hat{S}_2$ = 0.13 $\hat{S}_3$ = 0.60 $\hat{S}_4$ = 0.01 $\sum_{i=1}^{4} \hat{S}_i$ = 0.79	Main effect indices, $\hat{S}_i$ $\hat{S}_1$ = 0.05 $\hat{S}_2$ = 0.13 $\hat{S}_3$ = 0.60 $\hat{S}_4$ = 0.02 $\sum_{i=1}^{4} \hat{S}_i$ = 0.80	Main effect indices, $\hat{S}_i$ $\hat{S}_1$ = 0.05 $\hat{S}_2$ = 0.13 $\hat{S}_3$ = 0.61 $\hat{S}_4$ = 0.02 $\sum_{i=1}^{4} \hat{S}_i$ = 0.81
	Total-effect indices, $\hat{S}_{Ti}$ $\hat{S}_{T1}$ = 0.05 $\hat{S}_{T2}$ = 0.13 $\hat{S}_{T3}$ = 0.61 $\hat{S}_{T4}$ = 0.01 $\sum_{i=1}^{4} \hat{S}_{Ti}$ = 0.80	Total-effect indices, $\hat{S}_{Ti}$ $\hat{S}_{T1}$ = 0.06 $\hat{S}_{T2}$ = 0.13 $\hat{S}_{T3}$ = 0.61 $\hat{S}_{T4}$ = 0.02 $\sum_{i=1}^{4} \hat{S}_{Ti}$ = 0.82	Total-effect indices, $\hat{S}_{Ti}$ $\hat{S}_{T1}$ = 0.07 $\hat{S}_{T2}$ = 0.13 $\hat{S}_{T3}$ = 0.61 $\hat{S}_{T4}$ = 0.03 $\sum_{i=1}^{4} \hat{S}_{Ti}$ = 0.84

Table 3.8: Main effect and total-effects sensitivity indices of uncertainty parameters on *MataBerkait*-dry woven fabric elastic properties under biaxial loading: 1 - yarn spacing; 2 - yarn width; 3 - yarn height; 4 - friction coefficient

Material properties	Linear regression	Quadratic without mixed term	Full quadratic
E_{xx}	Main effect indices, $\hat{S}_i$ $\hat{S}_1$ = 0.02 $\hat{S}_2$ = 0.00 $\hat{S}_3$ = 0.06 $\hat{S}_4$ = 0.86 $\sum_{i=1}^{4} \hat{S}_i$ = 0.94	Main effect indices, $\hat{S}_i$ $\hat{S}_1$ = 0.02 $\hat{S}_2$ = 0.00 $\hat{S}_3$ = 0.05 $\hat{S}_4$ = 0.89 $\sum_{i=1}^{4} \hat{S}_i$ = 0.96	Main effect indices, $\hat{S}_i$ $\hat{S}_1$ = 0.05 $\hat{S}_2$ = 0.00 $\hat{S}_3$ = 0.06 $\hat{S}_4$ = 0.86 $\sum_{i=1}^{4} \hat{S}_i$ = 0.97
	Total-effect	Total-effect	Total-effect

Continued on next page

Table 3.8 – continued from previous page

Material properties	Linear regression	Quadratic without mixed term	Full quadratic
	indices, $\hat{S}_{Ti}$ $\hat{S}_{T1}$ = 0.03 $\hat{S}_{T2}$ = 0.02 $\hat{S}_{T3}$ = 0.08 $\hat{S}_{T4}$ = 0.86 $\sum_{i=1}^{4} \hat{S}_{Ti}$ = 0.99	indices, $\hat{S}_{Ti}$ $\hat{S}_{T1}$ = 0.03 $\hat{S}_{T2}$ = 0.02 $\hat{S}_{T3}$ = 0.08 $\hat{S}_{T4}$ = 0.89 $\sum_{i=1}^{4} \hat{S}_{Ti}$ = 1.02	indices, $\hat{S}_{Ti}$ $\hat{S}_{T1}$ = 0.03 $\hat{S}_{T2}$ = 0.01 $\hat{S}_{T3}$ = 0.09 $\hat{S}_{T4}$ = 0.94 $\sum_{i=1}^{4} \hat{S}_{Ti}$ = 1.07
E_{yy}	Main effect indices, $\hat{S}_i$ $\hat{S}_1$ = 0.03 $\hat{S}_2$ = 0.01 $\hat{S}_3$ = 0.07 $\hat{S}_4$ = 0.40 $\sum_{i=1}^{4} \hat{S}_i$ = 0.51	Main effect indices, $\hat{S}_i$ $\hat{S}_1$ = 0.03 $\hat{S}_2$ = 0.01 $\hat{S}_3$ = 0.09 $\hat{S}_4$ = 0.41 $\sum_{i=1}^{4} \hat{S}_i$ = 0.54	Main effect indices, $\hat{S}_i$ $\hat{S}_1$ = 0.01 $\hat{S}_2$ = 0.00 $\hat{S}_3$ = 0.08 $\hat{S}_4$ = 0.48 $\sum_{i=1}^{4} \hat{S}_i$ = 0.57
	Total-effect indices, $\hat{S}_{Ti}$ $\hat{S}_{T1}$ = 0.03 $\hat{S}_{T2}$ = 0.01 $\hat{S}_{T3}$ = 0.08 $\hat{S}_{T4}$ = 0.42 $\sum_{i=1}^{4} \hat{S}_{Ti}$ = 0.54	Total-effect indices, $\hat{S}_{Ti}$ $\hat{S}_{T1}$ = 0.04 $\hat{S}_{T2}$ = 0.02 $\hat{S}_{T3}$ = 0.10 $\hat{S}_{T4}$ = 0.42 $\sum_{i=1}^{4} \hat{S}_{Ti}$ = 0.58	Total-effect indices, $\hat{S}_{Ti}$ $\hat{S}_{T1}$ = 0.01 $\hat{S}_{T2}$ = 0.00 $\hat{S}_{T3}$ = 0.10 $\hat{S}_{T4}$ = 0.49 $\sum_{i=1}^{4} \hat{S}_{Ti}$ = 0.60
E_{zz}	Main effect indices, $\hat{S}_i$ $\hat{S}_1$ = 0.00 $\hat{S}_2$ = 0.09 $\hat{S}_3$ = 0.03 $\hat{S}_4$ = 0.04 $\sum_{i=1}^{4} \hat{S}_i$ = 0.17	Main effect indices, $\hat{S}_i$ $\hat{S}_1$ = 0.01 $\hat{S}_2$ = 0.10 $\hat{S}_3$ = 0.03 $\hat{S}_4$ = 0.04 $\sum_{i=1}^{4} \hat{S}_i$ = 0.18	Main effect indices, $\hat{S}_i$ $\hat{S}_1$ = 0.03 $\hat{S}_2$ = 0.10 $\hat{S}_3$ = 0.04 $\hat{S}_4$ = 0.06 $\sum_{i=1}^{4} \hat{S}_i$ = 0.23
	Total-effect indices, $\hat{S}_{Ti}$ $\hat{S}_{T1}$ = 0.04 $\hat{S}_{T2}$ = 0.14	Total-effect indices, $\hat{S}_{Ti}$ $\hat{S}_{T1}$ = 0.01 $\hat{S}_{T2}$ = 0.10	Total-effect indices, $\hat{S}_{Ti}$ $\hat{S}_{T1}$ = 0.03 $\hat{S}_{T2}$ = 0.10

Continued on next page

Table 3.8 – continued from previous page

Material properties	Linear regression	Quadratic without mixed term	Full quadratic
	$\hat{S}_{T3}$ = 0.07 $\hat{S}_{T4}$ = 0.00 $\sum_{i=1}^{4} \hat{S}_{Ti}$ = 0.25	$\hat{S}_{T3}$ = 0.03 $\hat{S}_{T4}$ = 0.05 $\sum_{i=1}^{4} \hat{S}_{Ti}$ = 0.19	$\hat{S}_{T3}$ = 0.04 $\hat{S}_{T4}$ = 0.07 $\sum_{i=1}^{4} \hat{S}_{Ti}$ = 0.24

Based on the results in Tab. 3.7, it can clearly be observed that a strong interaction between the uncertain input variables lies in E_{xx}. A relative difference can be measured as such E_{xx} under uni-axial loading where the difference, $\hat{S}_{Ti} - \hat{S}_i$ are 0.07, 0.05 and 0.06 for linear, quadratic without mixed term and full quadratic regressions, respectively. The difference between $\hat{S}_i$ and $\hat{S}_{Ti}$ values for E_{yy} can be concluded as 0.01 : 0.03 : 0.03 whilst E_{zz} with 0.01 : 0.02 : 0.03. It seems that the differences are considered small for transverse directions.

Furthermore, it is found that the friction coefficient is the most influential uncertain variable in E_{xx} values. The $\hat{S}_4$ (friction coefficient) in each regression modes are obtained as 0.39 for E_{xx}. The yarn height $\hat{S}_3$ followed the rank with 0.33 for all regression modes. The least influential variable in E_{xx} values is yarn width variations. This is agreeable due to the relationship between yarn height and yarn width ratio. This is because the yarn width and yarn height are correlated with the yarn cross-sectional aspect ratio, AR_y. Concurrently, the decreases of yarn width indices increase the yarn height indices or vice versa. In contrast, the most dominant variable in E_{yy} and E_{zz} values is yarn height variation. Again, the yarn width is the least contributor to the E_{yy} values however shows a better performance in E_{zz} for all regression modes. It is also discovered that the yarn spacing presented itself as a variable with marginal importance in all regression modes under uni-axial loading case.

Under biaxial loading case, it is observed that the friction coefficient behaves dominantly in E_{xx} and E_{yy} with more than 80% and 40%, respectively. Contradictorily, the dominant variable in E_{zz} is given by yarn width variable with 10% of the total contribution. It is also discovered that the value of $\hat{S}_{Ti}$ is greater than $\hat{S}_i$ for all mode of regression in each stiffness properties. The presence of interactions in the model can be calculated by $1-\Sigma_i S_i$. With the presence of interaction between the uncertainty variable and the response output (stiffness properties), significantly the value of S_{Ti} is greater than S_i. The difference, $S_{Ti} - S_i$ is a measure of how much uncertainty variable is involved in interactions with any other uncertainty variable.

In addition, it is observed that most of the total-effect indices are less than 1 except for E_{xx} under biaxial loading. This shows that the uncertain input variable is non-additive to all stiffness properties under uni-axial loading and similarly to E_{yy} and E_{zz} for biaxial loading. Overall, the dominance of each uncertain input variable also affected by the loading modes and the yarn properties. Again, the yarn properties that include the orientation of the yarns, size and shape of the yarns and the fibrous composite may affect the stiffness values. For instance, the friction coefficient variable becomes dominant in both loading cases for E_{xx} and only for E_{yy} under biaxial loading.

By definition, S_{Ti} is greater than S_i or equal to S_i in the case that one uncertainty variable is not involved in any interaction with other uncertainty variables. However, if $S_{Ti} = 0$, it reflects that uncertainty variable is non-influential and can be fixed anywhere in its distribution without affecting the variance of the response output. Furthermore, the sum of all S_i is equal to 1 for additive models whilst less than 1 for non-additive models. Conclusively, a reliable result has been obtained through Sobol's indices compared to other approaches.

Chapter 4

Probabilistic multi-scale optimization of hybrid laminated composites

This chapter delineates the concept of EA and ACO for multi-objective optimization in hybrid laminated composites as a whole. The metric of performance is evaluated through the evaluation of the optimization tasks given. This chapter also elaborates on how the structure in the mesoscopic level incorporates the micro-mechanical performance of the yarns (fine-scale optimization) whereas the modelling of the structure in the macroscopic level incorporates the mesoscopic performance of the unit cells and therefore the microscopic performance of the yarns (coarse-scale optimization). In Section 4.3, the fine-scale optimization problem is described wherein the single objective optimization is done with stochastic effects for a selected set of uncertainties. In Section 4.4, the coarse-scale formulation is elaborated considering the multi-objective optimization for hybrid laminated composites. The mathematical formulation of the fundamental frequency and buckling load factor for hybrid laminated composites are derived in subsection 4.4.2. The application of ACO to analyse the multi-objective optimization problems is formulated in subsection 4.4.1. Section 4.3.1 and 4.4.3 delineate the single- and multi-objective optimization problems, respectively.

4.1 Literature review

4.1.1 Review of hybrid laminated composites

The use of hybrid laminated composites in aerospace, defense, marine, and automotive industries have been dominated in recent years due to their outstanding properties. Unlike isotropic materials, hybrid laminated composites hold a great strength/weight or elasticity/weight ratios. Their inherent tailorability (RL09b) have made them popular among the hybrid laminates. Thus, the lay-up sequence optimization of hybrid laminated composite structures is crucial for improving the specific design objectives in advanced industries. There are numerous of hybrid laminated composites available for instance interply hybrid, intraply hybrid, intermingled mixed hybrid, selective placement hybrid and super hybrids laminates, see Fig. 4.1. The hybrid laminates are defined as follows: (i) interply hybrids are the stacking ply of two or more homogeneous reinforcements; (ii) intraply hybrids consist a mixture of tows with two or more constituent fibre types in the same ply; (iii) intermingled mixed hybrids are a random mixture of the constituent fibre types with no concentrations of

either type are present in the material; (iv) selective placement is referred to the placing of reinforcements wherein additional strength is needed on top of the base reinforcing laminate ply; and (v) super-hybrid composites are composed by specified orientations and sequences of foils or metal stacking (PFMP04).

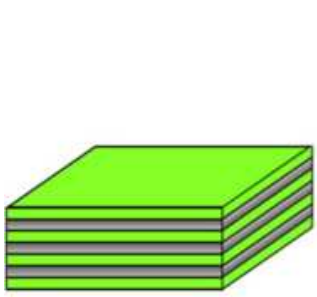

(a) Interply hybrid (SCB$^+$14)

(b) Intraply hybrid (SCB$^+$14)

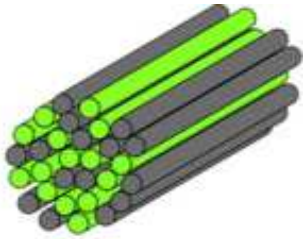

(c) Intermingled mixed hybrid (SCB$^+$14)

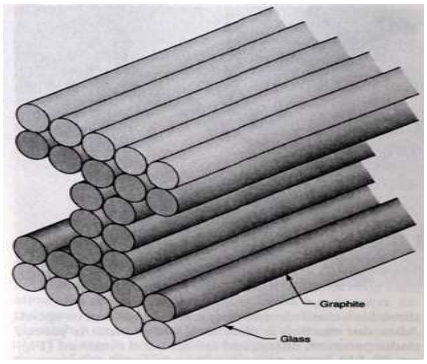

(d) Selective placement hybrid

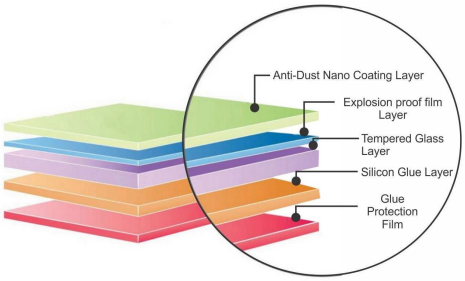

(e) Super-hybrid

Figure 4.1: Types of hybrid laminated composites

Laminates are referred to multiple stacking plies of fibre-reinforced composites that binded permanently. A lamina is a flat or a curved arrangement of unidirectional or woven fibres embedded in a matrix material. It is commonly assumed to be orthotropic, and its thickness depends on the material from which it is made. Their properties mainly depend on a complicated combination of their structural units and their interactions. The complicated nature of the laminated textiles mechanics makes them ideal candidates for a mechanical analysis using computer-based methods. According to the integrated textile modelling concept, the only inputs in the total design procedure are the fibre properties, the yarn structure and the fabric structure (VKDP11). Correspondingly, these could be the basis in predicting the mesoscopic uncertainty parameters for laminated textile composites. In many engineering applications, it is reasonable to make use of standard layers with certain thicknesses and limited number of angles. Furthermore, in the most practical laminate applications only the fibre directions in plies and ply thicknesses are different - the material remains the same.

Practically, the lay-up sequence problems are designed as follows: Consider a laminate made up of N plies which consist of different orientation for m number of distinct plies from 1 to N. The algorithm is generated through the sequence of complete lay-ups and

this algorithm is used to find the best lay-ups which satisfies several design constraints. Since it is essential to specify a solution coding, the choice of the coding that provides effectiveness in the moves and solution evaluations is determined to ensure the success of the heuristic search. For laminate lay-up sequence optimizations, each string candidate represents a lay-up sequence design of a composite laminate. Each string is encoded in an array of r ($r_i; i = 1, 2, ..N$) by stacking all ply-angles of the given composite laminate system. The r stands for the ply angles and N is the number of plies. For instance, a laminate with $[30^\circ{}_2, \pm 45^\circ, 90^\circ{}_2, 0^\circ{}_2]_s$ array. The rightmost number refers to the ply that closest to the laminate plane of symmetry whilst the leftmost 3 numbers describe the outer ply. The knowledge of dynamic characteristics, i.e. natural frequencies and mode shapes of structural components has been a great interest in the study of structural responses to various excitations (KLTM07). Resonance is a phenomenon of external excitation and relevant to maximum frequency problems in laminated structures.

4.1.2 Meta-heuristics operators in optimization problems

Numerous computational approaches have been implemented for dynamic analysis of complex structures utilizing the finite element method and fast growth of high-speed computing capability (KLTM07). In the context of multi-objective optimization, the conventional mathematical optimization algorithms are irrelevant due to the problematic in obtaining the set of Pareto optimal solutions of many multi-objective optimization problems. In light of this, stochastic methods have been introduced to solve the respective issues.

Variety of meta-heuristics have been developed and widely utilized, such as genetic algorithm (GA), ant colony optimization (ACO), simulated annealing (SA), scatter search (SS), non-dominated sorting genetic algorithm (NSGA-II), particle swarm optimization (PSO) and others (AE07, CJKO01, NLA$^+$08, LFZ$^+$10, HL92, OK95). A meta-heuristic is an iterative generation process which guides a subordinate heuristic by combining intelligently different concepts for exploring and exploiting the search space, learning strategies are used to structure information in order to find efficiently near-optimal solutions. To summarize, the fundamental properties of meta-heuristics are as follows (BR03);

a. Meta-heuristics are strategies that "guide" the search process.

b. Able to efficiently explore the search space in order to find optimal solutions.

c. Meta-heuristic algorithms techniques range from simple local search procedures to complex learning processes.

d. Meta-heuristic algorithms are approximate and usually non-deterministic.

e. Meta-heuristics may incorporate mechanisms to avoid getting trapped in confined areas of the search space.

f. The fundamental concepts of meta-heuristics permit an abstract level description.

g. Meta-heuristics are not problem-specific.

h. Meta-heuristics may make use of domain-specific knowledge in the form of heuristics that are controlled by the upper level strategy.

i. Advanced meta-heuristics use search experience (embodied in some form of memory) to guide the search.

Tab. 4.1 shows the most important components in classifying the meta-heuristics.

Table 4.1: Classification of Meta-heuristics

Meta-Heuristics Component	Attributes
Nature-inspired vs. non-nature inspired	Nature-inspired algorithms: Genetic Algorithm, Ant Algorithms Non-nature-inspired algorithms: Tabu Search, Iterated Local Search.
Population-based vs. Single point search	Population-based algorithm: Ant-Colony (perform search processes which describe the evolution of set of points in the search space. Single-point search: Tabu Search, Iterated Local Search, Variable Neighbourhood Search
Dynamic vs. Static Objective Function	Static objective function: Keep objective function ”as-it-is” Dynamic objective function: Guided Local Search
One vs. Various Neighbourhood Structures	One Neighbourhood Structure: Most meta-heuristics algorithm work on one single neighbourhood structure. Various Neighbourhood Structure: Variable Neighbourhood Search (VNS)
Memory usage vs. Memory-loss methods	Memory-less algorithms perform a Markov process. Normally differentiate between te use of short term memory or long term memory.

An important task in multi-objective optimization is to identify a set of optimal trade-off solutions (called a Pareto-optimal solution) between the conflicting objectives, which helps gain a better understanding of the problem structure and supports the decision-maker in choosing the best compromise solution for the considered problem. It can be regarded as a population-based stochastic generate-and-test algorithm. It deals simultaneously with a set of possible solutions (so-called population), which allows to find an entire set of Pareto-optimal solutions in a single run of the algorithm. This approach is differently to the traditional mathematical programming techniques, which performing a series of separate runs in finding the optimal solution. In addition, evolutionary algorithm is less liable to the shape or continuity of the Pareto-optimal solution, whereas these two factors are the main interest for mathematical programming techniques (Coe99).

Various types of solution strategy have been adopted in solving the optimization problems with respect to the cost, the weight and the fundamental frequency. Grenestedt (Gre89), Reiss and Ramachandran (RR87) and Bert (Ber77) explored the single optimization of fundamental frequency for hybrid laminated composites by implementing continuous design variables. Duffy and Adali (AS92, DA91) delineated the cost minimization, the fundamental frequency and frequency separation on cross-ply laminates as an extension of Adali’s

work (Ada84) for anisotropic laminates. More investigations on weight and cost minimization and fundamental frequency maximization can be retrieved in Fukunaga *et al.* (FSS94), Adali and Verijenko (AV01), Tahani and Abachizadeh (AT09), Grosset *et al.* (GVH01), Kolahan *et al.* (KTS05) and the most recent by Hemmatian *et al.* (HFSB13). Grosset *et al.* (GVH01) adopted the approach of genetic algorithm (GA) whilst Kolahan *et al.* (KTS05) and Hemmatian *et al.* (HFSB13) simulated with simulated annealing and ant colony optimization, respectively.

EA and ACO are chosen as the optimization problem operators in this study. The EA is used due to the ability of genetic operators to explore the search space (the most typical genetic operators are reproduction, mutation, and recombination). It is also robust with respect to noisy evaluation functions. In addition, the reproduction operator uses a bias toward good-quality individuals wherein the better the fitness function value of an individual, the higher the probability that the individual will be selected and therefore be part of the next generation. The EA is less liable to the shape or continuity of the Pareto-optimal solution, thus we proposed the ACO as helping factor to guide the exploration and to increase the control of exploitation. The ACO is employed to speed up the local search and improve precision of solutions. The artificial ants implement a randomized construction heuristic which makes probabilistic decisions. Pheromone evaporation also has the advantage of avoiding the convergence to a locally optimal solution. This is differently to the gradient based numerical optimization technology which often gives local optima in non-linear problem and optimization algorithm can easily get stuck in one of local optima.

4.2 Mesoscopic uncertainty parameters

Experimental test are the most reliable and common source to identify material properties. However, via numerical models, deterministic results are obtained in output whereas in actual experiments there are usually probabilistic results every time that the tests are repeated. Although the experimental results may having acceptable standard deviations, their differences are still indicative of unavoidable noise tolerances in fabric responses. This is caused by the presence of uncertainties that are intrinsic to the nature of fabric materials and test set-ups. Thus, it is essential to design an ideal unit cell models that are incapable of representing uncertainties in the real fabric behaviour. This study focuses on geometrical uncertainty parameters only that commonly present in the fabric at unloaded configurations which caused by poor manufacturing procedures (KM10).

Among the geometrical parameters, yarn spacing, height, width and misalignment of yarn angles (under a closer view) are the most important parameters for woven fabric unit cells. The configuration of yarn geometry is given in Fig. 3.3. Yarn spacing primarily relates to the fabric arrangement and has a major influence on fabric macro-scale mechanical properties and the appearance (IB96). Here, the yarn spacing is defined as the distance between the right-hand edges of the picks in woven fabric. The geometrical designation of basic yarn is given in (ALB$^+$14). A uniform yarn spacing in fabrics is prominent and excessive variation of yarn spacing can be considered as a fabric imperfection. Commonly, a yarn spacing variation exists due to the yarn count variation, improper settings and adjustments of the machine parameters, eccentricity and wear in the motion transmission system.

Yarn weight refers to the thickness of yarn (yarn height), t_y. The higher the yarn weight,

the heavier the yarn (ALB$^+$14). The yarn width w_y, has an inter-related correlation with the yarn height, t_y. The details of positive- and negative-yarn misalignments are depicted in Fig. 4.2(a) and Fig. 4.2(b), respectively. The yarn alignment depends on the way the yarn is placed in the fixture or how it was prepared.

In fact, misalignment of the yarns angle is an important factor as the misaligned orientation of the fibrils in the yarn significantly affect the stiffness and failure pattern of the yarn in contrast to a yarn of perfectly aligned fibrils (XN11). The experimental work by Lussier and Chen (LC02) confirmed that misalignment in a yarn under tension condition, causes large increases in load and stiffness rather than under shear condition. Milani *et al.* (MNAH07) added that the effect of misalignment of yarn angles becomes more significant as the weave structure becomes more complicated. Correct estimates of the tolerance value intervals are crucial for reliable output predictions.

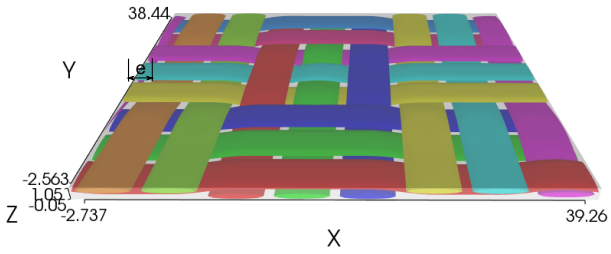

(a) Positive misalignment

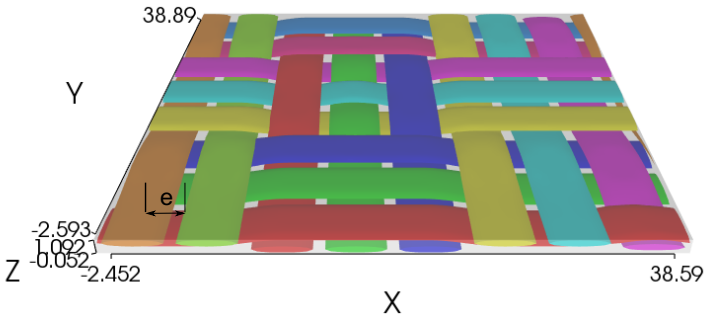

(b) Negative misalignment

Figure 4.2: Misalignments in yarns

Stochastic variation of input parameters like material properties, geometry thicknesses, load cases, etc. can significantly affect the results of simulations obtained at nominal values of input parameters (PGWT10). A normal distribution is the common applied statistical distribution in engineering industry. During the fabrication process, uncertainties (e.g. measurement errors) may occur and contribute to the variations of fabric strengths which follow a normal distribution (Zha10b). The details of uncertain mesoscopic parameters in optimizing the lamina are delineated as follows (KM12):

a. **Yarn spacing,** s_y

b. **Yarn width,** w_y

c. **Yarn height,** t_y

d. **Misalignment in yarn angle,** e°**.**

Tab. 4.2 shows the tolerances of the four uncertain mesoscopic parameters used in the optimization problem analyses.

Table 4.2: The tolerance value intervals of mesoscopic uncertainty parameters (KM12)

Uncertain mesoscopic parameter	**Base parameter value**	**Lower bound**	**Upper bound**	**Data sources**
Yarn spacing, s_y	5.13 mm	-2.5 %	2.5 %	Peng and Cao(PC02)
Yarn width, w_y	4.44 mm	-3.55 %	3.55 %	Peng and Cao(PC02)
Yarn height, t_y	0.5 mm	-4.0 %	4.0 %	upper estimation of Komeili and Milani(KM12)
Misalignment in yarn angle, e°	0°	-5°	+5°	Milani *et al.*(MNAH07) Komeili and Milani(KM12)

4.3 Optimization at the fine-scale

We consider a single-objective optimization of a lamina under uncertain mesoscopic parameters and apply the evolutionary algorithm (EA) for arbitrary complex computational models in fine-scale optimization problem. An evolutionary algorithm (EA) is a population-based stochastic meta-heuristic for optimization. Candidate solutions are iteratively optimized with respect to a fitness function that measures the solution quality (ES03, BKBR13).

This section also explains the uncertainties that often exist in lamina at meso-level and elaborates the influence on the macroscopic elastic properties of lamina at macro-level. This study considers only on geometrical uncertainty parameters and a range of variation has been identified as in 4.2. The goal of the evolutionary optimization process is to find the best lamina pattern that maximizes its macroscopic elastic properties, conducted by EA under the following uncertain mesoscopic parameters: yarn spacing, yarn height, yarn width and misalignment of yarn angle. The conducted optimization processes are inspired by (BKBR13) with a consideration of sensitivity analysis in the geometrical uncertainty parameters. An equal representation of the upper and lower bounds of the variables are presented to ensure a significant statistical analysis. In this case, the Latin Hypercube Sampling (LHS) is used as a random sample parameter distribution into equal probability intervals (IC80). Each variable is assumed to be uniformly distributed due to insufficient information with respect to the meso-scale uncertain input parameters.

4.3.1 A fine-scale optimization problem formulation

The optimization begins with a random initialization of weave patterns in population. The weave patterns are inspired by patterns that commonly applied in Malaysian craft products

motivated by Ilyani *et al.* (BKBR13) with a number notation 8X8. There are 66 weave patterns chosen as shown in Fig. 4.3 (MHD89). The first number in the notation defines the number of warp yarns and the later number refers to weft yarns.

The algorithm illustrated in Fig. 2.12 is adopted in our fine-scale optimization problem. The fitness function is evaluated for each pattern and each uncertain mesoscopic parameter set. The sets of uncertain mesoscopic parameters are designed by utilizing LHS. The lamina is modelled by TexGen (LBL11) package and analysed by ABAQUS/Standard Version 6.12 (HIoRI12). Periodic boundary conditions are applied using 'Equation' option in ABAQUS based on voxel-based meshing using 8 node 3D linear brick elements (BKBR13). The basic idea of using periodic boundary conditions is to assume that a part on macro level consists of a number of lamina's in which each basic mechanical element determines the global constitutive law of the material on macro level. We adopt the approach by Li and Wongsto (LW04) for periodic boundary condition in our study.

The initial population of this study is produced according to the optimization flow scheme as illustrated in Fig. 2.13. Unlike evolutionary technique in Section 2.6, we utilize the Latin Hypercube Sampling to generates the combination of the uncertain geometric parameters in all sets of population in this study. We employ the Rank Selection that similar to Fitness-Proportionate Selection except that selection probability is proportional to relative fitness rather than absolute fitness. It is repeated 10 times to ensure the analysis convergence. The silicon carbide (SiC) and alumina oxide (Al_2O_3) woven fabrics are chosen in this study and embedded in aluminum matrix systems.

Fitness function evaluation

A weighted sum fitness function is utilized in this study in order to maximize an equally weighted average of the elastic properties of a silicon carbide (SiC) and alumina oxide (Al_2O_3) composite. The design problem is represented by the following optimization problem:

$$\textbf{max} \ \left(0.1667E_x + 0.1667E_y + 0.1667E_z + 0.1667G_{xy} + 0.1667G_{xz} + 0.1667G_{yz}\right), \tag{4.1}$$

subject to multiple weave patterns preform.

Parent Selection

We utilize the Rank Selection in the study due to the individuals in the population have very close fitness values. This leads to each individual having an almost equal share of the pie (like in case of Fitness-Proportionate Selection) and hence each individual no matter how fit relative to each other has an approximately same probability of getting selected as a parent. This in turn leads to a loss in the selection pressure towards fitter individuals. In this, we remove the concept of a fitness value while selecting a parent. However, every individual in the population is ranked according to their fitness. The selection of the parents depends on the rank of each individual and not the fitness. The higher ranked individuals are preferred more than the lower ranked ones.

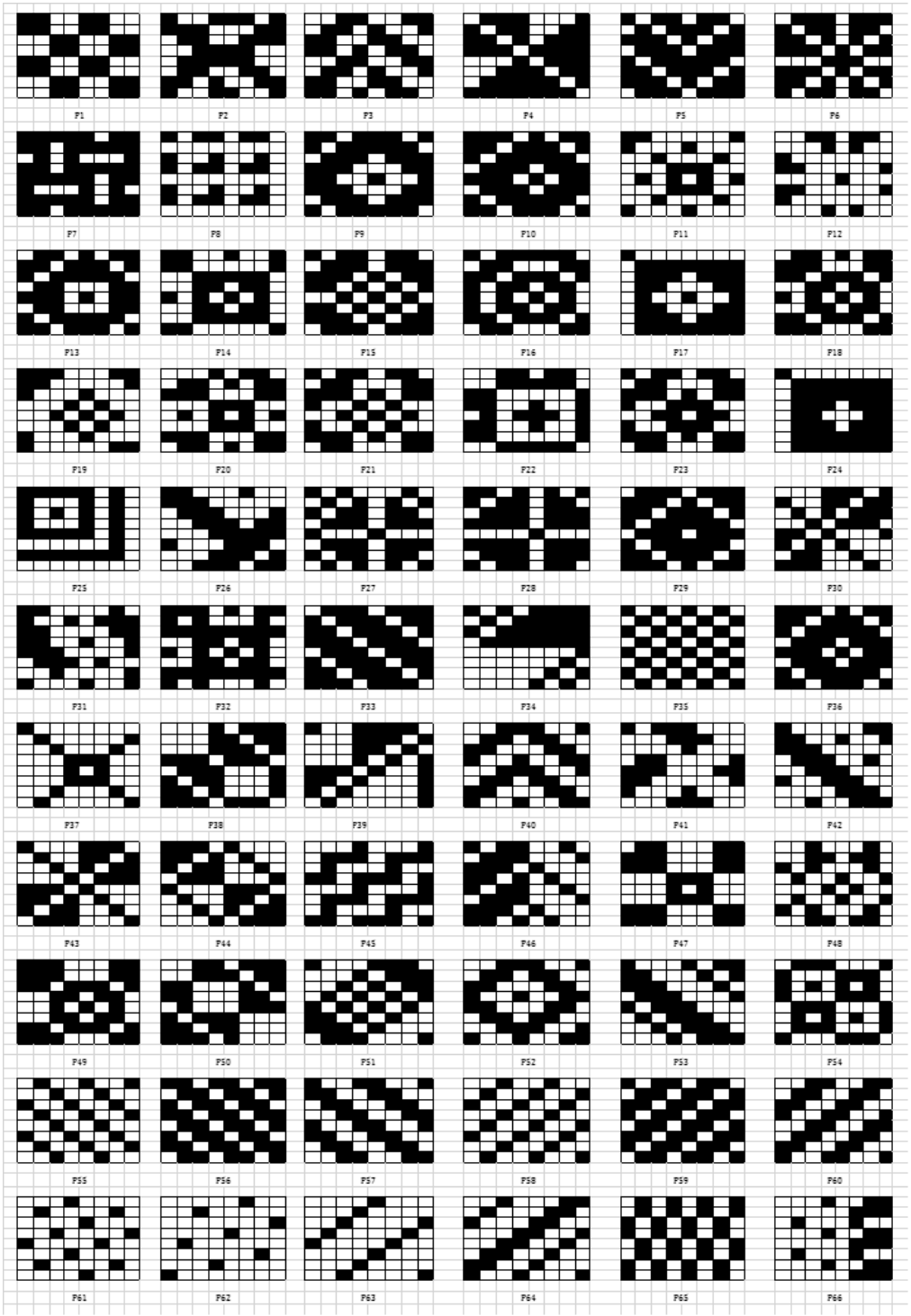

Figure 4.3: The selection of weave patterns used in fine-scale optimization with evolutionary algorithm (EA) - black squares corresponding to crossovers where the warp yarn is on top and white squares refer to the underlying weft yarn

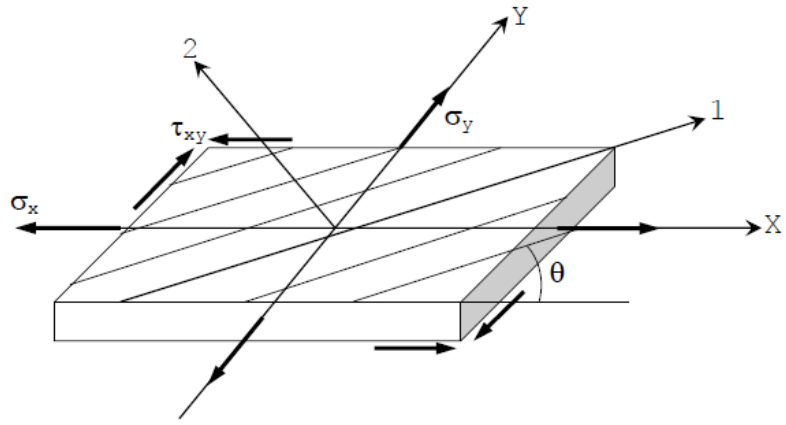

Figure 4.4: The tensor's components in terms of a coordinate basis (parallel and normal to the fibre axis

Recombination/Crossover

We utilize the uniform crossover which a fixed mixing ratio between two parents. Unlike single- and two-point crossover, the uniform crossover enables the parent chromosomes to contribute the gene level rather than the segment level. The uniform crossover evaluates each point in the parent strings for exchange with a probability of 0.5. This means that the offspring has approximately half of the genes from first parent and the other half from second parent, although crossover points can be randomly chosen.

Mutation

Swap mutation is employed by selecting two positions with an equally point on the chromosome at random, and interchange the patterns. By mutation individuals are altered. The purpose of mutation is preserving and introducing diversity. The mutation allows the algorithm to avoid local minima by preventing the population of chromosomes from becoming too similar to each other, thus slowing or even stopping evolution. This explains the fact that the mutation avoid only taking the fittest of the population in generating the next but rather a random (or semi-random) selection with a weighting toward those that are fitter (Obi11).

4.3.2 Computation of macroscopic elastic properties of lamina

The macroscopic elastic properties of a lamina can be modelled under plane-stress conditions by simplifying an orthotropic constitutive model. We adopt the same approach as mentioned in subsection 2.5.2 for the macroscopic elastic properties of a lamina of this study.

The Poisson's ratios $(\nu_{yx}, \nu_{zy}, \nu_{xz})$ are related to the aforementioned moduli and Poisson's ratios as in Eq. (2.1) (Lon05, BKBR13). Consequently, the macroscopic elastic properties are expressed as in Eq. (2.2). Since we are only concerned with stresses and strains within the plane of the lamina, only two normal and one shear are involved (see Fig. 4.4),

reducing Eq. (2.2) to Eq. (2.3): Therefore only four independent constants (E_x, E_y, G_{xy} and either of the Poisson's ratios) are needed to define the in-plane elastic properties of a lamina (Lon05). The work done by the force is expressed by Eq. (2.33) and the strain energy can be written as in Eq. (2.34).Simplifying W to E yields a relationship between the concentrated forces and the macroscopic stress applied as given by Eq. (2.35).The macroscopic elastic properties are then computed by Eq. (2.36). Further computational descriptions of the lamina macroscopic elastic properties can be found in (LW04) and (BKBR13).

We extract the macroscopic elastic properties under uni-axial tension. The sensitivity analysis is done based on surrogate model due to computational savings. We used polynomial regression fit to a simulated data set. The geometrical sensitivity analysis shows that the misalignment is a very important factor regardless of the loading mode (KM10) especially in the context of dry woven. Commonly, the deformation of ply depends on the orientation at which the ply has been cut. Laminates with warp and weft yarns at $\pm 45^{\circ}$ deform through shearing. In compression, the shearing process increases the angle between warp and weft yarns through increasing the overall width of the ply if the fabric is unconstrained (LWP13). The coarse-scale optimization is done only for a selected set of uncertainties, i.e. the ones who have the key influence based on the result of the fine-scale optimization. Uncertain mesoscopic parameters that barely influence the macroscopic elastic properties is considered deterministic.

4.4 Optimization at the coarse-scale

We further utilized the best weave pattern obtained in the fine-scale optimization into the coarse-scale optimization. In this study, optimization analyses have been carried out to optimize the stacking sequences of symmetric hybrid laminated composite plate with uncertain mesoscopic parameters by employing the ACO algorithm. As the use of ACO in optimization is emerging, it is essential to allocate robust benchmarks to enlighten the algorithm's capabilities (AT09).

4.4.1 Ant Colony Optimization

Ant Colony Optimization (ACO) is a probabilistic technique and a novel technique for solving hard combinatorial optimization problem in a reasonable amount of computational time. Real ants communicate information through the pheromone paths in finding the shortest path from a food source to their nest. This pheromone leads the other ant to follow the path and reinforcing the path with its own pheromone. The more ants follow the path, the more attractive that the path becomes. However, this tendency is not deterministic. Fig. 4.5 demonstrates the shortest path finding capability of ant colonies. The artificial ants employed in ACO aim to mimic the real ants. Elitist Ant System (EAS) also known as a modification in the ACO concept is considered in this study.

Initialization

At this stage, each ant decides where to go for its next step by selecting among all unvisited candidate elements (HFSB13).

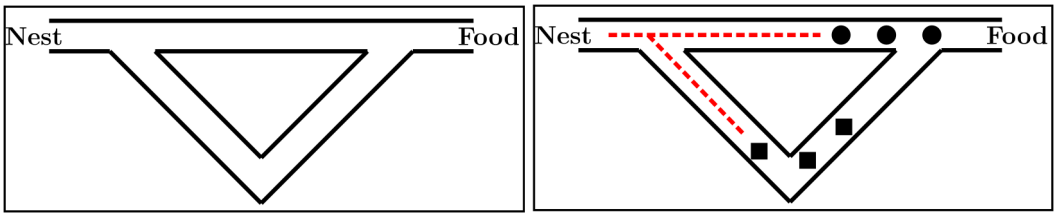

(a) All ants are in the nest. No pheromone is released.

(b) The foraging starts. In probability, 50% of the ants take the short path (circle shape) and 50% take the long path to the food source (rhomb shape).

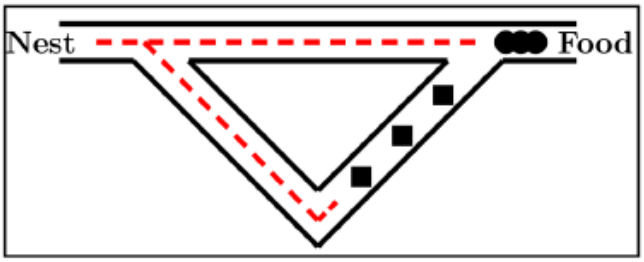

(c) The ants that have taken the short path have arrived earlier at the food source. Therefore, when return to the nest, the probability to take again the short path is higher.

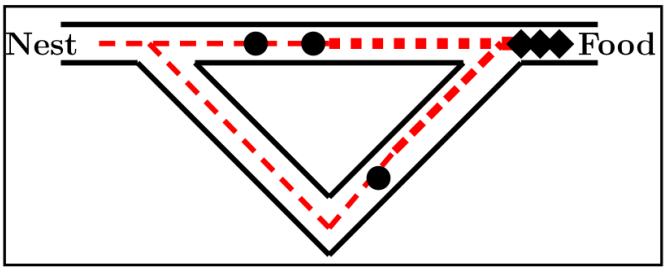

(d) The pheromone trail on the short path receives, in probability, a stronger enforcement and the probability to take this path grows. Finally, due to the evaporation of the pheromone on the long path, the whole colony will in probability use the short path.

Figure 4.5: The capability of ant colonies in finding the food source. Reproduced by Blum (Blu05).

Construction of Solution - State transition rule

The construction of solution used a combinatorial mechanism between directed greedy behaviour and Roulette-wheel known as state transition rule. An ant arriving at city i chooses the next city among unvisited cities according to the following mechanism (HFSB13):

$$S = \begin{cases} \arg\max \left\{ [\tau(i,j)]^{\alpha} \cdot [\eta(i,j)]^{\beta} \right\} & if \leq q_0 \\ s & otherwise \end{cases} \tag{4.2}$$

$$s = \begin{cases} \frac{[\tau(i,j)]^{\alpha} \cdot [\eta(i,j)]^{\beta}}{\sum [\tau(i,u)]^{\alpha} \cdot [\eta(i,u)]^{\beta}} & if \quad j \in allowed \quad j \\ u \in allowed \ u & \\ 0 & otherwise \end{cases} \tag{4.3}$$

where $\tau_{i,j}$ is the amount of pheromone related to the path between cities i and j and $\eta i, j$ is the heuristic function defined here as the inverse of distance between two cities. As can be seen from Eq. (4.3), the total decision term is a combination of both pheromone and heuristic functions with the latter having a power of β. The state transition rule consists of two sub-rules, while q and q_0 determine which one to be used. The constant parameter q_0 demonstrates the relative importance of sub-rules. However, q is a randomly generated number, uniformly distributed in range of 0 to 1. If $q \leq q_0$ is the case of exploitation, the city with the largest combination of pheromone and heuristic is chosen. Otherwise, the city with the largest calculated term may not be necessarily chosen. Thus, the exploration of candidates with smaller function values is made feasible. In general, the ants act in a parallel manner. Their first elements of solution are assigned randomly and then to the end of constructing the solution, state transition rule is repeated (HFSB13).

Pheromone updating rule - Global and Local updating rule

In EAS, the ant which constructed the shortest tour from the beginning of the trial along with other ants are allowed to deposit pheromone. By combining the mechanism of pseudo-random-proportional rule with EAS, the search becomes more directed. Ants search in a neighborhood of the best tour found up to the current iteration of the algorithm. Global updating is performed after all ants have completed their tours. The pheromone level is updated by applying the global updating rule as in Eq. (4.4) (HFSB13):

$$\tau(r,p) = (1-\rho)\,\tau(r,p) + \rho \Delta \tau(r,p) \tag{4.4}$$

$$\Delta \tau_{ij}^{k} = \begin{cases} \frac{\tau_0}{2J(\psi^{+})}, & l_{ij} \in \psi^{k} \in \{\psi^{+}, \psi^{*}\} \\ 0 & otherwise \end{cases} \tag{4.5}$$

The parameter $\rho \in (0,1]$ is a parameter that regulates the pheromone evaporation. τ_0 and k are the initial amount of the pheromone and the index number for each ants, respectively. The ψ^{+} and ψ^{*} are the best obtained tour in each iteration and the best-so-far solution using the best ant, respectively.

While generating a solution, changes occur to pheromone level by applying the local updating rule to Eq. (4.4) that yields Eq. (4.6) (HFSB13):

$$\Delta \tau(r,p) = \tau_0. \tag{4.6}$$

In practice, the role of local updating rule is to decrease the pheromone values on the visited solution components, making in this way these components less desirable for the following ants due to the loses of its pheromone. This mechanism increases the exploration of the search space within each iteration (HFSB13, Blu05).

Elitist Ant System

In exploiting information of global-best solution, Elitist Ant System (EAS) is proposed (DMC96). The updating rule in EAS performs the same rule as rank-based Ant system however the global-best ant in EAS allows pheromone change contribution n times in each iteration. The updating rule for EAS encourages both exploration as each of the m solutions found by the colony receive a pheromone addition and exploitation, as the global-best path is reinforced with the greatest amount of pheromone. As the value of n increases, the emphasis on exploitation is greater.

For constrained optimization, the solutions which do not satisfy the constraints may be omitted. Infeasible solutions may be identified and omitted prior to the evaluation of the fitness function. The status of infeasible solutions may also be checked and assigned a considerably large value to them. The latter case which known as penalty function approach is used in this study as it involves simple modifications in the original code. At the end of this section, it might be helpful to summarize the above explanations in the following pseudo-code format for EAS method (HFSB13):

```
Initial parameter setting
Repeat for each iteration
   Repeat for each ant
      Set the initial point for each ant
      Repeat for (No. of design variables - 1)
         Perform "the state transition rule"
         Perform "the local updating rule"
      Update the best global solution
   Perform "the global updating rule"
   Check the stopping conditions
Report the best solution
```

Figure 4.6: The pseudo-code of EAS method

4.4.2 Mathematical formulation for fundamental frequency and buckling load factor

Consider a simply supported symmetric hybrid laminated composite plate of length a, width b, and total laminate thickness h in the x, y, and z directions, respectively. Layer thickness t are assumed constant and total laminate thickness h is taken by $h = N \times t$ where N is the sum of plies. The outer ply N_o and inner ply N_i contribute to the hybrid laminated composite $N = N_o + N_i$. The equation governing the free vibrations of these laminates is

given by (Red04, TK$^+$05, HFSB13)

$$D_{11}\frac{\partial^4 w}{\partial x^4} + 4D_{16}\frac{\partial^4 w}{\partial x^3 \partial y} + 2\left(D_{12} + 2D_{66}\right)\frac{\partial^4 w}{\partial x^2 \partial y^2} + 4D_{26}\frac{\partial^4}{\partial x \partial y^3} + D_{22}\frac{\partial^4 w}{\partial y^4} = \rho h \frac{\partial^2 w}{\partial t^2} \tag{4.7}$$

where w denotes the deflection in the z direction and ρ is the mass density averaged in the thickness directions shown in Eq. (4.7). The mass density of a hybrid laminated composite is formulated as a thickness weighted average given by Eq. (4.8)

$$\rho = h^{-1}\int_{-h/2}^{h/2} \rho^{(k)} dz = \frac{1}{N}\sum_{k=1}^{N} \rho^{(k)} \tag{4.8}$$

where $\rho^{(k)}$ is the mass density of the material in the k^{th} ply.

The bending stiffness D_{ij} in Eq. (4.9) are formulated as

$$D_{ij} = \int_{-h/2}^{h/2} \left(z^{(k)}\right)^2 \bar{Q}_{ij}^{(k)} dz \tag{4.9}$$

where $z^{(k)}$ is the distance from the middle plane of the laminate to the top of the k^{th} ply. The $\bar{Q}_{ij}^{(k)}$ in Eq. (4.10) defines the plane stress reduced stiffness component of the k^{th} ply that derived from the function of fibre orientations and material properties using standard transformation relations given by

$$\begin{aligned}
\overline{Q}_{11} &= Q_{11}\cos^4\theta + 2\left(Q_{12} + 2Q_{66}\right)\sin^2\theta\cos^2\theta + Q_{22}\sin^4\theta \\
\overline{Q}_{12} &= \left(Q_{11} + Q_{22} - 4Q_{66}\right)\sin^2\theta\cos^2\theta + Q_{12}\left(\sin^4\theta + \cos^4\theta\right) \\
\overline{Q}_{22} &= Q_{11}\sin^4\theta + 2\left(Q_{12} + 2Q_{66}\right)\sin^2\theta\cos^2\theta + Q_{22}\cos^4\theta \\
\overline{Q}_{16} &= \left(Q_{11} - Q_{12} - 2Q_{66}\right)\sin\theta\cos^3\theta + \left(Q_{12} - Q_{22} + 2Q_{66}\right)\sin^3\theta\cos\theta \\
\overline{Q}_{26} &= \left(Q_{11} - Q_{12} - 2Q_{66}\right)\sin^3\theta\cos\theta + \left(Q_{12} - Q_{22} + 2Q_{66}\right)\sin\theta\cos^3\theta \\
\overline{Q}_{66} &= \left(Q_{11} + Q_{22} - 2Q_{12} - 2Q_{66}\right)\sin^2\theta\cos^2\theta + Q_{66}\left(\sin^4\theta + \cos^4\theta\right)
\end{aligned} \tag{4.10}$$

where Q_{ij} is the stiffness of composite along principal axes calculated as in Eq. (4.11)

$$\begin{aligned}
Q_{11} &= \tfrac{E_x}{1-\upsilon_{xy}\upsilon_{yx}} \\
Q_{12} = Q_{21} &= \tfrac{\upsilon_{yx}E_x}{1-\upsilon_{xy}\upsilon_{yx}} \\
Q_{22} &= \tfrac{E_y}{1-\upsilon_{xy}\upsilon_{yx}} \\
Q_{66} &= G_{xy}.
\end{aligned} \tag{4.11}$$

The macroscopic elastic properties (E_x, E_y, G_{xy} and the Poisson's ratios) are extracted from fine-scale optimization analysis. As aforementioned, this study deals with a hierarchical stochastic multi-scale optimization approach. There are several types of boundary conditions could in principle be used for this study, however we adopt simply-supported as our assumptions. Theoretically, this boundary condition is free to rotate and does not experience any torque. Practically, there is usually a small torque due to friction between the structure and its pin, but if the pin is well-greased, this torque may be ignored. The boundary conditions for the simply supported plate are computed as in Eq. (4.12)

$$\begin{aligned}
w = 0, \quad M_x = 0 \quad &\text{at x = 0,a} \\
w = 0, \quad M_y = 0 \quad &\text{at y = 0,b}
\end{aligned} \tag{4.12}$$

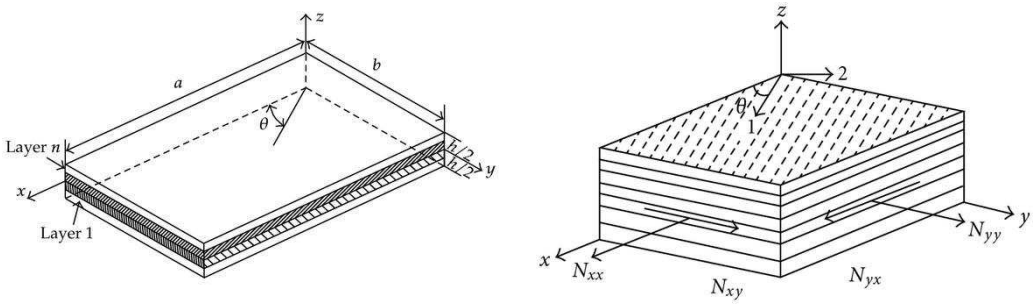

Figure 4.7: A simply supported hybrid laminated composite subjected to biaxial loadings

where M_x and M_y in Eq. (4.13) represents the bending moments in the x and y directions, respectively. The resultant of moments is formulated as

$$(M_x, M_y) = \int_{-h/2}^{h/2} (\sigma_x, \sigma_y) dz. \tag{4.13}$$

The influence of bending-twisting coupling stiffness D_{16} and D_{26} are assumed insignificant and can be omitted if the following non-dimensional parameters satisfy the following constraints

$$\begin{aligned} \gamma &= D_{16}\left(D_{11}{}^3 D_{22}\right)^{-1/4} \\ \delta &= D_{26}\left(D_{11} D_{22}{}^3\right)^{-1/4} \\ \gamma &\leq 0.2 \\ \delta &\leq 0.2. \end{aligned} \tag{4.14}$$

A detail explanation on reducing bending-twisting coupling can be found in Nemeth (Nem86). Due to similarity of expressions for buckling load and frequencies, the same constraints are used to reduce the error introduced by neglecting D_{16} and D_{26}. Adopting Eq. (4.7) with respect to the boundary conditions in Eq. (4.12), we could formulate the deflection w for the vibration mode (m, n) as (TK$^+$05, HFSB13)

$$w(x, y, t) = \sum_{m=1}^{\infty} \sum_{n=1}^{\infty} A_{mn} \sin \frac{m\pi x}{a} \sin \frac{n\pi y}{b} e^{i\omega_{mn} t} \tag{4.15}$$

where ω_{mn} is the natural frequency of the vibration mode (m,n) and $i = \sqrt{-1}$. By substituting Eq. (4.15) into Eq. (4.7), yielding to

$${\omega_{mn}}^2 = \frac{\pi^4}{\rho h} \left[D_{11} \frac{m^4}{a^4} + 2\left(D_{12} + 2D_{66}\right) \frac{m^2}{a^2} \frac{n^2}{b^2} + D_{22} \frac{n^4}{b^4} \right] \tag{4.16}$$

where the various frequencies ω_{mn} correspond to different mode shapes (different values of m and n in Eq. (4.16)). The fundamental frequency is obtained when m and n are both

one. For the rectangular plate given in Fig. 4.7, the fundamental frequency (first frequency) is given as (TK^{+}05, HFSB13)

$$f = \frac{\pi}{2\sqrt{\rho h}}\sqrt{\frac{D_{11}}{a^4} + \frac{2\left(D_{12}+2D_{66}\right)}{a^2b^2} + \frac{D_{22}}{b^4}} \tag{4.17}$$

where a and b are the dimensions of the plate, ρ is the average density and h is the total thickness of the plate.

Identically, the laminate buckles into m and n half-waves in the x and y directions when the amplitude parameter reaches the value of λ_b given by (RL11)

$$\frac{\lambda_b}{\pi^2} = \frac{D_{11}\left(\frac{m}{a}\right)^4 + 2\left(D_{12}+2D_{66}\right)\left(\frac{m}{a}\right)^2\left(\frac{n}{b}\right)^2 + D_{22}\left(\frac{n}{b}\right)^4}{N_x\left(\frac{m}{a}\right)^2 + N_y\left(\frac{n}{b}\right)^2 + N_{xy}\left(\frac{mn}{ab}\right)}. \tag{4.18}$$

The critical buckling load λ_{cb} is achieved when the λ_b is minimum wherein λ_{cb} is the function of (m,n) with respect to the plate aspect ratio (AR). It is assumed that the simply-supported plate is loaded with an axial load in x-direction N_x for the value of λ_{cb} by utilizing Eq. (4.18).

4.4.3 A coarse-scale optimization problem formulation

The selection of the optimal stacking sequence with uncertain mesoscopic parameters to obtain the simultaneous minimization of the weight and the cost of a rectangular hybrid laminated composite plate is presented as the design problem. The hybrid laminated composites dimensions are a = 1167.87 mm, b = 1146.09 mm which has been enlarged about 33 times from the original dimension of the best weave pattern. This is adopted to represent a macro-scale scenario of the ply. The ply thickness t is taken by 0.98 mm. The Pareto-optimal solution of hybrid laminated composite using multi-objective ACO algorithms is generated for simultaneous optimization cost as well as weight with design constraints on fundamental frequency of 30 Hz, and buckling load factor of 50, respectively.

In this study, the concept of hybridization using two material composites is adopted. The macroscopic elastic properties for both laminate plies are extracted from fine-scale optimizations and it is found that these plies are optimal. The high stiffness-to-weight ratio and more expensive Silicon Carbide-Aluminum ($SiC-Al$) is used for the outer laminate ply whilst less expensive and low stiffness-to-weight ratio Alumina Oxide-Aluminum (Al_2O_3-Al) for the inner laminate plies is considered. The stiffness-to-weight ratio of Silicon Carbide-Aluminum ($SiC-Al$) and Alumina Oxide-Aluminum (Al_2O_3-Al) are about 420 against 34, respectively. The cost of Silicon Carbide-Aluminum ($SiC-Al$) is about three times higher than Alumina Oxide-Aluminum (Al_2O_3-Al). If the weight is the priority, then Silicon Carbide-Aluminum ($SiC-Al$) is preferable. However, if the cost is concerned, the optimum Alumina Oxide-Aluminum (Al_2O_3-Al) plies is the options.

Initially, the hybrid laminated composite has 44 plies, however this may vary by the algorithm in determining the optimal ply sequence. The stacking sequence is constrained to be symmetric about the laminate mid-plane, requiring only 1/2 of the laminate stacking sequence to be designed. In addition, the requirement that the laminate is balanced can be enforced by using pairs of $\pm\theta$ plies at symmetric state. With this, shear-extension and

bending-twisting effects are minimized. The ply angles are varying from 0^o to 90^o in steps of 5^o. As mentioned in Section 4.3.1, only an uncertain parameter is considered with respect to the most sensitive uncertain mesoscopic parameter. It is evident that the most dominant uncertain mesoscopic parameter is the misalignment in lamina angle as similar to Komeili (KM12). The numbers of pair laminates vary from 6 to 11 for half of the hybrid laminated composite. In this study, the number of zone is set to equal number of pairs and each zone contains 38 cities with different material properties and orientation angles. Tab. 4.3 explains the number of cities that designed for each investigated materials and related angles. Number 1-19 and 20-38 indicate the Alumina Oxide-Aluminum ($Al_2O_3 - Al$) and Silicon Carbide-Aluminum ($SiC - Al$) materials, respectively, with corresponding angles and misalignment in ply angles.

Table 4.3: Number of cities for Alumina Oxide-Aluminum and Silicon Carbide-Aluminum

Angles, θ°	Misalignment of yarn angles, e°	Alumina Oxide-Aluminum, $Al_2O_3 - Al$	Silicon Carbide-Aluminum, $SiC - Al$
0	2.47	1	20
-5/+5	2.47	2	21
-10/+10	2.47	3	22
-15/+15	2.47	4	23
-20/+20	2.47	5	24
-25/+25	2.47	6	25
-30/+30	2.47	7	26
-35/+35	2.47	8	27
-40/+40	2.47	9	28
-45/+45	2.47	10	29
-50/+50	2.47	11	30
-55/+55	2.47	12	31
-60/+60	2.47	13	32
-65/+65	2.47	14	33
-70/+70	2.47	15	34
-75/+75	2.47	16	35
-80/+80	2.47	17	36
-85/+85	2.47	18	37
90	2.47	19	38

Ant colony optimization (ACO) is utilized to formulate the Pareto-optimal solutions by optimizing a convex combination of the two non-linear objectives, weight (W) and cost (C) based on a series of multiplier values (α). The multiplier values (α) employs the concept of weighted sum method in order to solve the optimization problem. The objective functions for multi-objective optimization of hybrid laminated composites can be defined as

(a) Cost minimization, C

$$C = [N_{AlO} c_{AlO} \rho_{AlO} + N_{SiC} c_{SiC} \rho_{SiC}]\, tab \tag{4.19}$$

(b) Weight minimization, W

$$W = [N_{AlO}\rho_{AlO} + N_{SiC}\rho_{SiC}]\, tab \tag{4.20}$$

(c) Pareto-optimal solutions minimization, F

$$F = \alpha W + (1 - \alpha)C. \tag{4.21}$$

Design constraints are defined as

(a) Fundamental frequency, f

$$f = \min\left(f(m, n)\right) \tag{4.22}$$

(b) Buckling load factor, λ_b

$$\lambda_{cb} = \min(\lambda_b(m, n)) \tag{4.23}$$

where c_{AlO} the unit cost of Alumina Oxide-Aluminum ply $(1/m^3)$, c_{SiC} is the unit cost of the Silicon Carbide-Aluminum ply $(1/m^3)$, a, b, t, N_{AlO}, N_{SiC}, ρ_{AlO} and ρ_{SiC} are the length, the width, the ply thickness, the number of Alumina Oxide-Aluminum ply, the number of Silicon Carbide-Aluminum ply, the density of Alumina Oxide-Aluminum and Silicon Carbide-Aluminum, respectively. The values of weighting factor α are selected and the multi-objective function is minimized (see, Eq. (4.21)) using a single-objective optimizer based on ACO.

4.5 Numerical Results and Discussions

EA is used to solve the optimization problem described in Section 4.3.1. This section represents the hierarchical multi-scale optimization results based on aforementioned explanation. We quantify the macroscopic elastic properties of the best weave pattern under uncertain mesoscopic parameters from the fine-scale optimization problem formulation. In course-scale optimization problem formulation, the minimization of weight and cost are determined with respect to the aforementioned uncertain mesoscopic parameters. ACO has been employed to optimize the stacking sequence of the hybrid laminated composite plate. It is also determined their orientation and macroscopic elastic properties of each ply that gives the desired properties: fundamental frequency and buckling load factor.

4.5.1 Fine-scale's numerical results

We first study the influence of the mesh refinement on the macroscopic material properties in the fine-scale's optimization. We evaluate the quality of the mesh by refining the mesh until a steady-state of fitness function value is obtained. This is due to the approach of voxel-based meshing in TexGen application. Further explanation on voxel-base meshing can be retrieved in (LW04). It is a clear difference on the relative CPU time between the coarse mesh (level 1) and other four meshes. It can be concluded from the Fig. 4.8 and Tab. 4.4 that the mesh 3 is sufficient to provide the accurate results.

The selection of weave patterns is made corresponding to the best fitness function evaluation as stated in Section 4.3.1. Using Latin Hypercube Sampling (LHS), 100 sampling

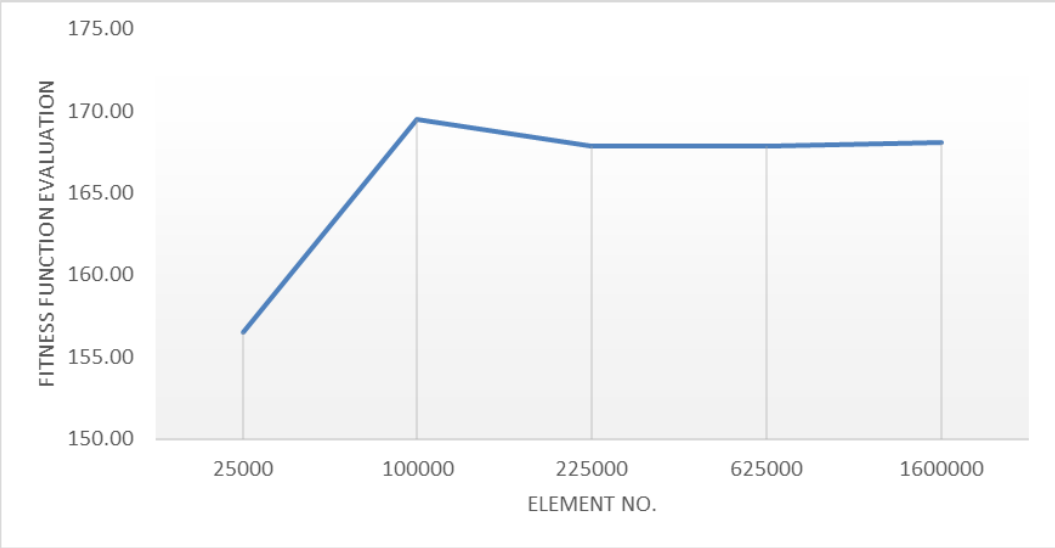

Figure 4.8: Mesh sensitivity based on the relationship between fitness function evaluation and number of elements

Table 4.4: Mesh statistics of fine-scale's optimization

Mesh	**Number of nodes**	**Number of elements**	**DOF DOF**	**Relative CPU time** (sec)
1 $(coarse)$	28617	25000	85839	27.4
2	112217	100000	336639	171.80
3	250817	225000	752439	569.20
4	693017	625000	2079039	2473.70
5 $(fine)$	1768817	1600000	5306439	11292.00

Table 4.5: The ranking of fitness function evaluation according to the weave pattern, see Fig. 4.3

Rank No.	Pattern No.	Fitness Values	Rank No.	Pattern No.	Fitness Values	Rank No.	Pattern No.	Fitness Values
1	P47	159.47	23	P54	158.48	45	P63	157.78
2	P66	159.30	24	P8	158.45	46	P52	157.77
3	P62	159.27	25	P17	158.40	47	P20	157.72
4	P41	159.21	26	P2	158.39	48	P40	157.71
5	P11	159.16	27	P34	158.37	49	P43	157.65
6	P49	159.11	28	P50	158.35	50	P51	157.64
7	P7	159.09	29	P4	158.34	51	P44	157.63
8	P19	159.06	30	P18	158.34	52	P65	157.61
9	P22	159.02	31	P10	158.29	53	P64	157.58
10	P53	159.01	32	P36	158.29	54	P16	157.49
11	P45	158.90	33	P61	158.28	55	P23	157.33
12	P12	158.90	34	P29	158.27	56	P27	157.08
13	P14	158.89	35	P28	158.09	57	P21	156.99
14	P42	158.88	36	P31	158.04	58	P35	156.64
15	P33	158.88	37	P30	158.03	59	P55	156.50
16	P25	158.87	38	P15	157.92	60	P56	156.48
17	P24	158.84	39	P46	157.92	61	P3	156.29
18	P37	158.75	40	P39	157.90	62	P60	156.25
19	P38	158.70	41	P6	157.90	63	P58	156.24
20	P32	158.69	42	P5	157.89	64	P57	156.04
21	P9	158.58	43	P48	157.85	65	P59	155.90
22	P26	158.58	44	P13	157.80	66	P1	155.72

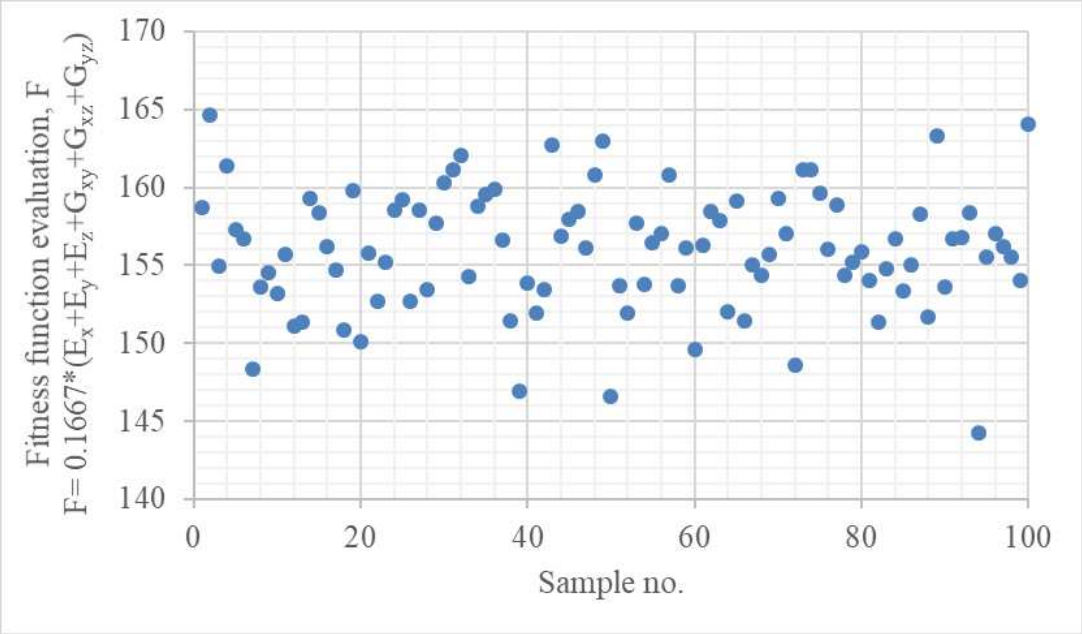

Figure 4.9: The fitness evaluation with all uncertain parameters under LHS on $TampukJantung$ weave

points are generated for each pair-wise of uncertain mesoscopic parameters between the tolerance values as mentioned in Tab. 4.2. Two parents are randomly chosen and evaluated with the 100 sampling points which consist all combinations of mesoscopic uncertain parameters as tabulated in Fig. 4.9. At this stage, we could determine which combination of mesoscopic uncertain parameter is dominant. The first rank of mesoscopic uncertain parameter combination is defined as a dominant combination. Consequently, the most dominant combination is evaluated on all patterns. With respect to this, we save the computational time in the analysis. Fig. 4.10 and Tab. 4.5 show the parent selection operator results to determine the best parents for the next generation (offspring). The best fitness is ranked as 1, second best as 2 etc. and the worst fitness is ranked as P (number of patterns in population). It is clearly observed that the individuals in the population have very close fitness values. This shows that the adopted parent selection operator is adequate. We adopt the first two parents of the rank to undergo recombination and mutation with pair-wise of uncertain mesoscopic parameters. The offsprings generated from both parents are evaluated with pair-wise of uncertain mesoscopic parameters generated using LHS are ranked and optimized with respect to the fitness function evaluation. Correspondingly, the best weave pattern is determined based on the first weave of the rank. The best weave pattern designation under uncertainty parameters and its material properties are depicted in Fig. 4.11 and Fig. 4.12, respectively. It is observed that the best pattern is given by offspring number $P353$ (combination patterns of $P47$ and $P24$)with 165.56 of fitness function. With a fixed geometry specification (optimized uncertain mesoscopic parameters), we also evaluated the lamina with three different material constituents for fibres and matrix. Tab. 4.7 shows the

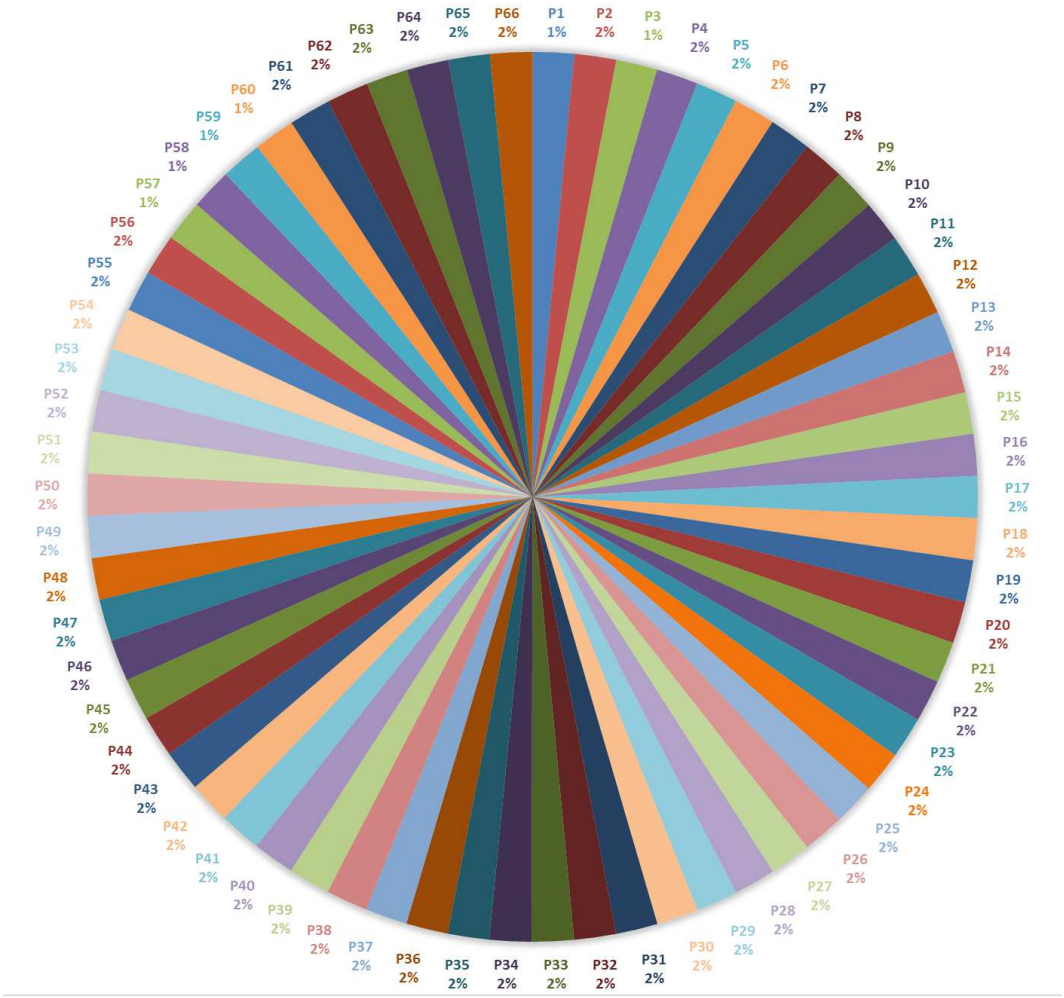

Figure 4.10: Rank Selection for parent selection. $P1 - P66$ refers to the pattern number, see Fig. 4.3 for the pattern design

list of various fibres and matrix used that contributes the result in Tab. 4.6.

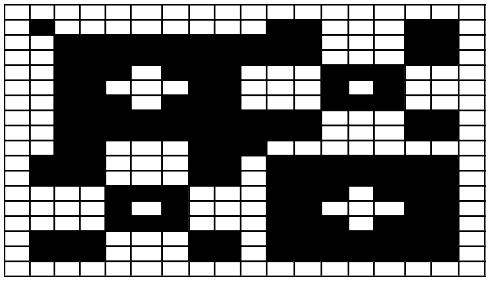

(a) The best pattern in black-paper diagram (combination patterns of P47 and P24)

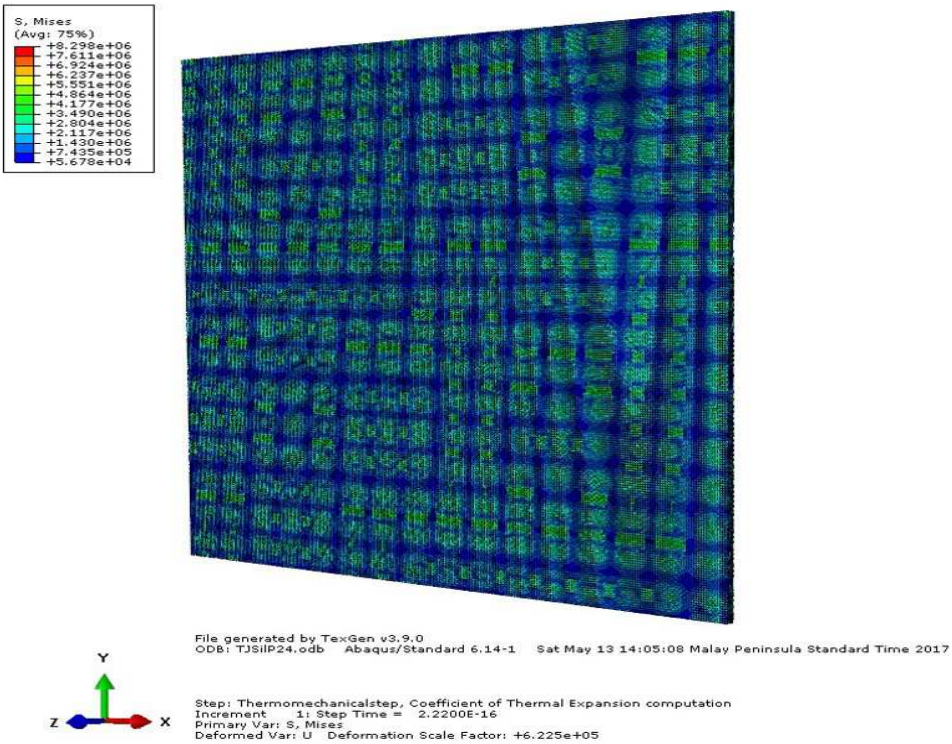

(b) Best pattern in ABAQUS visualization

Figure 4.11: Fine-scale optimization result

The weave pattern of lamina is characterized by the interlacement of the warp and weft yarns orthogonal to each other, resulting in undulation or waviness in both directions (BKBR13). This study founds that the effect of misalignment of yarn angles becomes more significant as the weave structure becomes more complicated. This shows that the study has a good agreement with the findings by Milani *et al.*(MNAH07). The macroscopic elastic properties of best weave pattern (see, Fig. 4.12) is influenced by the bridging effect between the adjacent yarns (i.e., the capacity of adjacent yarns to transmit loads from each other, due to the matrix connection between them) due to the presence of non-interlacing regions.

Pattern no.	Uncertain parameter dimension					Material Properties (GPa)						
P353 (mix of P24 & P47)	Yarn spacing (warp/weft)	Yarn height (warp/weft)	Yarn width (warp/weft)	Misalignment of yarn angles (e)	Fabric thickness (warp/weft)	E_{xx}	E_{yy}	E_{zz}	G_{yz}	G_{xz}	G_{xy}	Fitness value
	5.03/5.02	0.49/0.49	4.44/4.59	2.47	0.98/0.98	270.9	268.5	217.3	68.5	67.0	100.8	165.6

Figure 4.12: Best pattern designation

Table 4.6: Macroscopic elastic properties of Alumina Oxide-Aluminum ($Al_2O_3 - Al$) and Silicon Carbide-Aluminum ($SiC - Al$)

Parameters	Alumina oxide -aluminum ($Al_2O_3 - Al$)	Silicon carbide -aluminum ($SiC - Al$)
Longitudinal modulus E_x (GPa)	258.6	271.0
Transverse modulus E_y (GPa)	256.4	269.0
In-plane shear modulus G_{12} (GPa)	93.96	101.0
Poisson ratio μ_{12}	0.29	0.21
Density (kg/m^3)	3690	3100
Ply-thickness t (m)	0.00098	0.00098
Cost factor c	1	3

Table 4.7: Material constituents for fibres and matrix

Material Parameters	Fibres		Matrix
	SiC	Al_2O_3	Aluminum, Al
Density (gcm^{-3})	3.2	3.9	2.71
Longitudinal Tensile Modulus, E_x (GPa)	406	385	69
Transverse Tensile Modulus, E_y (GPa)	406	385	-
Poisson's ratio, μ_{xy}	0.2	0.3	0.32
Shear modulus G_{xy} (GPa)	169	154	26
Longitudinal Tensile Strength (MPa)	3395	1400	74
Longitudinal Thermal Expansion ($10^{-6}K^{-1}$)	5.2	8.5	23.6
Transverse Thermal Expansion ($10^{-6}K^{-1}$)	5.2	8.5	-
Glass transition melting point ($\circ C$)	-	-	660
Cost (/kg)	75	25	2

The bridging effect considers the undulation in the loading direction that yield an optimized macroscopic elastic properties. It may be noted that the in-plane properties of lamina are compromised with the undulation of warp and weft, interlacement of warp and weft as well as the reinforcement in fabric. When misalignment is present, the yarns elongate, as well as reorient at the same time.

The results of the macroscopic elastic properties are strongly dependent on the assumptions of the variability of the uncertain mesoscopic parameters. Referring to Fig. 4.12, the optimized dimension of lamina is varying on the warp and weft directions. This approach is implemented due to the parametric study carried by Ilyani *et al.* (BKBR13). It is observed that the elastic and shear moduli reduces corresponding to yarn spacing changes with fixed values of yarn thickness and width. Naik *et al.*(NS92a) and Lee *et.al.*(LBH03) highlighted that an optimum spacing between adjacent yarns gives higher elastic moduli. Based on Komeili and Milani (KM12), it is identified that the misalignment of the yarn angle is the most influential uncertain mesoscopic parameter for the macroscopic elastic properties. It has been a significant criterion due to the low shear stiffness values used in the analysis. With the use of low shear stiffness materials, the yarns tend to be aligned first along the loading direction with no high resistance before other effect of uncertainty criteria. Contradictorily, the use of high shear stiffness materials allows the yarns to behave like a beam which is able to resist shearing during the loading condition. In light of this, the misalignment of yarn angle is highlighted in the course-scale optimization problem as the design variables. The other uncertain mesoscopic parameters are demonstrated to be unimportant.

4.5.2 Coarse-scale's numerical results

ACO is utilized to solve the problem described in Section 4.4.3. The ACO algorithm has proved its efficiency in many optimization problems although several parameters acting need to be well-tuned (AT09). In order to solve the course-scale optimization problem, different values of α multiplier are chosen varying from 0 to 1. The idea of locating expensive material in the outer layer and inexpensive material in the inner layer can reduce the material costs while satisfies the design specifications. The macroscopic elastic properties of Alumina Oxide-Aluminum ($Al_2O_3 - Al$) and Silicon Carbide-Aluminum ($SiC - Al$) adopted for the optimal stacking sequence task are given in Tab. 4.6. Since a classical laminated plate theory is adopted, only 5 macroscopic elastic properties are utilized as elaborated in Eq. (4.10). In this study, the parameter setting employed for ACO is given in Tab. 4.8.

Table 4.8: The user parameters and settings for ACO (HFSB13)(AT09)

Number of ants	ρ	q_0	τ_0	No. of iteration
10	0.5	0.9	0.5	2000

The Pareto-optimal solution, F is minimized by assigning α = 0, 0.75, 0.85, 0.89, 0.93, 0.98 and 1. Tab. 4.9 shows the optimal stacking sequence and optimum values of the Pareto-optimal solution, F with variation of α values and respective design constraints. It is observed that the minimum cost, C is at 58.083 whilst the minimum weight W is at

Table 4.9: Stacking sequence and optimum values of hybrid laminated plate with variation of α

a/b = 1.0; $\lambda_b^{min} = 50$; $f_{min} = 30$;						
α	Stacking sequence	C	W	F	λ_b	f
0	8 1 1 1 1 1	67.763	67.763	67.763	96.067	84.201
	13 1 1 1 1 1	67.763	67.763	67.763	96.120	84.224
	5 1 1 1 1 1	67.763	67.763	67.763	96.170	84.245
	2 1 1 1 1 1	67.763	67.763	67.763	96.130	84.228
	15 1 1 1 1 1	67.763	67.763	67.763	96.062	84.198
0.75	19 1 1 1 1 1	58.083	58.083	58.083	60.579	72.220
0.85	20 1 1 1 1 1	72.800	56.535	58.975	60.602	73.217
0.89	14 1 19 1 19 1	67.763	67.763	67.763	93.315	82.985
	15 1 1 1 1 1	67.763	67.763	67.763	96.062	84.198
	13 1 19 1 19 1	67.763	67.763	67.763	93.404	83.025
	16 1 1 1 1 1	67.763	67.763	67.763	96.179	84.249
	8 1 1 1 1 1	67.763	67.763	67.763	96.067	84.201
0.93	36 1 1 1 1 1	97.198	64.668	66.945	96.263	86.280
	27 1 1 1 1 1	97.198	64.668	66.945	96.050	86.184
0.98	37 1 1 1 1 1	97.198	64.668	65.318	96.183	86.244
	36 1 1 1 1 1	97.198	64.668	65.318	96.263	86.280
	26 1 1 1 1 1	97.198	64.668	65.318	96.193	86.249
	33 1 1 1 1 1	97.198	64.668	65.318	96.004	86.164
1.0	25 1 1 1 1 1	97.198	64.668	64.668	96.262	86.280
	24 1 1 1 1 1	97.198	64.668	64.668	96.175	86.241
	35 1 1 1 1 1	97.198	64.668	64.668	96.186	86.245

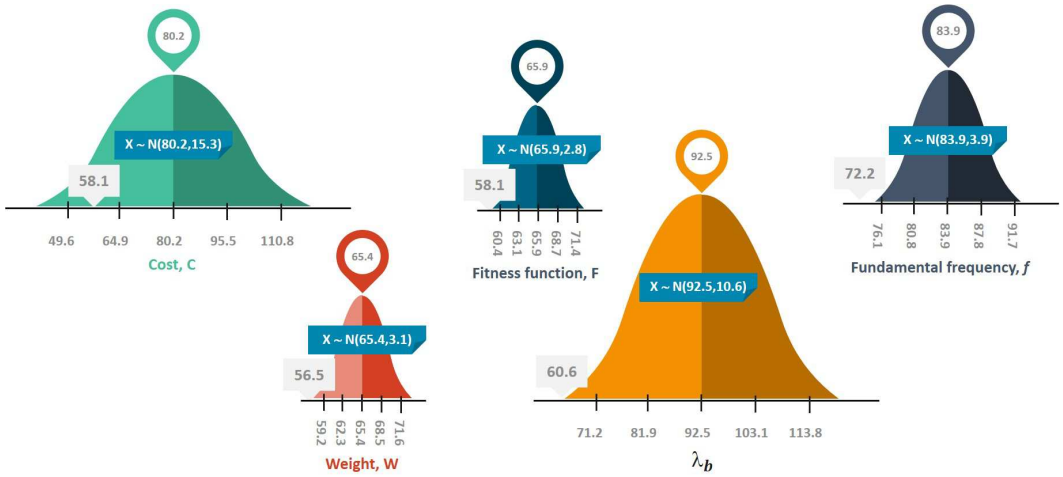

Figure 4.13: Summary of the statistical results between fitness functions and design constraints

56.535 kg. The corresponding stacking sequence consists of 16 Alumina Oxide-Aluminum ($Al_2O_3 - Al$) and 28 Silicon Carbide-Aluminum ($SiC - Al$) plies is found as the optimum plies. It is also conservatively claimed that the C and W values are identical for $\alpha = 0$ and $\alpha = 0.89$. Similarly to $\alpha = 0.93$, $\alpha = 0.98$ and $\alpha = 1.0$ with 97.198 and 64.668 kg, respectively. It is quite understandable as with restricted number of plies, it is impossible to satisfy the design constraints only with minimal amount of Alumina Oxide-Aluminum ($Al_2O_3 - Al$) plies. The buckling load factors show almost about two times than the minimum buckling factor λ_b^{min} whilst the fundamental frequencies increases almost three times than the minimum value. The Pareto-optimal stacking sequences given in Tab. 4.9 are considerably high to the design constraints with the consideration of the misalignment yarn angles. The summary of the statistical results according to the fitness function and design constraint parameters are summarized in Tab. 4.10 and Fig. 4.13. The peak point shows the mean value of each parameters and it is found that the Cost C has the highest standard deviation value with 15.3, thus the more spread of the data is obtained. It is obviously seen that the Weight W, Fitness function F and fundamental frequency f have the steeper bell curve due to the smaller standard deviation. The best values for Weight W, fitness function F, buckling load factor λ_b and fundamental frequency f falls within 3 standard deviation. However, the best cost falls in 95% range which is within 2 standard deviation.

The Pareto-optimal solution between the two involved objective functions in multi-objective optimization designs with reasonable fundamental frequency, but notable and worthy reductions in cost, the latter objective always a demanding requirement in hybrid laminated composites. This study clearly illustrates that the constraints handling by way of considering it as additional design objectives is found to be effective for hybrid laminated stacking sequence optimization. It is evident that the chosen materials and number of plies give a significant influence to the cost of hybrid laminated composites. In addition, the plies angles and the misalignment in the yarn angles significantly affect the first fundamental frequency and the cost, C. The values of multiplier α also play an important role in opti-

Table 4.10: Statistical results of different parameter considering all multiplier values, α

Parameter	Best	Mean	Worst	Std Dev
Cost	58.083	80.157	97.198	15.315
Weight	56.535	65.441	67.763	3.104
Fitness function, F	58.083	65.898	67.763	2.756
λ_b	60.579	92.492	96.263	10.639
f	72.220	83.874	86.280	3.888

mizing the hybrid laminated stacking sequence. When α is set into 0, the multi-objective optimization formulation is reduced to single-optimization formulation wherein the cost C is minimized. However, when α is equal to 1 consequently the weight W is the optimized. Obviously, by considering cost as the single objective, the optimum design is that with all plies made up of Alumina Oxide-Aluminum ($Al_2O_3 - Al$).

Conclusively, the adoption of ACO offer an optimum design in which the plies made of Alumina Oxide-Aluminum ($Al_2O_3 - Al$) have appeared in the inner plies and those made of Silicon Carbide-Aluminum ($SiC - Al$) as the outer plies. This generates a hybridization in laminated composite wherein the structural function holds by the stiffer plies in outer side contribute to the flexural properties. Theoretically, the inner plies merely utilized to reduce the total cost while keep the distance of the outer plies from the neutral plane. In contrast, with the presence of misalignment in yarn angles, the cost, C increases notably.

Chapter 5

Conclusions

5.1 Summary of achievements

A summary of conclusions for each chapter are described as follows:

5.2 Optimization of Elastic Properties and Weaving Patterns of Woven Composites

Woven fabric composites differ considerably from conventional engineering materials in various ways. They are inhomogeneous, lack of continuity and are highly anisotropic. This is the reason why woven fabric composites are non-linear and plastic even at low stress and at room temperature. They also tend to deform easily, as well as suffering large strains and displacements even at low stress, under ordinary conditions or in normal use. In addition, woven fabric composites have a good drapability behaviour in which they do not forming the sharp corners which appear in the case of paper when it is folded. Thus, they possess unique characteristics suitable especially for body movement, aesthetic values and other physiological and psychological requirements.

This study has presented a genetic algorithm to optimize woven composites, able to address both the choice of elastic constants of the constituents and the weaving pattern. The so-obtained woven composites show an acceptable strength performance with considerable values of elastic properties and weave tightness. The best pattern not only provides high elastic properties but also could minimize the fray problem due to a high weave tightness. Effective elastic properties of woven fabric composites have also been evaluated following a procedure which does not require a numerical averaging process and the outcome is satisfactory.

TexGen and ABAQUS softwares are ideal partners for this analysis. TexGen gives a maximum flexibility to the desired model, thus permitting precise modelling of the textiles. It also ensures some realistic contact surface between the yarns with minimal interpenetration. The advantages of TexGen are the automated functions that able to discretize the model, attributing material orientations and properties to elements, and able to export the model to external analysis software in several data formats, e.g. ABAQUS. The remarkable functionality provides a cohesive foundation for a priori prediction of textile composite

Global sensitivity analysis	Uniaxial modes			Biaxial modes		
	E_{xx}	E_{yy}	E_{zz}	E_{xx}	E_{yy}	E_{zz}
Correlation analysis	$(R^2)_1 = 0.92$ $(R^2)_2 = 0.59$ $(R^2)_3 = 0.98$ $(R^2)_4 = 0.94$	$(R^2)_1 = 0.90$ $(R^2)_2 = 0.94$ $(R^2)_3 = 0.98$ $(R^2)_4 = 0.92$	$(R^2)_1 = 0.90$ $(R^2)_2 = 0.98$ $(R^2)_3 = 0.98$ $(R^2)_4 = 0.90$	$(R^2)_1 = 0.98$ $(R^2)_2 = 0.008$ $(R^2)_3 = 0.98$ $(R^2)_4 = 0.98$	$(R^2)_1 = 0.90$ $(R^2)_2 = 0.90$ $(R^2)_3 = 0.98$ $(R^2)_4 = 0.98$	$(R^2)_1 = 0.35$ $(R^2)_2 = 0.98$ $(R^2)_3 = 0.94$ $(R^2)_4 = 0.92$
Response Surface Method (full quadratic)	$R^2 = 0.91$ $R^2_{adj} = 0.90$	$R^2 = 0.84$ $R^2_{adj} = 0.83$	$R^2 = 0.81$ $R^2_{adj} = 0.80$	$R^2 = 0.97$ $R^2_{adj} = 0.97$	$R^2 = 0.57$ $R^2_{adj} = 0.54$	$R^2 = 0.23$ $R^2_{adj} = 0.17$
Sobol's indices	Total effect indices, $\hat{S}_{Ti}$ $\hat{S}_{T1} = 0.21$ $\hat{S}_{T2} = 0.04$ $\hat{S}_{T3} = 0.32$ $\hat{S}_{T4} = 0.39$ $\sum_{i=1}^{4} \hat{S}_{Ti} = 0.97$	Total effect indices, $\hat{S}_{Ti}$ $\hat{S}_{T1} = 0.09$ $\hat{S}_{T2} = 0.08$ $\hat{S}_{T3} = 0.60$ $\hat{S}_{T4} = 0.10$ $\sum_{i=1}^{4} \hat{S}_{Ti} = 0.87$	Total effect indices, $\hat{S}_{Ti}$ $\hat{S}_{T1} = 0.07$ $\hat{S}_{T2} = 0.13$ $\hat{S}_{T3} = 0.61$ $\hat{S}_{T4} = 0.03$ $\sum_{i=1}^{4} \hat{S}_{Ti} = 0.84$	Total effect indices, $\hat{S}_{Ti}$ $\hat{S}_{T1} = 0.03$ $\hat{S}_{T2} = 0.01$ $\hat{S}_{T3} = 0.09$ $\hat{S}_{T4} = 0.94$ $\sum_{i=1}^{4} \hat{S}_{Ti} = 1.07$	Total effect indices, $\hat{S}_{Ti}$ $\hat{S}_{T1} = 0.01$ $\hat{S}_{T2} = 0.00$ $\hat{S}_{T3} = 0.10$ $\hat{S}_{T4} = 0.49$ $\sum_{i=1}^{4} \hat{S}_{Ti} = 0.60$	Total effect indices, $\hat{S}_{Ti}$ $\hat{S}_{T1} = 0.03$ $\hat{S}_{T2} = 0.10$ $\hat{S}_{T3} = 0.04$ $\hat{S}_{T4} = 0.07$ $\sum_{i=1}^{4} \hat{S}_{Ti} = 0.24$

Figure 5.1: Global sensitivity analysis results based on R^2 values under uni-axial and biaxial loadings

physical properties as illustrated by other applications.

A parametric study has been conducted to investigate the effect of various geometric parameters of optimized woven pattern on the elastic properties of the composite. The gap length, yarn thickness, material constituents and effect of shape factor have been selected to investigate the elastic properties of optimized woven fabric composites. Overall, an understanding of the designation mechanisms of fabrics is beneficial for fabric design and process control, which comprehends investigation of the relationships between fibre properties, structure of the yarn, process of fabric construction and physical properties of the fabric.

5.3 Uncertainty Quantification of Dry Woven Fabrics: A Sensitivity Analysis on Material Properties

In this study, two global sensitivity analyses are presented with particular consideration of the influences of four uncertainty criteria on $MataBerkait$-dry woven fabric material properties. They are presented in order to quantify the significant factor that influenced *MataBerkait*-dry woven fabric material properties under uni-axial and biaxial loadings. Latin Hypercube Sampling (LHS) was used as random sampling plan in the analysis.

Furthermore, it is highlighted that the sensitivity analyses conducted are based on surrogate model predictions. The four uncertainty criteria of interest are defined as the yarn width, spacing, height and friction coefficient. These four uncertainty criteria are highlighted due to the importance in geometrical factors and the mechanical responses of fabric unit cells. The most significant uncertainty criterion that affects the material properties of

the fabric was identified by the global sensitivity analyses. Overall, the reasons that influenced the material properties results based on uncertainty criteria are varies. Fig. 5.1 summarizes the coefficient of determination, R^2 between uncertainty parameters and the *MataBerkait*-dry woven fabric material properties based on the global sensitivity analysis. To conclude, the type of weave, the properties of the yarns, the properties of the fibrous composite, the orientation of the yarns, and the size and shape of the yarns affect the stiffness values. The effect of loading also plays an important role in predicting the stiffness values.

A regression-based method helps in determining on how the output of the dependent variable changes when any one of the independent variables is varied, while the other independent variables are held fixed. Correlation analysis is conducted by varying one uncertainty variable at a time. The scatter plots are beneficial for quick overviews and for showing patterns between the uncertainty criteria and responses (material properties). It shows large quantities of data and easy to interpret the correlation between variables and clustering effects. However, scatter plots confront with difficulties in discovering relationships which span more than two dimensions.

On the other hand, the correlation analysis (scatter plot) measures the linear relation between the uncertainty criteria which shows that the friction coefficient and yarn height are dominantly influenced the material properties of the *MataBerkait*-dry woven fabric. The contribution of correlation ratio obtained by these two factors are extremely high (more than 0.90) in both loading cases evaluated. Shear moduli are found to have the weakest correlation compared to elastic moduli results. Moreover, the observations from the results of scatter plots provided valuable insight in the effects of uncertainty criteria on the response of the fabric. Indeed, the correlation analysis is a preliminary evaluation of the uncertainty criteria.

Unlike, regression-based, variance-based methods allow full exploration of the input space, which account for interactions, and non-linear responses. Response surface model is an iterative process and involves only the main effects and interactions or may also have quadratic and possibly cubic terms to visualize the curvature. It is also known as surrogate models which commonly employed for design optimization and sensitivity analyses. Three types of regression modes (Linear, quadratic without mixed term and full quadratic regressions) are presented in the response surface model. Again, it is impossible to visualize the response shape for more than 3 dimensional cases. R^2 values from response surface model showing an increase as the order of regression is increased.

However, the high values of R^2 could not guarantee the fitness of the model. Therefore, R_{adj} is used to help the overall explanatory power of the regression. R_{adj} value will be higher as more extra variables are added. However, the small difference between R_{adj} and R^2 reflects that the material properties response are not affected with any extra variables in the analysis. The evaluation of R^2 values cannot be fully-taken as an evaluation of sensitivity analysis for the uncertainty criteria because the approach does not quantify the dominant factor significantly. The response surface model results on shear properties might be misleading but also indicate some effects due to the variation of uncertainty criteria.

Another approach of a variance-based method utilized is the Sobol's indices. The Sobol's sensitivity indices are ratios of partial variances to total variance, and none of the sensitivity indices may be negative or exceed 1. Importantly, first-order sensitivity index

does not measure the uncertainty caused by interactions with other variables. A first-order sensitivity index is estimated directly because it measures the effect of one varying variable. The total-effect index places an upper bound on the importance of a given input by crediting the full effect of all relevant interactions to the given input. Eventually, the sensitivity indices (Sobol's indices) provide a clear idea of the effect of each uncertain variable onto the variance of the result responses. Indeed, the sum of all total-effect sensitivity indices is always greater than 1 and the model is perfectly additive if its equal to 1.

However, a more general study can be conducted to consider the effect of combined loading, as such combination of shear and biaxial loadings. It is also be worthwhile to investigate a series of loading magnitudes, yarn shapes and material properties of fibrous composite on the sensitivity analysis results as it was observed here some factors can either loosen or strengthen their significance by the increment of the loading magnitudes (only displacement is applied here). Lenticular or power ellipse can be chosen as an option to the yarn shape selection.

Other fibrous composite like E-Glass/Polyester also contributes some difference in the results. Most of the observations and conclusions made are limited to the 2D-weave of *Mata-Berkait*-dry woven fabric. Adoption of several plies of *MataBerkait*-dry woven fabric also a worthwhile trial to be considered as here we only used a single ply dry-fabric. It would be of interest to study on how the same uncertainty criteria reflect the response in 3D-weave of various fabric architectures. In conjunction to that, the uncertainty in yarn materials may be used to quantify the significance of material properties with the similar approaches. It is also recommended to generate a comprehensive experimental test data specifically on uncertainty analysis. If a comprehensive macro-scale constitutive model is to be generated, thus these results can be practically used for manufacturing process simulations or quality control applications.

5.4 Probabilistic multi-scale optimization of hybrid laminated composites

The complexity in obtaining an optimum solution of engineering problems makes the use of heuristic algorithms becomes a compatible tool. Nevertheless, their applications are limited due to the high computational cost of the slow convergence rate. This study focuses on multiple scales of hybrid laminated composites: the fine-scale and the coarse-scale for multi-objective optimization. The fine-scale is the relative on single-objective optimization of a lamina under uncertain mesoscopic parameters using EA algorithm. The coarse-scale defines the optimization analysis to optimize the stacking sequences of symmetric hybrid laminated composite composite structure with uncertain mesoscopic parameters by employing the ACO algorithm.

Woven fabrics in lamina consist of yarns in two principal in-plane directions (the warp and weft direction). The mechanical response (macroscopic elastic properties) of a lamina is therefore governed by the two types of yarns and the interactions between them. In the fine-scale optimization problem, an optimized weave pattern is determined which holds the

best performance of macroscopic elastic properties under mesoscopic uncertainty parameters. The optimization process utilizes the concept of EA to optimize the macroscopic elastic properties. The fitness-oriented has been chosen in EA concept wherein a candidate solution in the population is evaluated by a fitness function. The foundation of the optimization process is based on the survival of the fittest solutions. The investigated uncertain mesoscopic parameters are yarn spacing, yarn height, yarn width and misalignment of yarn angle. The so-obtained lamina macroscopic elastic properties is utilized in the course-scale optimization problem. The misalignment of yarn angle has been pursued as the uncertain mesoscopic parameter for course-scale optimization in accordance with Komeili and Milani (KM12).

In order to deal with the deficiency of the global optimization methods, the ACO is developed. The idea of ACO algorithm employs as a local search and updating the positions of the subject matter is performed by a pheromone-guided mechanism. In course-scale optimization, we present the formulation and implementation details of ACO for combinatorial optimization of hybrid laminated composite structure with multiple objectives. A logical pattern for stacking sequence of hybrid laminated composite structure is obtained and adoption of a series of multiplier values (α) which applying the weighted sum method approach with the specified design constraints.

Hybrid laminates consisting of low stiffness and less expensive inner layers and high stiffness and expensive outer layers are considered. The evaluated objective functions are minimization of cost and weight for hybrid symmetric laminates made of Silicon Carbide-Aluminum ($SiC - Al$) and Alumina Oxide-Aluminum ($Al_2O_3 - Al$) plies. The number of plies of specified material and are taken as the design variables. The optimization process are constrained by predefined fundamental frequency and buckling load factor. The idea of hybridization ends with notably reduction in cost for a reasonable reduction in fundamental frequency. The results delineate that ACO is a reliable and efficient algorithm for obtaining optimum solutions. The final decision of the optimal design may depend on the additional information that allows a practitioner to highlight the priorities of the two objective functions. Practically, there is no single optimal design and consideration of influencing parameters on the application may produce a different choice.

References

[AC08] C. Ayranci and J. Carey. 2D braided composites: A review for stiffness critical applications. *Composite Structures*, 85:43–58, 2008.

[Ada84] S. Adali. Design of shear-deformable antisymmetric angle-ply laminates to maximize the fundamental frequency and frequency separation. *Composite Structures*, 2:349369, 1984.

[AE97] J. O. Ajayi and H. M. Elder. Fabric friction, handle, and compression. *Journal of The Textile Institute*, 88:232–241, 1997.

[AE07] V. J. Amuso and J. Enslin. The strength pareto evolutionary algorithm 2 (spea2) applied to simultaneous multi-mission waveform design. In *Waveform Diversity and Design Conference, 2007. International*. IEEE, 2007.

[AGL71] G. M. Abbott, P. Grossberg, and G. A. V. Leaf. The mechanical properties of woven fabric: Part VII-Hysteresis and bending of woven fabrics. *Textile Research Journal*, 41:345–348, 1971.

[AH89] J. Amirbayat and J. W. S. Hearle. The anatomy of buckling of textile fabrics: Drape and comformability of dimensionless groups. *Journal of the Textile Institute*, 80:51–70, 1989.

[AHW+12] S. Allaoui, G. Hivet, A. Wendling, P. Ouagne, and D. Soulat. Influence of the dry woven fabrics meso-structure on fabric/fabric contact behaviour. *Journal of Composite Materials*, 46:627–639, 2012.

[ALB+14] AB Ilyani Akmar, Tom Lahmer, SPA Bordas, LAA Beex, and Timon Rabczuk. Uncertainty quantification of dry woven fabrics: A sensitivity analysis on material properties. *Composite Structures*, 116:1–17, 2014.

[AS92] Duffy KJ Adali S. Minimum cost design of vibrating laminates by hybridization. *Engineering Optimization*, 19:255267, 1992.

[AS11] M. Akbulut and F. O. Sonmez. Design optimization of laminated composites using a new variant of simulated annealing. *Computers & Structures*, 89:1712–1724, 2011.

[AT07] S. Babu Aminjikarai and A. Tabiei. A strain-rate dependent 3-d micromechanical model for finite element simulations of plain weave composite structures. *Composite Structures*, 81(3):407 – 418, 2007.

[AT09] M. Abachizadeh and M. Tahani. An ant colony optimization approach to

multi-objective optimal design of symmetric hybrid laminates for maximum fundamental frequency and minimum cost. *Structural Multidisciplinary Optimization*, 37:367–376, 2009.

[AV01] S. Adali and V. E. Verijenko. Optimum stacking sequence design of symmetric hybrid laminates undergoing free vibrations. *Composite Structures*, 54:131–138, 2001.

[AXC11] M. Ansar, W. Xinwei, and Z. Chouwei. Modeling strategies of 3D woven composites: A review. *Composite Structures*, 93:1947–1963, 2011.

[AY04] A. Alamdar-Yazdi. Weave structure and the skewness of woven fabric. *Research Journal of Textile and Apparel*, 8:28–33, 2004.

[Bac52] S. Backer. The mechanics of bent yarns. *Textile Research Journal*, 22:668–681, 1952.

[BBBLR13] Loıc Brevault, Mathieu Balesdent, Nicolas Bérend, and Rodolphe Le Riche. Comparison of different global sensitivity analysis methods for aerospace vehicle optimal design. In *10th World Congress on Structural and Multidisciplinary Optimization, WCSMO-10*, 2013.

[BC89] J-H. Byun and T-W. Chou. Modelling and characterization of textile structural composites: A review. *The journal of Strain Analysis for Engineering Design*, 24:253–262, 1989.

[BC01] Lucia Breierova and Mark Choudhari. An introduction to sensitivity analysis. MIT System Dynamics in Education Project, 2001.

[Beh61] B. Behre. Mechanical properties of textile fabrics: Part I-Shearing. *Textile Research Journal*, 31:87–99, 1961.

[Ber77] C. W. Bert. Optimal design of a composite-material plate to maximize its fundamental frequency. *Journal of Sound Vibration*, 50:229237, 1977.

[BGB01] K. Buet-Gautier and P. Boisse. Experimental analysis and modeling of biaxial mechanical behavior of woven composite reinforcements. *Experimental Mechanics*, 41:260–269, 2001.

[BGGLB99] K. Buet-Gautier, A. Gasser, J. Launay, and P. Boisse. Meso-macro mechanical behaviour of dry fiber fabrics. In *Proceedings of International Committee on Composite Materials (ICCM)*, page 735, 1999.

[BKBR13] Ilyani Akmar Abu Bakar, Oliver Kramer, Stéphane Bordas, and Timon Rabczuk. Optimization of elastic properties and weaving patterns of woven composites. *Composite Structures*, 100:575–591, 2013.

[Blu05] C. Blum. Ant colony optimization: Introduction and recent trends. *Physics of Life Reviews*, 2:353373, 2005.

[Boi10] P. Boisse. Simulations of composite reinforcement forming. In *Woven Fabric Engineering*. 2010.

[BP89] N. S. Bakhvalov and G. Panasenko. *Homogenisation: Averaging Processes*

in Periodic Media: Mathematical Problems in the Mechanics of Composite Materials. Springer, 1989.

[BR03] C. Blum and A. Roli. Metaheuristics in combinatorial optimization: Overview and conceptual comparison. *ACM computing surveys (CSUR)*, 35:268–308, 2003.

[BS93] T. Bäck and H. P. Schwefel. An overview of evolutionary algorithms for parameter optimization. *Evolutionary Computation*, 1:1–23, 1993.

[BS02] H.G. Beyer and H.P. Schwefel. Evolution strategies a comprehensive introduction. 1:3–52, 2002.

[BSS04] K. Baba, R. Shibata, and M. Sibuya. Partial correlation and conditional correlation as measures of conditional independence. *Australian & New Zealand Journal of Statistics*, 46(4):657–664, 2004.

[Buc80] C. P. Buckley. *Mechanics of flexible fibre assemblies*, chapter Review of the mechanical properties of fibres, pages 35–49. Alpen aan den Rijn, Netherlands Germantown, Md. : Sijthoff and Noordhoff, 1980.

[BVP13] L. A. A. Beex, C. W. Verberne, and R. H. J. Peerlings. Experimental identification of a lattice model for woven fabrics: Application to electronic textile. *Composites: Part A*, 48:82–92, 2013.

[BVSB08] P. Badel, E. Vidal-Sall, and P. Boisse. Large deformation analysis of fibrous materials using rate constitutive equations. *Computers and Structures*, 86:1164 – 1175, 2008.

[CFF+04] L. Costa, L. Fernandes, I. Figueiredo, J. Júdice, R. Leal, and P. Oliveira. Multiple-and single-objective approaches to laminate optimization with genetic algorithms. *Structural and multidisciplinary optimization*, 27:55–65, 2004.

[Che98] K. Chee. *Pendidikan Seni Visual*. Pelangi Publishing Group Bhd., 1998.

[Chu11] T. W. Chua. Multi-scale modelling of textile composites, 2011.

[CJKO01] D. W. Corne, N. R. Jerram, J. D. Knowles, and M. J. Oates. Pesa-ii: Region-based selection in evolutionary multiobjective optimization. In *Proceedings of the Genetic and Evolutionary Computation Conference (GECCO2001*. Citeseer, 2001.

[CKG08] E.W.C. Coenen, V.G. Kouznetsova, and M.G.D. Geers. A multi-scale computational strategy for structured thin sheets. *International Journal of Material Forming*, 1:61–64, 2008.

[CLJ05] J.J. Crookston, A. C. Long, and I. A. Jones. A summary review of mechanical properties prediction methods for textile reinforced polymer composites. *Proceeding of the Instituition of Mechanical Engineers, Part L: Journal of Materials Design and Applications*, 219:91–109, 2005.

[Coe99] C. A. C. Coello. An updated survey of evolutionary multiobjective optimiza-

tion techniques: State of the art and future trends. In *Evolutionary Computation, 1999. CEC 99.*, volume 1. IEEE, 1999.

[CSQ07] P. V. Cavallaro, A. M. Sadegh, and C. J. Quigley. Decrimping behavior of uncoated plain-woven fabrics subjected to combined biaxial tension and shear stresses. *Textile Research Journal*, 77:403–416, 2007.

[CT63] E. E. Clulow and H. M. Taylor. An experimental and theoretical investigation of biaxial stress-strain relations in a plain weave cloth. *Journal of the Textile Institute Transactions*, 54:323–347, 1963.

[CT06] K. F. Choi and S. K. Tandon. An energy model of yarn bending. *Journal of the Textile Institute*, 97:49–56, 2006.

[DA91] K. J. Duffy and S. Adali. Maximum frequency design of pre-stressed symmetric, crossply laminates of hybrid construction. 2:477–484, 1991.

[Dah61] B. Dahlberg. Mechanical properties of textile fabrics: Part II-Buckling. *Textile Research Journal*, 31:94–99, 1961.

[Deb01] K. Deb. *Multi-objective optimization using evolutionary algorithms*. Wiley, 2001.

[DGBH94] P. H. Dastoor, T. K. Ghosh, S. K. Batra, and S. P. Hersh. Computer-assisted structural design of industrial woven fabrics: Part III-Modelling of fabric uniaxial/biaxial load-deformation. *Journal of the Textile Institute*, 85:135–137, 1994.

[DMC96] M. Dorigo, V. Maniezzo, and A. Colorni. The ant system: Optimization by a colony of cooperating agents. *IEEE Trans Syst Man Cybernet*, 26:29–41, 1996.

[Dub10] P. D. Dubrovski. *Woven fabric engineering*. Sciyo, 2010.

[ES03] A. E. Eiben and J. E. Smith. *Introduction to Evolutionary Computing*. SpringerVerlag, 2003.

[FOW66] L. J. Fogel, A. J. Owens, and M. J. Walsh. *Artificial intelligence through simulated evolution*. John Wiley, 1966.

[FPS67] W. D. Freeston, M. M. Platt, and M. M. Schoppee. Mechanics of elastic performance of textile materials: Part XVIII- Stress-strain response of fabrics under two-dimensional loading. *Textile Research Journal*, 37:948–975, 1967.

[Fre09] D. A. Freedman. *Statistical Models: Theory and Practice*. Cambridge University Press, 2009.

[FS75] W. D. Freeston and M. M. Schoppee. Geometry of bent continuous-filament yarns. *Textile Research Journal*, 45:835–852, 1975.

[FS11] R. Fangueiro and F. Soutinho. 3 - textile structures. In R. Fangueiro, editor, *Fibrous and Composite Materials for Civil Engineering Applications*, Woodhead Publishing Series in Textiles, pages 62 – 91. Woodhead Publishing, 2011.

[FSS94] H. Fukunaga, H. Sekine, and M. Sato. Optimal design of symmetric laminated plates for fundamental frequency. *Journal of Sound and Vibration*, 171:219–229, 1994.

[GBH00] A. Gasser, P. Boisse, and S. Hanklar. Mechanical behaviour of dry fabric reinforcements. 3D simulations versus biaxial tests. *Computational Materials Science*, 17:7 – 20, 2000.

[GE07] M.R. Ghasemi and A. Ehsani. Multi-objective optimisation of composite laminates under heat and moisture effects using a hybrid neuro-ga algorithm. *Relation*, 1:12, 2007.

[Gel05] A. Gelman. Analysis of variancewhy it is more important than ever. *Ann. Statist.*, 33(1):1–53, 2005.

[GI12] G. Glen and K. Isaacs. Estimating sobol sensitivity indices using correlations. *Environmental Modelling and Software*, 37:157 – 166, 2012.

[GK66] P. Grossberg and S. Kedia. The mechanical properties of woven fabrics: Part I-The initial load extension modulus of woven fabrics. *Textile Research Journal*, 36:71–79, 1966.

[GM91] B. S. Gupta and Y. E. El Mogahzy. Friction in fibrous materials: Part I-Structural model. *Textile Research Journal*, 61:547–555, 1991.

[Gra97] A. E. Soremekun Grant. Genetic algorithms for composite laminate design and optimization, 1997.

[Gre89] J. L. Grenestedt. Layup optimization and sensitivity analysis of the fundamental eigenfrequency of composite plates. *Composite Structures*, 12:193–209, 1989.

[Gro66] P. Grosberg. The mechanical properties of woven fabrics: Part II-The bending of woven fabrics. *Textile Research Journal*, 36:205–211, 1966.

[Gup08] B. S. Gupta. *Friction in textile materials*. Woodhead Publishing and CRC Press, 2008.

[GVH01] L. Grosset, S. Venkataraman, and R. T. Haftka. Genetic optimization of two-material composite laminates. In *Sixteenth technical conference of the American society for composites, USA*, 2001.

[GZŠ06] J. Gajdošík, J. Zeman, and M. Šejnoha. Qualitative analysis of fiber composite microstructure: Influence of boundary conditions. *Probabilistic Engineering Mechanics*, 21(4):317 – 329, 2006.

[HA00] A. R. Horrocks and S. C. Anand. *Handbook of Technical Textiles*. Woodhead Publishing Limited, 2000.

[HD18] R. Haas and A. Dietzius. The stretching of the fabric and the shape of the envelope in non-rigid ballons. Technical report, 1918.

[HD03] J. C. Helton and F. J. Davis. Latin hypercube sampling and the propagation of uncertainty in analyses of complex systems. *Reliability Engineering and*

System Safety, 81:23–69, 2003.

[HFSB13] H. Hemmatian, A. Fereidoon, A. Sadollah, and A. Bahreininejad. Optimization of laminate stacking sequence for minimizing weight and cost using elitist ant system optimization. *Advances in Engineering Software*, 57:8, 2013.

[HGB69] J. W. S. Hearle, P. Grosberg, and S. Backer. *Structural mechanics of fibers, yarns and fabrics, Vol. 1*. Wiley-Interscience, 1969.

[HIoRI12] USA HKS Inc. of Rhone Island. Abaqus/standard user's manual. *SIMULIA brand of Dassault systems S.A*, 2012.

[HKN72] J. W. S. Hearle, M. Konopasek, and A. Newton. On some general features of a computer-based system for calculation of the mechanics of textile structures. 42(10):613–626, 1972.

[HL92] P. Hajela and C.-Y. Lin. Genetic search strategies in multicriterion optimal design. *Structural optimization*, 4:99–107, 1992.

[Hua79a] N. C. Huang. Finite biaxial extension of completely set plain woven fabrics. *Journal of Applied Mechanics*, 46:651–655, 1979.

[Hua79b] N. C. Huang. Finite biaxial extension of partially set plain woven fabrics. *International Journal of Solids and Structures*, 15:615–623, 1979.

[IB96] A. T. M. S. Islam and M. P. U. Bandara. Yarn spacing measurement in woven fabrics with specific reference to start-up marks. *Journal of the Textile Institute*, 87:107–119, 1996.

[IC80] R. L. Iman and W. J. Conover. Small sample sensitivity analysis techniques for computer models with an application to risk assessment. *Communications in Statistics*, 9:749–842, 1980.

[IC82a] T. Ishikawa and T-W. Chou. Elastic behavior of woven hybrid composites. *Journal of Composite Materials*, 16(1):2–19, 1982.

[IC82b] T. Ishikawa and T-W. Chou. Stiffness and strength behaviour of woven fabric composites. *Journal of Materials Science*, 17:3211–3220, 1982.

[IT01] I. Ivanov and A. Tabiei. Three-dimensional computational micro-mechanical model for woven fabric composites. *Composite Structures*, 54(4):489 – 496, 2001.

[Jin04] H. U. Jinlian. *Structure and mechanics of woven fabrics*. Woodhead Publishing Ltd., 2004.

[JP77] S. De Jong and R. Postle. An energy analysis of woven fabric mechanics by means of optimal-control theory part i: tensile properties. *Journal of the Textile Institute*, 68(11):350–361, 1977.

[JP78] S. De Jong and R. Postle. A general energy analysis of fabric mechanics using optimal control theory. 48(3):127–135, 1978.

[JSNS03] A. A. A. Jeddi, S. Shams, H. Nosraty, and A. Sarsharzadeh. Relations between

fabric structure and friction: Part I-Woven fabrics. *Journal of The Textile Institute*, 94:223–234, 2003.

[Kei11] H. Keitel. *Evaluation Methods for Prediction Quality of Concrete Creep Models*. PhD thesis, Bauhaus Universitaet Weimar, 2011.

[Kem58] A. Kemp. An extension of peirce's cloth geometry to the treatment of non-circular threads. *Journal of the Textile Institute*, 49:44–48, 1958.

[Khu06] A. I. Khuri. *Response surface methodology and related topics*. World scientific, 2006.

[KJS05] M.J. King, P. Jearanaisilawong, and S. Socrate. A continuum constitutive model for the mechanical behavior of woven fabrics. *International journal of Solids and Structures*, 42(13):3867 – 3896, 2005.

[KKL+11] H. Keitel, G. Karaki, T. Lahmer, S. Nikulla, and V. Zabel. Evaluation of coupled partial models in structural engineering using graph theory and sensitivity analysis. *Engineering Structures*, 33:37263736, 2011.

[KLTM07] Y. Kerboua, A. A. Lakis, M. Thomas, and L Marcouiller. Hybrid method for vibration analysis of rectangular plates. *Nuclear Engineering and Design*, 237:791–801, 2007.

[KM10] M. Komeili and A.S. Milani. *Meso-level analysis of uncertainties in woven fabrics*. VDM Verlag Dr. Müller, 2010.

[KM12] M. Komeili and A. S. Milani. The effect of meso-level uncertainties on the mechanical response of woven fabric composites under axial loading. *Computers and Structures*, 90-91:163–171, 2012.

[KNK73a] S. Kawabata, M. Niwa, and H. Kawai. The finite deformation theory of plain weave fabrics: Part I-The biaxial deformation theory. *Journal of the Textile Institute*, 64:21–46, 1973.

[KNK73b] S. Kawabata, M. Niwa, and H. Kawai. The finite deformation theory of plain weave fabrics: Part II-The uni-axial deformation theory. *Journal of the Textile Institute*, 64:47–61, 1973.

[KNK73c] S. Kawabata, M. Niwa, and H. Kawai. The finite deformation theory of plain weave fabrics: Part III-The shear deformation theory. *Journal of the Textile Institute*, 64:62–85, 1973.

[Kon80a] M. Konopasek. *Mechanics of flexible fibre assemblies, Nato Advanced Study Institutes Series, Series E: Applied Science*, chapter Classical elastica theory and its generalizations, pages 255–274. USA : Sijthoff and Noordhoff, 1980.

[Kon80b] M. Konopasek. *Mechanics of flexible fibre assemblies, Nato Advanced Study Institutes Series, Series E: Applied Science*, chapter Computational aspects of large deflection analysis of slender bodies, pages 275–292. USA : Sijthoff and Noordhoff, 1980.

[Kon80c] M. Konopasek. *Mechanics of flexible fibre assemblies, Nato Advanced Study*

Institutes Series, Series E: Applied Science, chapter Textile application of slender body mechanics, pages 293–310. USA : Sijthoff and Noordhoff, 1980.

[KS11] Ş. Karakaya and Ömer. Soykasap. Natural frequency and buckling optimization of laminated hybrid composite plates using genetic algorithm and simulated annealing. *Structural and Multidisciplinary Optimization*, 43:61–72, 2011.

[KSMK05] H. Kumazawa, I. Susuki, T. Morita, and T. Kuwabara. Mechanical properties of coated plain weave fabrics under biaxial loads. *Transactions of the Japan society for aeronautical ans space sciences*, 48:117–123, 2005.

[KTS05] F. Kolahan, M. Tahani, and A. Sarhadi. *Optimal design of sandwich composite laminates for minimum cost and maximum frequency using simulated annealing*. 2005.

[LB11] A. C. Long and L. P. Brown. *Composite reinforcements for optimum performance: Modelling the geometry of textile reinforcements for composites: TexGen*. Woodhead Publishing Ltd, 2011.

[LBD61] J. Lindberg, B. Behre, and B. Dahlberg. Mechanical properties of textile fabric: Part III-Shearing and buckling of various commercial fabrics. *Textile Research Journal*, 31:99–122, 1961.

[LBH03] S.K. Lee, J. H. Byun, and S. Hyung. Effect of fiber geometry on the elastic constants of the plain woven fabric reinforced aluminum matrix composites. *Materials Science*, 347:346–358, 2003.

[LBL11] H. Lin, L. P. Brown, and A. C. Long. Modelling and simulating textile structures using texgen. *Advanced Materials Research*, 331:44–47, 2011.

[LC02] D. Lussier and J. Chen. Material characterization of woven fabrics for thermoforming of composites. *Journal of Thermoplastic Composite Materials*, 15:497–509, 2002.

[LFZ+10] B. Liu, F. V. Fernández, Q. Zhang, M. Pak, S. Sipahi, and G. Gielen. An enhanced moea/d-de and its application to multiobjective analog cell sizing. In *Evolutionary Computation (CEC), 2010 IEEE Congress on*. IEEE, 2010.

[LHL+01] S. V. Lomov, G. Huysmans, Y. Luo, R.S. Parnas, A. Prodromou, I. Verpoest, and F.R. Phelan. Textile composites: modelling strategies. *Composites Part A: Applied Science and Manufacturing*, 32:1379–1394, 2001.

[LHL02] W. M. Lo, J. L. Hu, and L. K. Li. Modelling a fabric drape profile. *Textile Research Journal*, 72:454–463, 2002.

[LK80] G. A. V. Leaf and K. H. Kandil. The initial load-extension behaviour of plain woven fabrics. *Journal of the Textile Institute*, 71(1):1–7, 1980.

[LMH96] D. W. Lloyd, F. Mete, and K. Hussain. An approach to the theoretical mechanics of static drape. *International Journal of Clothing Science Technology*, 8:43–58, 1996.

[Lon05] A. C. Long. *Design and manufacture of textile composites*. Woodhead Publishing Limited, Cambridge, 2005.

[Lon11] A. C. Long. Modelling of processing and performance for textile composites. Lecture Notes, TexGen Workshop, 2011.

[Lov54] L. Love. Graphical relationships in cloth geometry for plain, twill, and sateen weaves. *Textile Research Journal*, 24:1073–1083, 1954.

[LPI+10] S. Lomov, G. Perie, D. Ivanov, I. Verpoest, and D. Marsal. Modeling three-dimensional fabrics and three-dimensional reinforced composites: challenges and solutions. *Textile Research journal*, 81:28–41, 2010.

[LR10] K Lakshmi and A Rama Mohan Rao. A memetic algorithm for combinatorial problems with multiple objectives. In *Advanced Computing (ICoAC), 2010 Second International Conference on*, 2010.

[LVSC09] M. Lima, R. M. Vasconcelos, L. F. Silva, and J. Cunha. Fabrics made from non-conventional blends: What can we expect from them related to frictional properties? *Textile Research Journal*, 79:337–342, 2009.

[LW04] S. Li and A. Wongsto. Unit cells for micromechanical analyses of particle-reinforced composites. *Mechanics of Materials*, 36:543–572, 2004.

[LWP13] J. S. Lightfoot, M. R. Wisnom, and K. Potter. Defects in woven preforms: Formation mechanisms and the effects of laminate design and layup protocol. *Composites Part A: Applied Science and Manufacturing*, 51:99–107, 2013.

[LZS+12] H. Lin, X. Zeng, M. Sherburn, A. C. Long, and M. J. Clifford. Automated geometric modelling of textile structures. *Textile Research Journal*, pages 1–14, 2012.

[MHD89] MHDC. *Anyaman : Pandan dan Mengkuang*. Malaysian Handicraft Development Corporation, Kuala Lumpur, Malaysia, 1989.

[MNAH07] A. S Milani, J. A. Nemes, R. C. Abeyaratne, and G. A. Holzapfel. A method for the approximation of non-uniform fibre misalignment in textile composites using picture frame test. *Composites Part A: Applied Science and Manufacturing*, 38:1493–1501, 2007.

[MR03] D. C. Montgomery and G. C. Runger. *Applied Statistics and Probability for Engineers:Third Edition*. John Wiley, 2003.

[Nai95] R. A. Naik. Failure analysis of woven and braided fabric reinforced composites. *Journal of Composite Materials*, 29:2334–2363, 1995.

[Nem86] M. P. Nemeth. Importance of anisotropy on buckling of compression-loaded symmetriccomposite plates. *AIAA journal*, 24:1831–1835, 1986.

[NG96] N.K. Naik and V.K. Ganesh. Failure behavior of plain weave fabric laminates under on-axis uniaxial tensile loading: Ianalytical predictions. *Journal of Composite Materials*, 30(16):1779–1822, 1996.

[NLA+08] A. J. Nebro, F. Luna, E. Alba, B. Dorronsoro, J. J. Durillo, and A. Beham.

Abyss: Adapting scatter search to multiobjective optimization. *Evolutionary Computation, IEEE Transactions on 12.4*, 12:439 – 457, 2008.

[NS92a] N. K. Naik and P. S. Shembekar. Elastic behavior of woven fabric composites: Iii - laminate design. *Journal of Composite Materials*, 26:2522–2541, 1992.

[NS92b] N. K. Naik and P. S. Shembekar. Elastic behavior of woven fabric composites: Ilamina analysis. *Journal of Composite Materials*, 26:2196–2225, 1992.

[Obi11] M. Obitko. "xi. crossover and mutation", 2011.

[OG11] B. Ozgen and H. Gong. Yarn geometry in woven fabrics. *Textile Research Journal*, 81:738–745, 2011.

[OK95] A. Osyczka and S. Kundu. A new method to solve generalized multicriteria optimization problems using the simple genetic algorithm. *Structural optimization*, 10:94–99, 1995.

[Olo64] B. Olofsson. The setting of wool fabrics - a theoretical study. *Journal of the Textile Institute*, 20:272–273, 1964.

[Pai52] E. V. Painter. Mechanics of elastic performance of textile materials: Graphical analysis of fabric geometry. Technical report, 1952.

[Pan96] N. Pan. Analysis of woven fabric strengths: Prediction of fabric strength under uniaxial and biaxial extensions. *Composites Science and Technology*, 56:311 – 327, 1996.

[PC00] X. Q. Peng and J. Cao. Numerical determination of mechanical elastic constants of textile composites. In *Proceedings of American Soceity for Composite*, pages 677–688, 2000.

[PC02] X. Peng and J. Cao. A dual homogenization and finite element approach for material characterization of textile composites. *Composites Part B: Engineering*, 33:45–56, 2002.

[Pei37] F. T. Peirce. The geometry of cloth structure. *Journal of the Textile Institute Transactions*, 28(3):45–96, 1937.

[PFMP04] A. Pegoretti, E. Fabbri, C. Migliaresi, and F. Pilati. Intraply and interply hybrid composites based on e-glass and poly (vinyl alcohol) woven fabrics: tensile and impact properties. *Polymer international*, 53:1290–1297, 2004.

[PGWT10] A. Ptchelintsev, G. Grewolls, J. Will, and M. Theman. Applying sensitivity analysis and robustness evaluation in virtual prototyping on product level using optislang. In *Proceeding of Simulia Customer Conference*, 2010.

[PKH59] M. M. Platt, W. G. Klein, and W. J. Hamburger. Mechanics of elastic performance of textile materials: Part XIV-Some aspects of bending rigidity of single yarns. *Textile Research Journal*, 29:611, 1959.

[PKN83] R. Postle, S. Kawabata, and M. Niwa. *Objective evaluation of apparel fabrics*. Textile Machinery Society of Japan, 1983.

[PO06] J. Park and A. Oh. Bending rigidity of yarns. *Textile Research Journal*, 76:478–485, 2006.

[PP96] J. R. Postle and R. Postle. Modelling fabric deformation as a nonlinear dynamical system using bäcklund transformations. *International Journal of Clothing Science and Technology*, 8:22–42, 1996.

[PT07] P. Potluri and V. S. Thammandra. Influence of uniaxial and biaxial tension on meso-scale geometry and strain fields in a woven composite. *Composite Structures*, 77:405–418, 2007.

[QMM03] J. Quinn, R. McIlhagger, and A. T. McIlhagger. A modified system for design and analysis of 3D woven preforms. *Composites Part A: Applied Science and Manufacturing*, 34:503–509, 2003.

[QWK+15] Z. Quan, A. Wu, M. Keefe, X. Qin, J. Yu, J. Suhr, J.H. Byun, B.S. Kim, and T.W. Chou. Additive manufacturing of multi-directional preforms for composites: opportunities and challenges. *Materials Today*, 18(9):503–512, 2015.

[Ram06] James O. Ramsay. *Principal Differential Analysis*. American Cancer Society, 2006.

[Red04] J.N. Reddy. *Mechanics of laminated composite plates and shells theory and analysis: 2nd edition*. CRC Press Inc., 2004.

[RKSB04] T. Rabczuk, J. Y. Kim, E. Samaniego, and T. Belytschko. Homogenization of sandwich structures. *International journal for numerical methods in engineering*, 61:1009 – 1027, 2004.

[RL08] U. Reuter and M. Liebscher. Global sensitivity analysis in view of nonlinear structural behavior. *LSDYNA Anwenderforum, Bamberg*, 2008.

[RL09a] A. R. M. Rao and K. Lakshmi. Multi-objective optimal design of hybrid laminate composite structures using scatter search. *Journal of Composite Materials*, 43:2157–2182, 2009.

[RL09b] A. R. M. Rao and K. Lakshmi. Multi-objective optimal design of hybrid laminate composite structures using scatter search. *Journal of Composite Materials*, 0:1–26, 2009.

[RL11] A. R. M. Rao and K. Lakshmi. Discrete hybrid pso algorithm for design of laminate composites with multiple objectives. *Journal of Reinforced Plastics and Composites*, 30:1703–1727, 2011.

[RR87] R. Reiss and S. Ramachandran. Maximum frequency design of symmetric angle-ply laminates. *Composite Structures*, 4:14761487, 1987.

[Sal08] A. Saltelli. *Global Sensitivity Analysis: The Primer*. John Wiley, 2008.

[SCB+14] Y. Swolfs, L. Crauwels, E. V. Breda, L. Gorbatikh, P. Hine, I. Ward, and I. Verpoest. Tensile behaviour of intralayer hybrid composites of carbon fibre and self-reinforced polypropylene. *Composites Part A: Applied Science and*

Manufacturing, 59:78–84, 2014.

[Sei09] M. Seidel. *Tensile Surface Structures: A practical Guide to Cable and Membrane Construction. Materials, Design, Assembly and Erection*. Ernst and Sohn, Berlin, 2009.

[SF96] D. M. Stump and W. B. Fraser. A simplified model of fabric drape based on ring theory. *Textile Research Journal*, 66:506–514, 1996.

[She07] M. Sherbun. *Geometric and Mechanical Modelling of Textiles*. PhD thesis, University of Nottingham, 2007.

[SLH78] W. J. Shanahan, D. W. Lloyd, and J. W. S. Hearle. Characterizing the elastic behaviour of textile fabrics in complex deformation. *Textile Research Journal*, 48:495–505, 1978.

[Sob01] I. M. Sobol. Global sensitivity indices for nonlinear mathematical models and their monte carlo estimates. *Mathematical and Computers in Simulation*, 55:271–280, 2001.

[SPH03] T.V. Sagar, P. Potluri, and J.W.S. Hearle. Mesoscale modelling of interlaced fibre assemblies using energy method. *Computational Materials Science*, 28:49 – 62, 2003.

[SS89] A. A. Shahpurwala and P. Schwartz. Modeling woven fabric tensile strength using statistical bundle theory. *Textile Research journal*, 59(1):26–32, 1989.

[STC+00] Andrea Saltelli, Stefano Tarantola, Francesca Campolongo, et al. Sensitivity anaysis as an ingredient of modeling. *Statistical Science*, 15(4):377–395, 2000.

[TI03] A. Tabiei and I. Ivanov. Fiber reorientation in laminated and woven composites for finite element simulations. *Journal of Thermoplastic Composite Materials*, 16:457–474, 2003.

[TK+05] M. Tahani, F. Kolahan, et al. Genetic algorithm for multi-objective optimal design of sandwich composite laminates with minimum cost and maximum frequency. In *International Conference on Advances in Materials, Product Design & Manufacturing Systems (ICMPM 2005)*, 2005.

[TSJ03] A. Tabiei, G. Song, and Y. Jiang. Strength simulation of woven fabric composite materials with material non- linearity using micro-mechanics based model. *Journal of Thermoplastic Composite Materials*, 16(1):5–20, 2003.

[TTS97] P. Tan, L. Tong, and G. P. Steven. Modelling for predicting the mechanical properties of textile compositesa review. *Composites Part A: Applied Science and Manufacturing*, 28:903–922, 1997.

[TUKZ99] N. Takano, Y. Uetsuji, Y. Kashiwagi, and M. Zako. Hierarchical modelling of textile composite materials and structures by the homogenization method. *Modelling and simulation in materials science and engineering*, 7:207–231, 1999.

[TY87] R. Testa and L. Yu. Stress-strain relation for coated fabrics. *Journal of Engineering Mechanics*, 113:1631–1646, 1987.

[TY02] A. Tabiei and W. Yi. Comparative study of predictive methods for woven fabric composite elastic properties. *Composite Structures*, 58:149 – 164, 2002.

[Una12] P. G. Unal. 3d woven fabrics. In *Woven fabrics*. 2012.

[VBLK+13] N. Vu-Bac, T. Lahmer, H. Keitel, J. Zhao, and T. Rabczuk. Stochastic prediction of bulk properties of amorphous polyethylene based on molecular dynamics simulations. *Mechanics of materials*, 2013.

[VG96] R. Vaidyanathan and Y. A. Gowayed. Optimization of elastic properties in the design of textile composites. *Polymer composites*, 17:305–311, 1996.

[VIV96] Ph. Vandeurzen, J. Ivens, and I. Verpoest. A three-dimensional micromechanical analysis of woven-fabric composites:i.geometric analysis. *Composites Science and Technology*, 56:1303–1315, 1996.

[VKDP11] S. Vassiliadis, A. Kallivretaki, D. Domvoglou, and C. Provatidis. Mechanical analysis of woven fabrics: The state of the art. *InTech*, pages 41–64, 2011.

[VN00] L. Virto and A. Naik. Frictional behavior of textile fabrics: Part II-Dynamic response for sliding friction. *Textile Research Journal*, 70:256–260, 2000.

[Wu09] Z. Wu. Three dimensional exact modelling of geometric and mechanical propeties of woven composites. *Acta Mechanica Solida Sinica*, 22:479–486, 2009.

[XN11] W. Xia and B. Nadler. Three-scale modeling and numerical simulations of fabric materials. *International Journal of Engineering Science*, 49:229–239, 2011.

[YDC06] H. Yi, X. Ding, and S. Chen. Estimation of the elastic constants of architectural membrane under bi-axial tensile loading. *Engineering Mechanics*, 10:033, 2006.

[YG10] X. Yu and M. Gen. *Introduction to Evolutionary Algorithms*. 2010.

[YPC+02] W. R. Yu, F. Pourboghrat, K. Chung, M. Zampaloni, and T. J. Kang. Non-orthogonal constitutive equation for woven fabric reinforced thermoplastic composites. *Composites Part A: Applied Science and Manufacturing*, 33(8):1095–1105, 2002.

[Zha10a] L. Zhang. *Reliability analysis of fabric structures*. PhD thesis, Newcastle Upon Tyne, 2010.

[Zha10b] L. Zhang. *Reliability analysis of fabric structures*. PhD thesis, Newcastle Upon Tyne, 2010.

[ZŠ07] J. Zeman and M. Šejnoha. From random microstructures to representative volume elements. *Modelling and Simulation in Materials Science and Engineering*, 15(4):S325, 2007.